PHYSICAL LAYER MODEL DESIGN FOR WIRELESS NETWORKS

A Dissertation

by

YI YU

Submitted to the Office of Graduate Studies of
Texas A&M University
in partial fulfillment of the requirements for the degree of

DOCTOR OF PHILOSOPHY

August 2006

Major Subject: Electrical Engineering

PHYSICAL LAYER MODEL DESIGN FOR WIRELESS NETWORKS

A Dissertation

by

YI YU

Submitted to the Office of Graduate Studies of
Texas A&M University
in partial fulfillment of the requirements for the degree of

DOCTOR OF PHILOSOPHY

Approved by:

Chair of Committee,	Scott L. Miller
Committee Members,	Costas N. Georghiades
	A. L. Narasimha Reddy
	Marina Vannucci
Head of Department,	Costas N. Georghiades

August 2006

Major Subject: Electrical Engineering

ABSTRACT

Physical Layer Model Design for Wireless Networks. (August 2006)

Yi Yu, B.S., Southeast University;

M.S., Southeast University

Chair of Advisory Committee: Dr. Scott L. Miller

Wireless network analysis and simulations rely on accurate physical layer models. The increased interest in wireless network design and cross-layer design require an accurate and efficient physical layer model especially when a large number of nodes are to be studied and building the real network is not possible. For analysis of upper layer characteristics, a simplified physical layer model has to be chosen to model the physical layer.

In this dissertation, the widely used two-state Markov model is examined and shown to be deficient for low to moderate signal-to-noise ratios. The physical layer statistics are investigated, and the run length distributions of the good and bad frames are demonstrated to be the key statistics for accurate physical layer modeling. A four-state Markov model is proposed for the flat Rayleigh fading channel by approximating the run length distributions with a mixture of exponential distributions. The transition probabilities in the four-state Markov model can be established analytically without having to run extensive physical layer simulations, which are required for the two-state Markov model. Physical layer good and bad run length distributions are compared and it is shown that the four-state Markov model reasonably approximates the run length distributions. Ns2 simulations are performed and the four-state Markov model provides a much more realistic approximation compared to the popular two-state Markov model.

Achieving good results with the flat Rayleigh fading channel, the proposed four-state Markov model is applied to a few diversity channels. A coded orthogonal frequency division multiplexing (OFDM) system with a frequency selective channel and the Alamouti multiple-input multiple-output system are chosen to verify the accuracy of the four-state Markov model. The network simulation results show that the four-state Markov model approximates the physical layer with diversity channel well whereas the traditional two-state Markov model estimates the network throughput poorly. The success of adapting the four-state Markov model to the diversity channel also shows the flexibility of adapting the four-state Markov model to various channel conditions.

To my parents

ACKNOWLEDGMENTS

First of all, I wish to thank my advisor, Dr. Scott L.Miller, for his constant support, guidance and encouragement throughout my Ph.D. program. He instilled in me the knowledge and philosophy of being an independent researcher. This dissertation would not have been possible without his help.

I would also like to thank the members of my dissertation committee, Dr. Costas N. Georghiades, Dr. A.L. Narasimha Reddy and Dr. Marina Vannucci, for spending their invaluable time reviewing my dissertation and suggesting improvements.

Finally, I would like to thank my parents, Lehong Yu and Huizhen Zhang, for their unconditional love and support throughout my life. This work is dedicated to them.

TABLE OF CONTENTS

LIST OF TABLES

LIST OF FIGURES

CHAPTER I

INTRODUCTION

Wireless network protocol design has been a very interesting topic for various researchers especially since wireless LANs (Local Area Networks) have emerged as a prevailing technology for broadband mobile wireless access. Also the demand of high speed packet data service for the third generation mobile communication system brings the need of protocol design over wireless links to provide better service. The increased interests in wireless network protocol designs require an accurate and efficient physical layer model for simulation when a large number of nodes are to be studied and building the real network is not possible. In this chapter, the wireless network architecture will be presented. The principle of the TCP/IP (Transmission Control Protocol/Internet Protocol) and how the protocol affects network throughput will be discussed. This chapter will also give a brief introduction of current commonly used physical layer models. Finally, an overview of the dissertation will conclude this chapter.

A. Network Architecture

To understand the relationship between wireless protocol design and physical layer models, it is necessary to first comprehend the network architecture, which groups the communication functions into related and manageable layers.

––––––––––

The journal model is *IEEE Transactions on Automatic Control.*
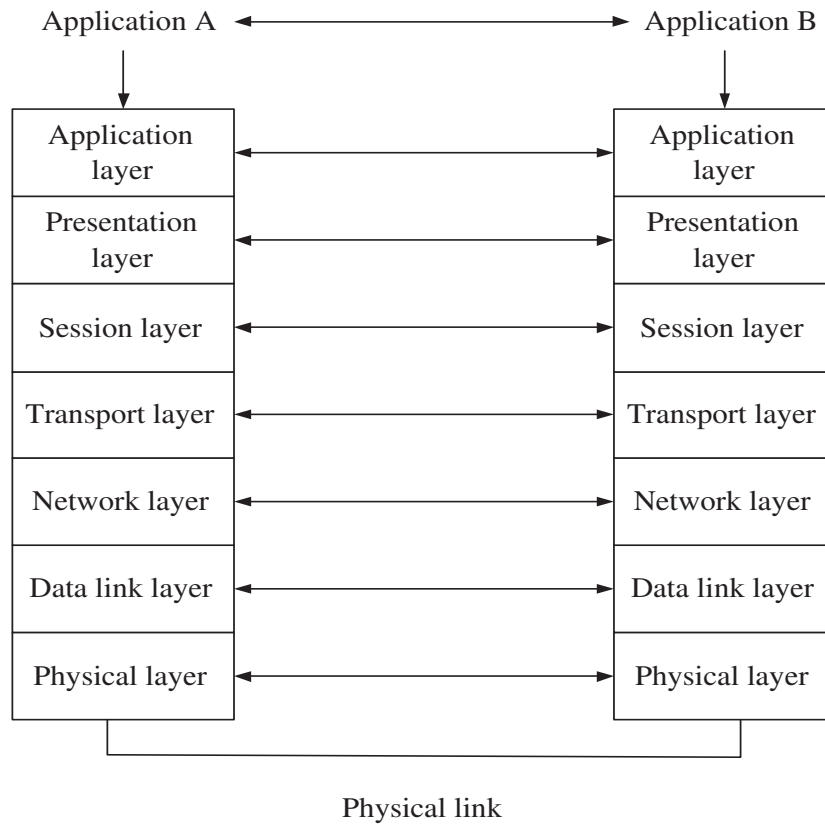
Fig. 1. The OSI reference model

1. The OSI Reference Model

The OSI(Open Systems Interconnection) reference model was developed to serve as a framework to facilitate the development of standards [1] [2]. It partitions the communication process into the seven layers shown in Fig. 1. Each layer is connected with a certain process that talks with a peer process on the other machine. Different layers communicate by exchanging protocol data units(PDU), which contain protocol control information and user information. The behavior of each layer is controlled by the layer protocol.

It is important to notice that there is no direct communication link between each

peer. For communication to take place, each layer attaches a header to the service data unit (SDU) transferred from the adjacent upper layer, forms the PDU and passes it to the next lower layer. In the mean time, each layer of the peer process extracts the SDU from the PDU delivered from the adjacent lower layer and passes the SDU to the adjacent upper layer. Each layer is supposed to function independently and the details of implementation of the layers are irrelevant to the other layers. The performance of each layer function relies on the correct execution of the tasks of other layers function.

The application layer supports application and end-user processes. This layer provides application services for file transfers,remote login, emails and other network software service. The presentation layer transforms application data to the network format and vice versa. It is intended to provide independence from different representations of application layer data. The session layer deals with sessions and connections between applications. It manages conversations between the applications at each end. The transport layer is responsible for end to end transfer of data between systems. In the transport layer, error recovery schemes and flow control are available to maintain a certain quality of service. Segmentation and reassembly can also be implemented to match the data size of the session layer to the size of the network layer data. These top four layers are end to end across the network while the lower three layers are involved with peer to peer processes across a single hop.

The network layer provides functions of switching, routing, addressing, internetworking, congestion control and packet sequencing. The data link layer involves transmission of frames across two nodes. It is divided into two sublayers: the Media Access Control (MAC) layer and the Logical Link Control (LLC) layer. The MAC sublayer coordinates the transmissions from a machine on the network into the medium. The LLC layer is responsible for transmission error recovery, flow control

and frame synchronization. The physical layer transfers the bit stream over a communication channel. The channel could be cable, copper wire, radio or optical fiber. The physical layer also deals with the hardware required to send and receive data on the carrier.

As we can see from Fig. 1, control is passed from one layer to the next. Each layer works independently from one another and all will have an influence on the final network throughput performance.

2.   TCP/IP over Wireless Link

TCP/IP protocol suites refer to a set of protocols that support network administration and maintenance. It not only includes the Transmission Control Protocol (TCP) and the Internet Protocol (IP) but also includes other related protocols such as the User Datagram Protocol (UDP), the Internet Control Message Protocol (ICMP), etc. The IP component performs network layer functions and provides routing between systems based on a four byte destination address. The IP layer is connectionless because every packet is routed independently and it does not guarantee the packet will be delivered to the destination or the packet will be received in sequence. The transport layer protocols, TCP and UDP perform transport layer functions based on the best-effort IP service.

TCP provides a connection-oriented,reliable, in-sequence and byte-stream service between applications [3] [4]. The Internet services such as the World Wide Web(WWW), terminal login, file transfer and mail transfer depend on the implementation of TCP and IP to supply solid application-to-application data connections. TCP employs sequence numbering and acknowledgment (ACK) to ensure reliable data transfer. Random intial sequence numbers are selected at the beginning of the connection. A selective Repeat ARQ mechanism is used in TCP to perform end-to-

end error control across a network. For each transmitted data sequence, the receiver is expected to send an ACK after receiving it. If an ACK does not arrive within a certain time interval, retransmission will be employed. In the TCP header, there is a window size field which specifies the number of bytes the sender is willing to accept. It is called the advertised window. The sender must stay within this limit. TCP uses this field to control the flow of data and congestion.

To avoid network overloading, TCP employs a congestion control algorithm to dynamically adjusts the congestion window according to the network state. By detecting the rate at which segments are sent and not acknowledged, a TCP device can infer the network congestion state and increase or decrease the congestion window size correspondingly. The maximum amount of data the sender can transmit is the minimum of the advertised window and the congestion window.

There are three phases of the congestion control algorithm during the TCP operation. Fig. 2 illustrates the dynamics of the TCP congestion window during a connection. The first phase is slow start, which is called when the algorithm starts or restarts. In slow start, the congestion window size grows exponentially upon the receiving of corresponding ACKs until the preset congestion threshold is met. After the congestion window size reaches to the value of congestion threshold, a congestion avoidance phase takes over. In this phase, the congestion window increases linearly rather than exponentially. When TCP detects network congestion, the algorithm enters the third phase, in which the congestion threshold is set to half of the current window size and the congestion window is set to one. After that, the algorithm restarts and enters the slow start phase again.

TCP assumes network congestion when an acknowledgement is not received before the time-out expires. Every time TCP detects congestion, the network throughput is cut due to the transmission window size being decreased to one. The assumption
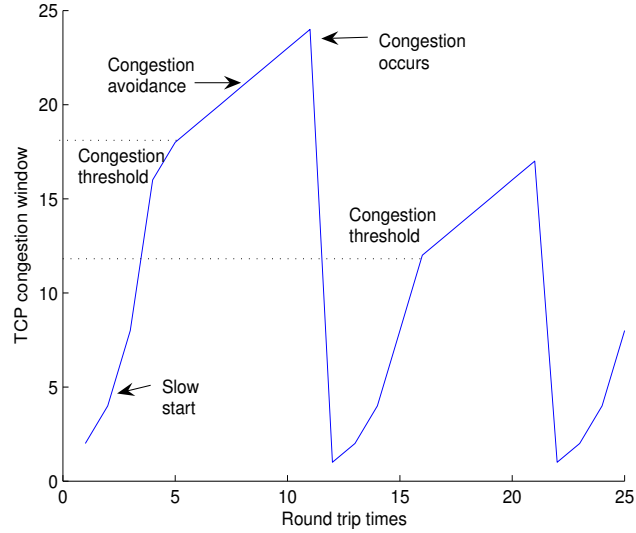
Fig. 2. Dynamics of TCP congestion window

of the algorithm is that the packet loss is caused by network congestion rather than transmission errors. However, the assumption is not valid for wireless environments. In wireless links, fading and noise become the major cause of packet loss. Transmission errors can be relatively high and physical layer packet losses are more often than in a wired network. If a packet is lost, TCP assumes it is dropped because of congestion and slows transmission drastically. In this case, the network throughput is reduced and the bandwidth is not used efficiently [5] [6] [7]. As a result, the statistics of packet errors in the physical layer can affect the TCP activities and thereby affect the network throughput.

To enhance the network performance, several improvements at the TCP layer are proposed such as the Split-TCP approach [8] [9], Snoop TCP [10] and Fast Retransmission and Recovery [11] [12]. In order to design an appropriate TCP protocol or compare the performance of different protocols for wireless environments, accurate modeling of wireless link characteristics has to be assured in the simulations.
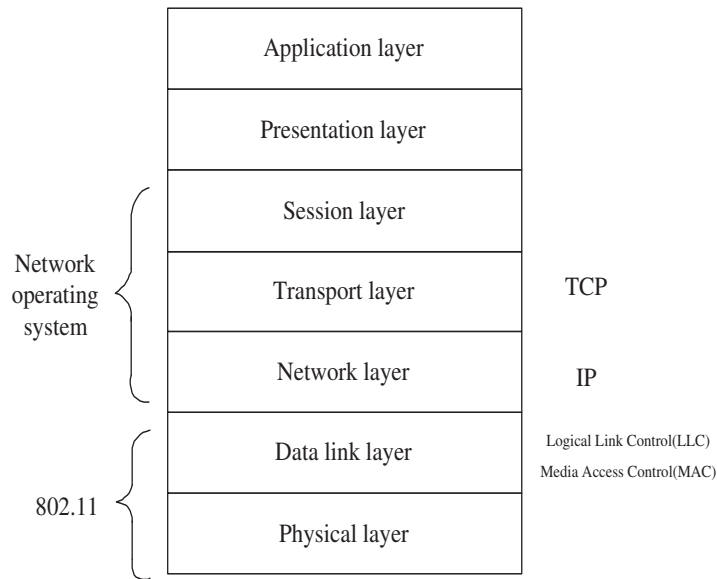
Fig. 3. IEEE 802.11 and the OSI model

3. Overview of Wireless Lan MAC Layer

The Wireless Local Area Network(WLAN) technology is defined by the IEEE 802.11 family of specifications. There are several specifications in the family: 802.11b, 802.11a, 802.11g, 802.11n, etc. The relationship of 802.11 and the OSI Model is shown in Fig. 3. The Ethernet protocol and CSMA/CA (Carrier Sense Multiple Access with Collision Avoidance) are used in the specifications. In addition to providing the standard MAC layer functions to coordinate multiple accesses, the 802.11 MAC also performs other functions to enhance communications over a wireless medium, such as fragmentation, packet retransmission and acknowledgements. Those functions are typically related to upper layer protocols.

Because on a radio link, the transceiver can not listen while transmitting as in a wired link, CSMA/CA is used by wireless LANs. In the Ethernet, CSMA/CD(Carrier Sense Multiple Access with Collision Detection) is used. In CSMA/CA, a station

listens to the channel before transmitting. If the channel is found to be idle, it starts to transmit. If the channel is busy, it waits for a random amount of time before trying to send it again. After a packet is transmitted, the receiving station will check the cyclic redundancy check (CRC) of the received packet and send an acknowledgment (ACK). If the sender does not get the acknowledgment it will have to retransmit the packet.

In a wireless LAN, MAC level retransmission is employed to detect and recover wireless link errors so that it appears to be a reliable channel to TCP. As we know, TCP slows down very quick by packet losses in radio links. Each time a station receives a packet, it sends back an ACK to the transmitter. If no ACK is received, the sender will assume the packet is lost and try to retransmit the packet (using the normal CSMA/CA procedures). Note that the ACKs are different from TCP acks, which belongs to a different layer function. In 802.11, typically the station transmits the next packet only when the previous packet has been acknowledged. There is no sliding window mechanism like in TCP to keep the protocol simple. If there is no ACK after the preset entry of retransmission, the operation will be abandoned and an error will be passed to the upper layers.

To decrease the probability of a packet being corrupted in a radio link, smaller packets are used in wireless LAN protocols. Because of the relatively high bit error rate, the smaller the packet size the less probability of packet error caused by the radio link. Since the Ethernet packets are usually longer, a fragmentation and reassembling mechanism is added at the MAC layer. Each fragment is individually checked and retransmitted. The transmission station is not allowed to transmit a new fragment until it receives an ACK for the previous fragment or if the fragment has been retransmitted too many times, the whole packet will be dropped.

Due to the retransmission and fragmentation scheme utilized in 802.11 MAC,

the pattern of radio link errors can make distinct upper layer activities. Continuous packet losses less than the threshold can be recovered locally without passing up to the TCP layer. On the other hand, continuous packet losses more than the threshold will be reported to the upper layer as an error, which will be considered as network congestion by TCP and slows down the transmission rapidly. Even with the same error rate, different distributions of radio link errors will result in varied network performance. For example, suppose the MAC retransmission threshold is 4 and the sender tries to send 100 frames to the receiver. The frame error rate is 0.1 so there will be approximately 10 frames in error . If the 10 error frames are distributed with a pattern of 3 frame error runs of length 3 and 1 single frame error runs of length 1, the loss of physical layer can be fully recovered by the MAC layer retransmission scheme and there will be no frame loss reported to the upper layer. The network throughput will be maximized in this case. However, if the 10 error frames are distributed with 2 frame error runs of length 5, the MAC layer can not recover from the physical layer frame error loss. The TCP layer will be informed of the packet loss and cut down the window size or TCP congestion threshold which will cause a significant loss of network throughput. Thus with a different distribution of the frame errors the network performance could completely differ.

4. Physical Layer Models

The performance of a wireless network is sensitive to the operation of the physical layer channel, where the statistics of the frame error process are intimately tied to higher layer network performance. Setting up a real environment simulation is found to be impractical most of the time especially when a large number of nodes are to be studied. Also it is difficult to adjust the physical layer parameters in a real physical environment simulation. Although simulating the equivalent baseband physical layer

channel with the actual modulation, coding and fading would be the optimum method to get the exact physical layer interactions, the complexity and particularly the running time consumption make this unbearable for researchers who are interested in network performance. Physical layer models come in handy in these situations and are adopted extensively in various research. The ease of using a physical layer model and the flexibility to adjust it make simulations which are unfeasible in a real physical environment possible. However, an inaccurate physical layer model could lead to misjudgement of upper layer protocol performance. Opportunities of designing protocols with a better knowledge of physical layer frame process statistics will be wasted with an inappropriate physical layer model.

Of all the current physical layer models, the two-state Markov Model (2SMM) is the most popular and widely used for network protocol research by all kinds of network simulators [13]. The model is particularly popular in wireless applications where the physical channel is of the flat Rayleigh fading type. It is frequently used for modeling the packet loss process associated with network congestion as well[14]. The memoryless two-state Markov process is illustrated in Fig. 4. In the good state, the transmission will be successful which means no error. Whereas in the bad state, the transmitted frame will be in error. The transition probabilities p and q are acquired from the physical layer frame error rate (FER) and the average frame error run length (AFEL). For the two-state Markov Model, the current frame state is dependent on the previous frame state and the corresponding transition probability while it has nothing to do with the frame states before the previous state.

Previous research shows that the two-state Markov Model is incapable of producing statistically accurate frame error processes for the case of low to moderate signal to noise ratios and hence inaccurate network simulation results are often encountered with the two-state Markov Model [15]. In most cases, we evaluate network protocols
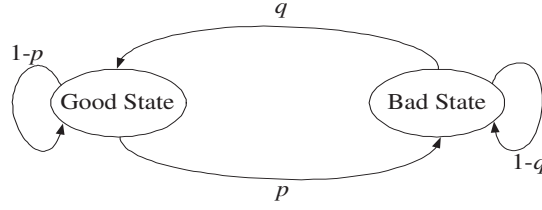
Fig. 4. Two-state Markov model

based on network simulation results. Failing to generate accurate network simulation results greatly affects the ability to execute correct protocol assessment.

An extended Gilbert model was proposed in [16] to characterize the queueing related packet losses in networks, in which the states of the model are described by the packet loss or reception run length. It could be used to model the packet loss in a wireless physical layer with fading. However, setting up the transition probabilities of the extended Gilbert model would not be an easy task. Moreover, there probably will be a large amount of states in the extended Gilbert model and thus will add a great deal of complexity in the model.

The finite-state Markov Model (FSMM) is proposed to improve the accuracy of two-state Markov Model [17] [18]. However, the finite-state Markov Model has limited application due of the complexity of setting up the model parameters. The diagram of the FSMM is show in Fig. 5. The main difference between the FSMM and the 2SMM is that the FSMM has several states which are partitioned by the received signal noise ratio. The principle of partitioning the states is to keep the average time duration in each state constant. As the normalized doppler rate decreases, the number of states needed increases. For a slow varying channel, with a large number of states, the complexity of implementing the FSMM and solving for the model parameters makes this model unfavorable for simulations.

Hidden Markov Models (HMMs) are used to model the fading processes as well
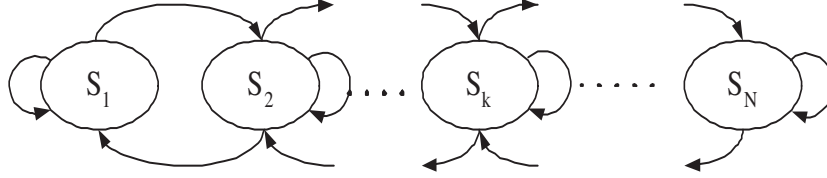
Fig. 5. Finite-state Markov model

[19] [20]. In [19], the HMM was fit to a fading process by either using the method of moments or approximating the multidimensional probability densities. Distributions of the fade duration and level crossing rates were computed analytically based on the extracted HMM. However, the complexity of generating the HMMs and the difficulty of computing the model parameters limit the application the the hidden Markov models.

Other channel models have been proposed recently for the purpose of accurate network layer performance, based on the statistics of the physical layer frame error process [21] [22]. With these newly proposed models, the network simulation accuracy is greatly improved, while the complexity of setting the model parameters is increased. A great deal of information has to be acquired in order to set model parameters, which means initial physical layer simulations are required for most cases. The complexity required to initialize the current physical layer channel models prompted us to develop an improved channel model where parameters can be set analytically.

All the physical layer models mentioned before are all designed for flat Rayleigh fading channels. For broadband wireless systems, those models do not apply anymore since the channel usually becomes frequency selective. With proper signal processing, frequency diversity can be achieved and the wireless link bit error rate will drop significantly. Appropriate approaches to design physical layer models for frequency selective channels are necessary in order to simulate a wideband communication system.

In [23], the two state Markov model was used to model the physical layer transmission success/failure of MIMO systems. The instantaneous mutual information was compared with the information rate to define the states of the Markov model. If the instantaneous mutual information was greater than the information rate, the channel was in a good state and otherwise the channel was in a bad state. The transition probabilities of the 2SMM were obtained by doing Monte-Carlo simulations. There was no validation of the 2SMM by comparing the frame error rate or average error frame run length with a simulated physical channel in this paper. For different Doppler rate, one has to rerun the Monte-Carlo simulations in order to set the transition probabilities. Especially for lower doppler rate, to obtain accurate transition probabilities from the simulation, the simulation time are significantly longer in order to capture the dynamics of the fading process.

B.   Overview of the Dissertation

The focus of the dissertation will be designing accurate, efficient and relatively simple physical layer models for wireless network simulations. The materials can be divided into three parts. First, the motivation and idea of designing a new physical layer model will be discussed in Chapter III. The structure of the proposed Four-State Markov model will also be introduced in this Chapter. Second, physical layer modeling for wireless systems with flat Rayleigh fading will be investigated thoroughly in Chapter IV. Chapter V will address the problem of physical layer modeling for a frequency selective channel and an Alamouti multiple-input multiple-output (MIMO) system.

In chapter II, the reader is introduced to the background of fading channels. The concepts of flat and frequency selective fading channels as well as the amplitude

distribution and correlation properties are described. The principles of Orthogonal Frequency Division Multiplexing (OFDM) and the Alamouti MIMO systems will also be presented.

Chapter III presents a new design of a four-state Markov Model (4SMM). First, the ns2 network simulator is introduced. The modifications of ns2 in order to embed an equivalent physical layer baseband and proposed physical layer models are described. Current physical layer models are investigated in detail. The popular two-state Markov Model is shown to be unable to capture the frame error run length distribution and provides poor network simulation results. The important characteristics of the frame error process are identified in order to provide accurate network results. It is found by the presented run length model that the run length distributions of physical layer frame process influences the network throughput in addition to the frame error rate. Finally, utilizing the properties of the frame error process, a simple four-state Markov Model is presented which captures the physical layer characteristics.

Chapter IV discusses the procedures to set up the four-state Markov Model for flat fading channels. The four-state Markov Model is built to match the good and bad frame run length distributions of the physical layer. By analyzing the underlying fading process, the parameters of four-state Markov Model can be set up analytically. With the model parameters analytically set up, the process of building the four-state Markov Model is very simple. Network Performance of the four-state Markov Model is presented and compared with other currently used models.

Chapter V presents the procedures to set up the four-state Markov Model for frequency selective channels and the Alamouti MIMO system. For both cases, certain diversity orders can be achieved and the four-state Markov Model is designed to match the physical layer statistics with diversity. The network performance of the four-state

Markov Model designed for a frequency selective channel and MIMO system are presented.

Finally, conclusions will be drawn in Chapter VI and related topics of future research will be discussed.

CHAPTER II

PHYSICAL LAYER CHARACTERISTICS

To design physical layer models for wireless network simulations, first one needs to understand the principles of wireless physical layer functions. The physical layer of a wireless system is intended to support reliable bit level transmission. Unlike a wired system, wireless channels are susceptible to a lot of impairments such as multi-path fading, interference and noise. These impairments cause the wireless channel to exhibit a higher error rate. The physical layer is designed to combat those drawbacks of wireless links at its best. In this chapter, the important concept of multi-path fading is introduced, which includes the flat fading channel and the frequency selective fading channel. A brief overview of an OFDM system structure and the Alamouti MIMO system structure is also provided in this chapter.

A.   Fading Channel

Fading is one of the major issues involved in a wireless communication system. As a result of multi-path propagation, fading is traditionally a pitfall of wireless transmission. In contrast to large scale path loss and shadowing, small scale fading is used to describe the rapid fluctuation of a signal over a short period of time [24] [25]. It is a result of multipath propagation caused by the reflections from the ground and surrounding structures. The combined signals at the receiver vary widely in amplitude and phase, depending on the amplitude and relative phases of the component signals. The multiple versions of signals may add constructively when their phases are aligned or cancel one another at other times.

Based on the relationship between the signal parameters and channel parameters, the fading process can be divided into different types. Fading can be slow or fast fading

depending on the relationship between the doppler rate and the symbol duration. On the other hand, fading can be flat or frequency selective depending on the relationship between the multipath time delay spread and the transmitted symbol duration.

1. Flat Fading Channel

With multiple versions of the delayed signal at the receiver due to multipath, the complex envelope of the received signal can be modeled as

$$r(t) = \sum_{k=1}^{N} \alpha_k(t) e^{j\theta_k(t)} s(t - \tau_k) + n(t), \tag{2.1}$$

where N is the number of multipath components, α_k and θ_k are the amplitude attenuation and phase shift of kth path respectively and τ_k is the delay for the kth path.

If the differential path delays $\tau_i - \tau_j \ll T_s$ for all paths, it can be assumed that $s(t - \tau_k) \approx s(t)$, in which case it is called flat fading. By utilizing this property, (2.1) can be written as

$$r(t) = \sum_{k=1}^{N} \alpha_k(t) e^{j\theta_k(t)} s(t) + n(t). \tag{2.2}$$

Define

$$g(t) = x(t) + jy(t) = \sum_{k=1}^{N} \alpha_k(t) e^{j\theta_k(t)}, \tag{2.3}$$

$$x(t) = \sum_{k=1}^{N} \alpha_k(t) \cos\theta_k(t), \tag{2.4}$$

$$y(t) = \sum_{k=1}^{N} \alpha_k(t) \sin\theta_k(t). \tag{2.5}$$

If there are a large number of paths available and each of the paths has approximately equal attenuation, then the central limit theorem can be invoked and both $x(t)$ and $y(t)$ can be treated as Gaussian random processes. This is well known as

Rayleigh fading since the magnitude of the received envelop, $|g(t)|$, follows a Rayleigh distribution. At any time t_1,

$$f_R(r) = \frac{r}{\sigma^2} \exp(-\frac{r^2}{2\sigma^2}), \ r \geq 0 \tag{2.6}$$

where $E[R^2] = 2\sigma^2$. This Rayleigh fading condition is typically encountered in urban areas where a line-of-sight or dominant path does not exist. The autocorrelation of the flat fading channel can be characterized by $\phi_{gg}(\tau)$.

$$
\begin{aligned}
\phi_{gg}(\tau) &= \frac{1}{2} E[g^*(t)g(t+\tau)] \\
&= \phi_{xx}(\tau) + j\phi_{xy}(\tau),
\end{aligned}
\tag{2.7}
$$

where

$$\phi_{xx}(\tau) = \phi_{yy}(\tau), \tag{2.8}$$

$$\phi_{xy}(\tau) = \phi_{yx}(-\tau). \tag{2.9}$$

Note that the phases $\theta_k(t)$ can be assumed to be uniformly distributed over $[-\pi, \pi]$ and independent for each $k_1 \neq k_2$. Let $\Omega_p = E[x^2(t)] + E[y^2(t)] = \sum_{k=1}^{N} \alpha_k^2$ and f_m be the Doppler rate. Then, it is straightforward to get the crosscorrelation

$$
\begin{aligned}
\phi_{xy}(\tau) &= E_\theta[x(t)y(t+\tau)] \\
&= \frac{\Omega_p}{2} E_\theta[\sin(2\pi f_m \tau \cos\theta)] \\
&= \frac{\Omega_p}{2} \frac{1}{2\pi} \int_{-\pi}^{\pi} \sin(2\pi f_m \tau \cos\theta)d\theta \\
&= 0.
\end{aligned}
\tag{2.10}
$$

This means $x(t)$ and $y(t)$ are uncorrelated and independent Gaussian random pro-
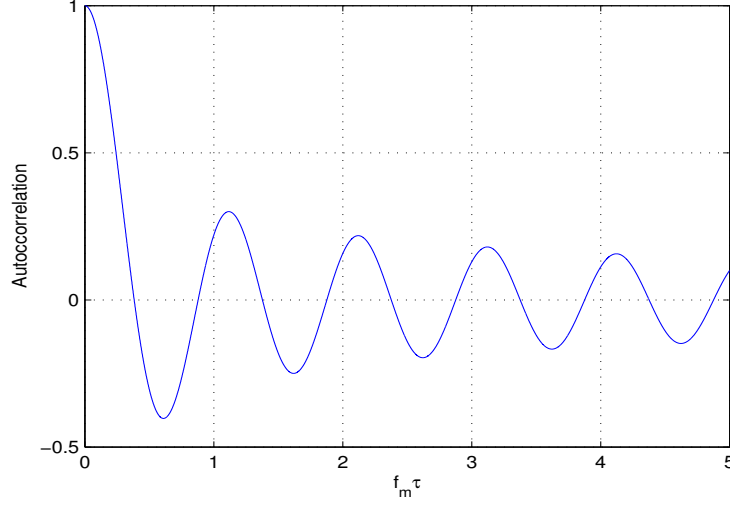
Fig. 6. Autocorrelation of the real and imaginary components of the Rayleigh fading process

cesses. The correlation ϕ_{xx} can be obtained as follows:

$$
\begin{aligned}
\phi_{xx}(\tau) &= E_\theta[x(t)x(t+\tau)] \\
&= \frac{\Omega_p}{2} E_\theta[\cos(2\pi f_m \tau \cos\theta)] \\
&= \frac{\Omega_p}{2} \frac{1}{2\pi} \int_{-\pi}^{\pi} \cos(2\pi f_m \tau \cos\theta)d\theta \\
&= \frac{\Omega_p}{2} \frac{1}{\pi} \int_{0}^{\pi} \cos(2\pi f_m \tau \cos\theta)d\theta \\
&= \frac{\Omega_p}{2} J_0(2\pi f_m \tau),
\end{aligned}
\tag{2.11}
$$

where $J_0(x)$ is the zero-order Bessel function of the first kind. The normalized auto-correlation function $\phi_{xx}\tau/(\Omega_p/2)$ is illustrated in Fig. 6.

The power spectral density (PSD) of $g(t)$ can be derived by the Fourier transform of $\phi_{gg}(\tau)$.

$$
S_{gg}(f) = F[\phi_{gg}(\tau)]
$$
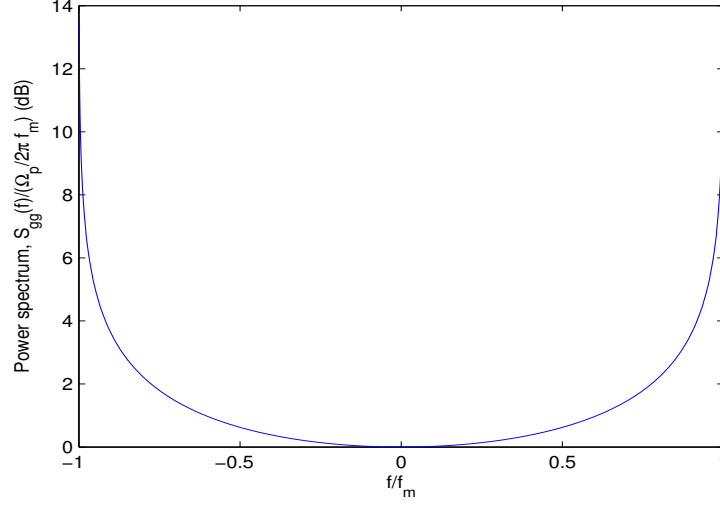
Fig. 7. PSD of the Rayleigh fading process

$$
\begin{aligned}
&= F[\phi_{xx}(\tau) + j\phi_{xy}(\tau)] \\
&= \frac{\Omega_p}{2\pi f_m} \frac{1}{\sqrt{1 - (\frac{f}{f_m})^2}}. \quad |f| \le f_m
\end{aligned}
\tag{2.12}
$$

The normalized PSD $S_{gg}(f)$ is plotted in Fig. 7. $S_{gg}(f)$ is limited to the frequency range of $|f| \le f_m$. The value of the spectral density is zero at the frequencies out of this range.

Two important second order statistics associated with Rayleigh fading are the level crossing rate L_R and the average fade duration $\bar{t}$. If R is the envelope threshold, define the normalized envelope threshold ρ as

$$
\rho = \frac{R}{\sqrt{\Omega_p}} = \frac{R}{R_{rms}}.
\tag{2.13}
$$

The level crossing rate and average fading duration for a Rayleigh fading channel are:

$$
L_R = \sqrt{2\pi} f_m \rho e^{-\rho^2},
\tag{2.14}
$$

$$\bar{t} = \frac{e^{\rho^2} - 1}{\rho f_m \sqrt{2\pi}}.$$ (2.15)

2. Frequency Selective Fading Channel

In the previous subsection, we have considered channel models that are appropriate for narrow band transmission, where the symbol duration is much larger than the delay spread of the channel. Under this condition, all frequency components of the transmitted signal will experience the same envelope attenuation and phase shift. However, this condition is not satisfied for the case of wideband signal transmission, where the symbol duration is small compared to the time spread of the propagation path delays. For a wideband signal, different frequency components will experience different phase shifts and thus will introduce amplitude and phase distortion into the transmitted signal. Such a channel is called a frequency selective fading channel.

In macro-cellular mobile radio, delay spreads are mostly in the range from about 100 nanoseconds to 10 microseconds. In indoor and micro-cellular channels, the delay spread is usually smaller. Most of the delay spreads for indoor environments are less than a few hundred nanoseconds. Denote T_d as the value of delay spread, for a wideband signal with symbol duration T_c the number of resolvable paths is

$$L = \lfloor T_d/T_c \rfloor + 1.$$ (2.16)

Frequency selective fading channels can be modeled by a τ spaced tapped delay line with L taps, as illustrated in Fig. 8.

$$g(t, \tau) = \sum_{i=1}^{L} g_i(t)\delta(\tau - \tau_i).$$ (2.17)

The complex envelope of the received signal is

$$r(t) = \sum_{i=1}^{L} g_i(t)s(t - \tau_i).$$ (2.18)
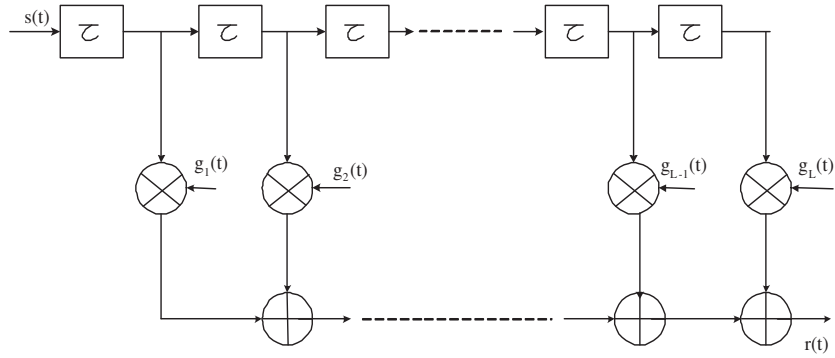
Fig. 8. Discrete-time tapped delay line model for a wideband multipath fading channel

If we assume a wide sense stationery uncorrelated scattering (WSSUS) channel, each tap will experience uncorrelated flat fading. The autocorrelation at each tap is

$$\phi_{g_k g_k}(\tau) = \frac{\Omega_k}{2} J_0(2\pi f_m \tau), \tag{2.19}$$

where Ω_k is the envelope power for the kth tap and f_m is the maximum Doppler shift. The total envelope power is

$$\Omega_p = \sum_{k=1}^{L} \Omega_k. \tag{2.20}$$

At the receiver, the transmitted signal arriving at various time slots will cause intersymbol interference (ISI). Certain signal processing techniques will have to be employed to reduce the ISI. On the other hand, diversity can be achieved by resolving multipath components at different time delays and combining them efficiently. By exploiting the frequency diversity inherent in the channel, system performance in terms of error rate can be improved considerably. Although ISI will be introduced by a frequency selective fading channel, it provides opportunities to decrease the bit error rate while there is no such opportunity to gain frequency diversity in a flat fading channel.
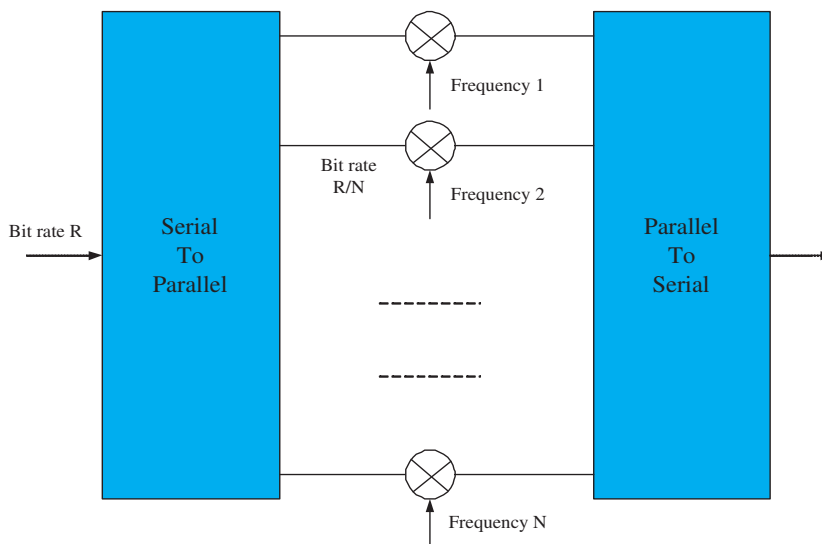
Fig. 9. OFDM multiplexing system

B.   Orthogonal Frequency Division Multiplexing (OFDM) System

Orthogonal frequency division multipexing (OFDM) is a modulation technique that
has been suggested for use in cellular radio, digital audio broadcasting, and wireless
LAN systems such as IEEE 802.11 [26] [27]. The OFDM technique distributes the
data over a large number of sub-carriers that are spaced in frequency. By spacing the
frequencies right, orthogonality is ensured so that data on different subcarriers does
not interfere with one another. The structure of an OFDM multiplexing system is
plotted in Fig. 9.

One of the key advantages of OFDM is that the modulation and demodulation
can be achieved by using the discrete Fourier transform, which can be efficiently
implemented by using the fast Fourier transform algorithm. Another key advantage
of OFDM is the easiness of eliminating Intersymol Interference (ISI) by adding a guard
interval to the data sequence. These attractive features make OFDM a very popular
modulation technique for high speed data transmission. Primary drawbacks of the

OFDM technique are the large peak to average power ratio (PAPR) it tends to create and tight synchronization required to ensure the orthogonality of the subcarriers.

As seen in Fig. 9, a block of N serial data symbols, each with duration T_s, is converted into a block of N parallel data symbols, each with duration $T = NT_s$. The N sub-carriers are spaced $1/T$ apart so that the transmitted data on different sub-carriers will not interfere. Assuming a rectangular pulse $u_T(t)$ is used for the amplitude shaping function, the complex envelope of an OFDM signal is

$$\tilde{s}(t) = A \sum_{k=0}^{N-1} x_k \exp\{\frac{j2\pi kt}{NT_s}\} u_T(t). \tag{2.21}$$

Sample the complex envelope at $t = nT_s$, then the sample sequence is

$$X_n = A \sum_{k=0}^{N-1} x_k \exp\{\frac{j2\pi kn}{N}\}, \ n = 0, 1, \ldots, \ldots, N-1. \tag{2.22}$$

This is equivalent to taking the IDFT (Inverse Discrete Fourier Transform) of the sequence $x_k, k = 0, 1, \ldots, N-1$, and multiplying with a constant value A.

Likewise, at the receiver side, the demodulated sequence can be acquired by performing a DFT (Discrete Fourier Transform) on the received vector $R_n, n = 0, 1, \ldots, N-1$. The demodulated sequence is

$$Z_i = \frac{1}{N} \sum_{n=0}^{N-1} R_n e^{-j\frac{2\pi ni}{N}}, \ i = 0, 1, \ldots, N-1. \tag{2.23}$$

Hence, by taking the IDFT and DFT of the transmitted sample sequence and the received sequence, OFDM can by implemented with one carrier modulation and demodulation. Further improvement can be achieved by using an IFFT and FFT algorithm to increase the efficiency and speed. This property greatly simplifies the OFDM system implementation and it is one of the main reasons that OFDM has received so much attention recently.

To mitigate the effects of ISI, a guard interval with a cyclic suffix of length G
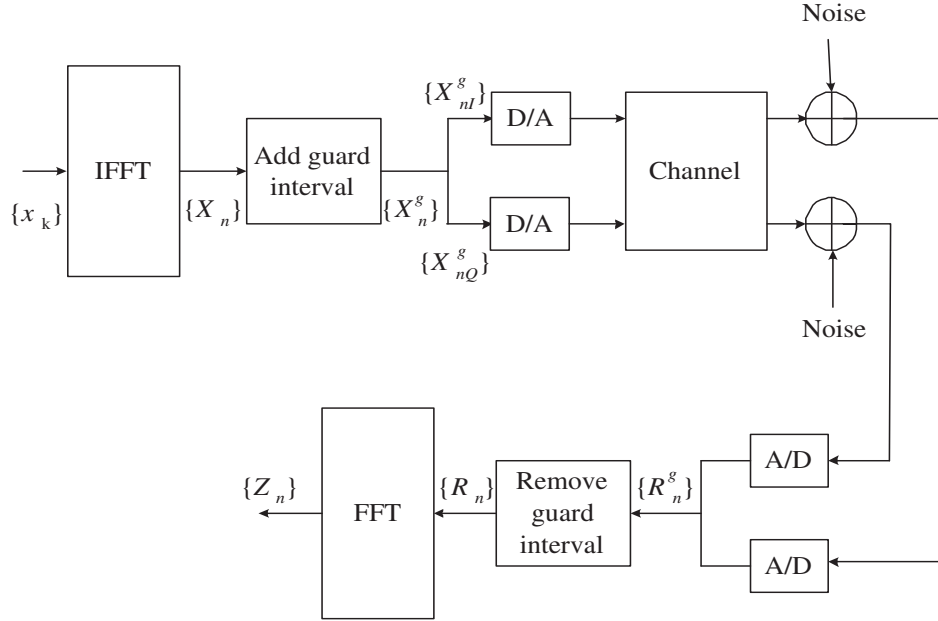
Fig. 10. Block diagram of OFDM transmitter and receiver

can be attached to the transmitted sequence X. The block diagram of an OFDM transmitter and receiver is shown in Fig. 10.

With a guard interval, the transmitted sequence becomes

$$X_n^g = A \sum_{k=0}^{N-1} x_k \exp\{\frac{j2\pi kn}{N}\}, \ n = 0, 1, \ldots, N + G - 1. \tag{2.24}$$

Suppose the channel impulse response is $\{g_m\}, m = 0, 1, \ldots, L$, ignoring the noise, the received sequence R_n^g is

$$R_n^g = \sum_{m=0}^{L} g_m X_{n-m}^g. \tag{2.25}$$

The first L received samples are corrupted by the ISI from the channel. If $G \geq L$, we can eleminate the ISI by removing the first G samples and replacing them with the last G samples. This way, the newly sequenced sample R_n are free of ISI. Denote

$(n)_N$ as the residue of n modulo N

$$
\begin{aligned}
R_n &= R_{G+(n-G)_N}^g \\
&= \sum_{m=0}^{L} g_m X_{(n-m)_N}, \ 0 \le n \le N-1
\end{aligned}
\tag{2.26}
$$

The OFDM demodulator performs a DFT on R_n

$$
\begin{aligned}
Z_i &= \frac{1}{N} \sum_{n=0}^{N-1} R_n e^{-j\frac{2\pi ni}{N}} \\
&= \lambda_i A x_i, \ 0 \le i \le N-1,
\end{aligned}
\tag{2.27}
$$

where

$$
\lambda_i = \sum_{m=0}^{L} g_m e^{-j\frac{2\pi mi}{N}}.
\tag{2.28}
$$

As shown in the above equation, after removing the cyclic prefix, the perfectly periodic signal can be transformed to the transmitted symbols by performing a DFT. The ISI caused by the channel has been completely removed. However, the addition of a guard interval will increase the bandwidth or reduce the data rate.

Another advantage of OFDM is that combined with appropriate coding, the frequency diversity inherent in the wideband channel can be exploited to improve the system performance greatly. A rule of thumb is that when the minimum free distance between the codewords is three times larger than the number of independent multipaths L provided by the channel, a diversity order of L can be achieved, which means the bit error rate will diminish with SNR L times faster than with a flat fading channel. This free frequency diversity gain makes a coded OFDM system highly desirable, especially in a fading environment. A considerable amount of recent research has focused on optimum coding and interleaving with OFDM systems.

One of the drawbacks with OFDM in implementation is that the peak to average power ratio (PAPR) is large, which makes the design of transmitter amplifier difficult

and not power efficient. Consider the case when all the subcarriers are at their maximum point, the PAPR can be as large as N times the power of each subcarrier. The large amplitude variation also increases the in-band noise and increases the BER when the signal has to go through amplifier non-linearities. Thus additional signal processing such as clipping and filtering is often needed to mitigate the large PAPR associated with OFDM systems.

The other problem with OFDM is that synchronization has to be kept tight otherwise the subchannel orthogonality will be impaired. If the subchannels are not orthogonal anymore, inter channel interference (ICI) will be introduced and cause an increase in the bit error rate. There will be a constant part added to $\lambda_i A x_i$ in (2.27) representing the interference. Loss of subchannel orthogonality will also arise in a fast fading channel. When there are variations in the channel gain over the duration of an OFDM block, the condition to guarantee the subchannel orthogonality is not satisfied anymore. Because of inter channel interference, an error floor will show up with the increase of signal noise ratio. Thus, one needs to be careful about choosing the number of subcarriers and block size when designing an OFDM system.

OFDM has been proposed and used for a lot of applications lately. Some parameters of the OFDM application used in the wireless LAN standard IEEE 802.11a are given below:

Data rates: 6Mbps to 48Mbps

Modulation: BPSK, QPSK, 16QAM and 64QAM

FFT size: 64, 52 subcarriers in use, 48 for data, 4 for pilots.

Subcarrier spacing: 0.3125 MHz

Guard duration: 0.8μsec

Symbol duration: 4μsec

C.   Alamouti MIMO System

To counter the fading effects on the wireless systems, which is typically a pitfall, various type of diversities are sought to improve the system performance in a fading environment. Frequency diversity is utilizing the independent fading in different frequency sub-bands of a wideband channel. Time diversity transmits the signal in different time slots where uncorrelated fading can be experienced. Space diversity is obtained by using multiple antennas, each placed at certain spacing so that the fading at each antenna is independent. To achieve frequency diversity, extra bandwidth is required. To gain time diversity, either data rate will be reduced or the bandwidth will increase. Also time delay will be introduced to transmit the same information at multiple time periods that are separated by the coherence time of the channel. In contrast, space diversity does not demand extra bandwidth or reduce the data rate, which is a very attractive feature. When the available radio spectrum is limited, extra bandwidth can not be afforded.

Multiple Input Multiple Output (MIMO) has recently emerged as one of the most significant techniques in wireless communication [28]. The diagram of a MIMO system is shown in Fig. 11. There are M and N antennas equipped at the transmitter and receiver respectively.

Define H as the $N \times M$ complex matrix of the channel. The ij-th component of H is denoted as h_{ij}, which represents the channel fading coefficient from the jth transmit antenna to the ith receive antenna. Assume there is no channel state information (CSI) at the transmitter, the MIMO system capacity is given by [29]

$$C = \log_2[\det(I_N + \frac{\rho}{M}HH^*)] \; bit/sec/Hz, \qquad (2.29)$$

where ρ is the SNR at any receive antenna.
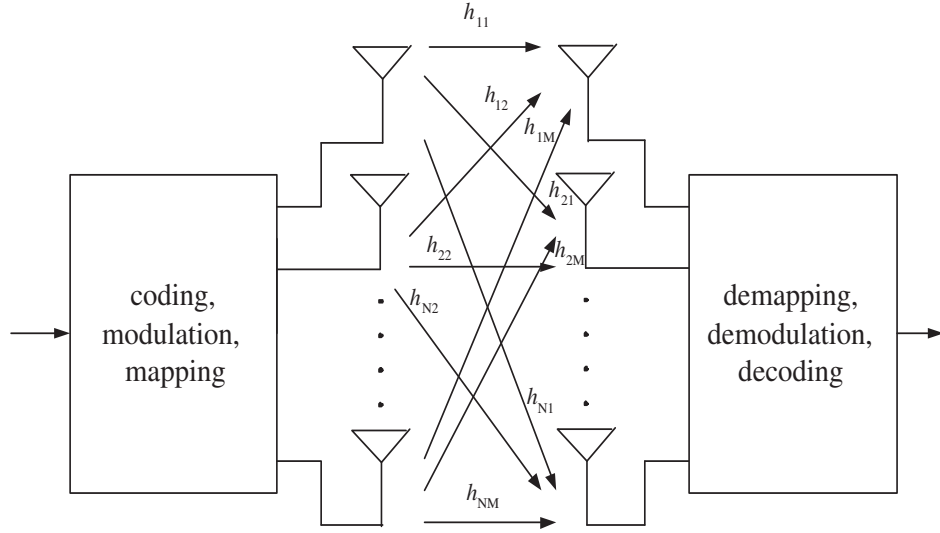
Fig. 11. Block diagram of a MIMO system

If the channel is known at the transmitter, a waterfilling mechanism can be used to optimize the system capacity [29]. In this situation, the capacity is

$$C_{WF} = \sum_{i=1}^{m} \log_2(\mu\lambda_i)^+ \ bit/sec/Hz, \qquad (2.30)$$

where a^+ denotes $\max(a, 0)$, $m = \min(M, N)$, λ_i are the nonzero eigenvalues of the matrix HH^* if $N \leq M$, while if $M < N$, λ_i are the nonzero eigenvalues of the matrix H^*H and μ is chosen to satisfy

$$\rho = \sum_{i=1}^{n} (\mu - \lambda_i^{-1})^+ \ bit/sec/Hz. \qquad (2.31)$$

In actual transmission systems, space-time coding is employed to approach the capacity of MIMO wireless channels. Space time coding is a coding technique designed to encode the multiple transmit antennas jointly. Space-time coding is performed in both the time domain and the spatial domain to introduce correlations between signals transmitted from various antennas at various times. By introducing the spatial-
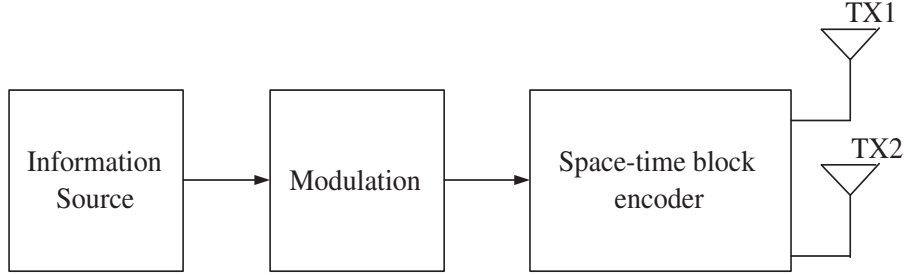
Fig. 12. Block diagram of the Alamouti space-time encoder

temporal correlation, transmit diversity can be achieved to minimize the errors at the receiver in a multipath fading channel. There are different type of space time coding structures available, including space-time block codes (STBC), space-time trellis codes (STTC), space-time turbo trellis codes and layered space-time codes. Below the basic concepts of the Alamouti space-time block coding scheme will be presented. Because of the simple structure and linear processing of the Alamouti scheme [30], it is a very attractive scheme in practice and is currently part of both the WCDMA and CDMA2000 standards.

The Alamouti code is designed to achieve transmitter diversity with two antennas at the transmitter. This scheme achieves a full diversity gain with a simple maximum-likelihood decoding algorithm. The block diagram of Alamouti space-time encoder is show in Fig. 12.

The modulated symbols are grouped into blocks of two modulated symbols each and space-time coding is performed for each block. Asssume the two modulated symbols in a block are $\{c_1, c_2\}$, the matrix that maps them to the transmit antenna is given by

$$\mathbf{C} = \begin{bmatrix} c_1 & -c_2^* \\ c_2 & c_1^* \end{bmatrix}. \tag{2.32}$$

The encoder outputs are transmitted from two antennas in two consecutive transmis-

sion periods. At the first transmission period, $[c_1\ c_2]$ are transmitted from antenna one and antenna two respectively. During the second transmission period, $[-c_2^*\ c_1^*]$ are transmitted from antenna one and antenna two.

Assume the fading coefficients are constant during two symbol periods, which are denoted as h_1 and h_2 for antenna one and antenna two respectively. Denote the received signal at the receiver antenna over two consecutive time periods as r_1 and r_2, which can be expressed as

$$r_1 \ = \ h_1c_1 + h_2c_2 + n_1, \tag{2.33}$$

$$r_2 \ = \ -h_1c_2^* + h_2c_1^* + n_2, \tag{2.34}$$

where n_1 and n_2 represents Gaussian noise sample at the two time intervals.

Suppose that the channel state information h_1 and h_2 are perfectly know at the receiver, by combining the received signal and the channel state information, two decision statistics can be constructed as

$$\tilde{c}_1 \ = \ h_1^*r_1 + h_2r_2^*, \tag{2.35}$$

$$\tilde{c}_2 \ = \ h_2^*r_1 - h_1r_2^*. \tag{2.36}$$

Substituting r_1 and r_2 from (2.33), (2.34) into the above equations,

$$\tilde{c}_1 \ = \ (|h_1|^2 + |h_2|^2)c_1 + h_1^*n_1 + h_2n_2^*, \tag{2.37}$$

$$\tilde{c}_2 \ = \ (|h_1|^2 + |h_2|^2)c_2 - h_1n_2^* + h_2^*n_1. \tag{2.38}$$

The maximum likelihood decision rule can be expressed as

$$\hat{c}_1 = \arg\min_{\hat{c}_1 \in S}(|h_1|^2 + |h_2|^2)|\hat{c}_1|^2 + d^2(\hat{c}_1, \tilde{c}_1), \tag{2.39}$$

$$\hat{c}_2 = \arg\min_{\hat{c}_2 \in S}(|h_1|^2 + |h_2|^2)|\hat{c}_2|^2 + d^2(\hat{c}_2, \tilde{c}_2). \tag{2.40}$$

Thus with simple linear combining at the receiver, maximum likelihood decoding can be performed for the Alamouti code. A diversity order of two can be achieved in this case.

The above discussions are for the Alamouti scheme with two transmit antennas and one receive antenna . It can be easily extended to the case of multiple receive antennas with similar linear combining. Assume there are a number, N, receive antennas, r_1^j, r_2^j are the received signals at two consecutive time t and $t + T$ at the jth receive antenna. T is the symbol duration.

$$
\begin{aligned}
r_1^j &= h_{j,1}c_1 + h_{j,2}c_2 + n_1^j, & (2.41) \\
r_2^j &= -h_{j,1}c_2^* + h_{j,2}c_1^* + n_2^j, & (2.42)
\end{aligned}
$$

where $h_{j,i}$ represents the fading coefficient for the path from the ith transmit antenna to the jth receive antenna, $i = 1, 2$, $1 \leq j \leq N$.

The two decision statistics $\tilde{c}_1$ and $\tilde{c}_2$ are given by

$$
\begin{aligned}
\tilde{c}_1 &= \sum_{j=1}^{N} h_{j,1}^* r_1^j + h_{j,2}(r_2^j)^*, & (2.43) \\
\tilde{c}_2 &= \sum_{j=1}^{N} h_{j,2}^* r_1^j - h_{j,1}(r_2^j)^*. & (2.44)
\end{aligned}
$$

Substituting r_1 and r_2 from (2.41), (2.42) into the above equations,

$$
\begin{aligned}
\tilde{c}_1 &= \sum_{i=1}^{2}\sum_{j=1}^{N} |h_{j,i}|^2 c_1 + \sum_{j=1}^{N}\left(h_{j,1}^* n_1^j + h_{j,2}(n_2^j)^* \right), & (2.45) \\
\tilde{c}_2 &= \sum_{i=1}^{2}\sum_{j=1}^{N} |h_{j,i}|^2 c_2 + \sum_{j=1}^{N}\left(h_{j,2}^* n_1^j - h_{j,1}(n_2^j)^* \right). & (2.46)
\end{aligned}
$$

The maximum likelihood decision rule can be expressed as

$$
\hat{c}_1 = \arg\min_{\hat{c}_1 \in S} \left[\left(\sum_{j=1}^{N}(|h_{j1}|^2 + |h_{j2}|^2) - 1 \right)|\hat{c}_1|^2 + d^2(\hat{c}_1, \tilde{c}_1) \right], \quad (2.47)
$$

$$\hat{c}_2 \;=\; \arg\min_{\hat{c}_2 \in S} \Big[\Big(\sum_{j=1}^{N}(|h_{j1}|^2 + |h_{j2}|^2) - 1\Big)|\hat{c}_2|^2 + d^2(\hat{c}_2, \tilde{c}_2)\Big]. \qquad (2.48)$$

Therefore, the Alamouti scheme can be easily applied to the environment of multiple receive antennas. Linear combining will be employed at the receiver and then maximum likelihood decoding can be performed. A diversity order of $2 \times N$ will be achieved. Following the Alamouti scheme, space time block codes with more than two transmit antennas have been studied and constructed to provide maximum diversity order [31]. However, the Alamouti scheme is the only space time block code with a complex transmission matrix to achieve the full transmission rate.

CHAPTER III

DESIGN OF PHYSICAL LAYER MODELS

Network performance relies on the characteristics of physical layer activities. Network simulator2 (ns2) is a popular network simulation software tool for evaluating network protocols under various network conditions. Ns2 has been widely accepted by the network communities and has proven itself as a valuable tool for network researchers. The basic structure of ns2 is introduced in the following. In order to investigate various physical channel models in wireless network simulation, some modifications to ns2 have been addressed, because of the fact that the models are not provided in the current software. In wireless network simulations, various physical layer models are employed according to the various circumstances. It is important that the appropriate physical layer models are adopted to obtain a proper view of the upper layer protocols. In this chapter, some popular physical layer models: the two-state Markov model and the finite-state Markov model are introduced. It is discovered that the two-state Markov model can not provide accurate network results especially for low to medium signal-to-noise ratios. The transition probabilities of the finite state Markov model are difficult to set and the complexity makes it impracticable for slow fadings. To solve this problem, the statistics of the physical layer frame error process are investigated. The physical layer good and bad frame run length distributions of the physical layer models are identified to be key factors for the purpose of providing accurate network throughput. A run length model is proposed and shown to have accurate network results. Inspired by the run length model, a simple four-state Markov model is presented. The structure of the four-state Markov model is detailed in this chapter.

A.   Network Simulator Ns2

Network simulator2 originated from the Realistic and Large (REAL) network simulator in 1989 [32]. Developed through the Virtual Inter Network Testbed (VINT) project funded by the Defense Advanced Research Projects Agency (DARPA) in 1995, ns was a collaborative effort at Lawrence Berkeley National Laboratories (LBNL), Xerox Palo Alto Research Center(PARC), University of California Berkeley(UCB) and the University of Southern California/Information Sciences Institute (USC/ISI). The simulator was updated to ns2 and released to the public. Currently the development of the simulator is supported by DARPA and National Science Foundation (NSF) with the projects Simulation Augmented by Measurement and Analysis of Networks (SAMAN) and Collaborative Simulation for Education and Research (CONSER), respectively. Carnegie Mellon University (CMU), Sun Microsystems and AT&T Center for Internet Research at ICSI (ACIRI) also contributed to the development of ns2. Ns2 provides support for simulation of TCP, routing, and multicast protocols over wired and wireless networks [33]. With its increasing popularity, ns2 has become a standard experiment environment for network researchers to evaluate protocols and validate the design of new approaches.

1.   Ns2 Overview

Ns2 is an object-oriented, discrete event driven network simulator. It covers multiple layers including the application layer, transport layer, network layer and the link layer and supports simulations at the packet level [33]. Network protocols such as TCP and UDP, traffic source behavior such as File Transfer Protocol (FTP), Telnet, Web, router queue management mechanisms such as Drop Tail, RED (Random Early Detection) and CBQ (Class-Based Queueing) and routing algorithms such as Dijkstra,
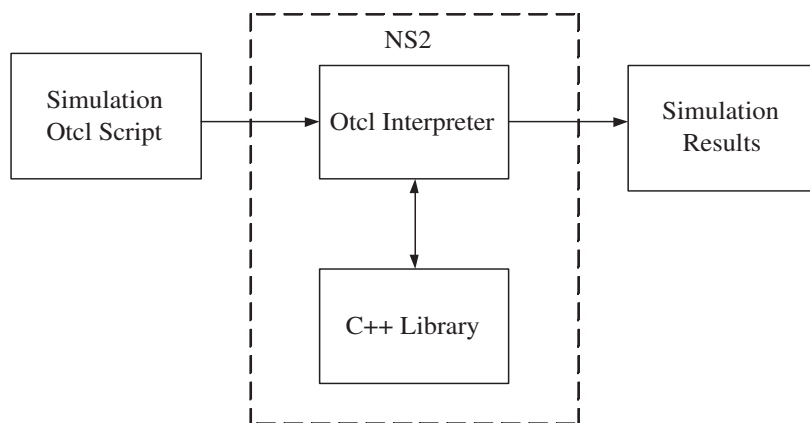
Fig. 13. Otcl and C++ in ns2 simulation

are implemented in ns2. Ns2 also implements multicasting and some of the MAC layer protocols for LAN simulations.

Ns2 is written in the C++ language and uses Object Tool Command Language (Otcl) as a front-end interpreter. Back-end C++ language implements the codes for defining protocols, agents, byte/bit level processing that are executed frequently. Otcl scripts performs the setup of the simulation scenarios, topologies and control of the simulation. The relationship between Otcl and C++ in a ns2 simulation is shown in Fig. 13. The dual language approach enables a high run-time speed and easiness to adapt the simulation parameters or configuration. The C++ language is fast to run but it is not convenient to change, compile and debugging especially for people who are not familiar with the structure of the program code. On the other hand, Otcl runs slower but it has a user friendly feature. Otcl script is simple for modifications and programming. Combining these two languages together, ns2 provides the user an easy to use and reconfigurable interface with fast running time.

Ns2 is discrete event driven which means that the simulator has list of events ordered by simulation time and each event happens at an instant of virtual time. An

Fig. 14. Two node link in ns2 simulation

event in ns2 is a packet ID that is unique for every packet with scheduled time and the pointer to an network object that handles the packet.

Ns2 network topology usually includes four major types of components: Application, Agent, nodes and link. Application represents the communication instigator. Agent refers to the packet generator or consumer. Application is attached to transport agents, which are responsible for handling transport data from an application to another agent. Node is the addressable entity. Link stands for the set of queues and contains information about how nodes are connected with regard to the data rate, delay and queue type. There are various integrated protocol modules from the physical layer to the application layer offered by ns2 to choose from, which means various types of applications, agents and links can be specified in ns2. To build a simple ns2 network scenario, first one would create two nodes and then create a source/sink agent to attach to each node. Connect the two agents, and then create the application such as FTP to attach to one of the nodes. For post simulation analysis, trace files are provided with information about the packets.

A simple example of two nodes connected over a link is shown in Fig. 14. Node 0 is connected with TCP/Reno agent and Node 1 is connected with null agent to receive data. An FTP application is attached to the TCP/Reno agent at node 0. The Otcl scripts of trying to send data between these two nodes are followed.

```
set ns_ [new Simulator]

set tracefd [open tracefile.tr w]
$ns_ trace-all $tracefd
set node0 [$ns_ node]
```

```
set node1 [$ns_ node]


set tcp_reno [new Agent/TCP/Reno]
$ns_ attach-agent $node0 $tcp_reno
set sink_reno [new Agent/TCPSink]
$ns_ attach-agent $node1 $sink_reno

$tcp_reno set packetSize_ 512
$tcp_reno set window_ 100
$sink_reno set packetSize_ 40

$ns duplex-link $node0 $node1 10Mb 1ms Droptail

set ftp0 [new Application/FTP]
$ftp0 attach-agent $tcp_reno
$ns_ connect $tcp_reno $sink_reno
$ns_ at 1.0 "$ftp0 start"
$ns_ at  100 "$ftp0 stop"
proc stop {} {
    global ns_ tracefd

    $ns_ flush-trace

    close $tracefd

}

$ns_ run
```

2.   Ns2 Simulation Over Wireless Link

The Rice Monarch Project at Carnegie Melon University (CMU) has made substantial extensions to the ns2 network simulator [34]. It enables mobile nodes simulations under a wireless network environment. A radio propagation model is used in ns2 wireless simulations to decide whether a packet will be received correctly through the wireless channel. IEEE 802.11 Media Access Control Protocols, a carrier-sense multiple access (CSMA) MAC protocol and Address Resolution Protocol (ARP) are added to the Link Layer protocol stack. A series of Mobile Routing Protocols such as dynamic source routing (DSR), destination sequence distance vector (DSDV), tem-

porally ordered routing algorithm (TORA) and ad-hoc on demand distance vector (ADOV) are also added to the network layer to simulate multi-hop wireless networks. A CMU trace file is generated for analysis of the simulation.

To account for the packet loss in a wireless channel, radio propagation models are implemented in ns2. These models are used to predict the received signal power of each packet. When a packet is received, the signal power is compared to a receiving threshold. If the signal power exceeds the receiving threshold, the packet will be assumed correct. Otherwise, it will be marked as error and abandoned by the MAC layer. There are several radio propagation models provided by the ns2, including a free space model, a two-ray ground reflection model and a shadowing model.

It should be noted that the radio propagation models only represent the large scale path loss. Small scale multipath fading, such as Rayleigh fading and Ricean fading, is not incorporated in these models. Since in digital mobile communication systems multipath fading is traditionally a pitfall, it should not be ignored in wireless network simulations with mobile terminal movement. An add-on package is available to simulate Ricean and Rayleigh fading developed by the Antenna & Radio Communication Group at CMU [35]. In this package, a pre-computed data set is used for the calculation of the fading envelope [36]. The dataset will be stretched or squeezed according to the value of the maximum Doppler frequency. Since the data set only represents a limited period of time, it is used repeatedly if the simulation runs for a long period of time. Although the CMU Ricean fading package results in an accurate simulation of the wireless channel for each individual flow, it generates identical fading components for different flows, which is not the scenario in reality. While reusing the dataset affects the accuracy, the required time to generate the pre-computed dataset also causes a time delay for ns2 simulations.

Therefore, with ns2 providing a variety of protocol stacks for wireless network

simulations, the simulation of physical layer multipath fading environment is not accurate and there are issues that still need to be addressed.

3.   Ns2 Modifications

To investigate the influence of various physical layer models on wireless network simulations, the ns2 simulator is adapted for our purpose.

Ns2 implements the functions which are related to sending and receiving frames in a single MAC object. In order to embed a new physical layer function into ns2, the MAC is modified by adopting a customized function each time the physical layer receives a frame. This customized physical layer function will decide whether the received frame is correct or not. Information about the packet length, transmission time and node positions are passed to the physical layer function. The physical layer function invokes a specific module according to the physical layer environment.

The major modification to ns2 is to build appropriate physical layer modules for our research purpose. To compare the performance of various physical layer models, first it is essential to build a module which simulates the real physical layer activities as close as possible. It will set a benchmark for all kinds of physical layer models. Therefore, multipath fading, corresponding modulation and coding schemes are all included in the baseline physical layer module. The specific modulation and coding schemes are simulated as the 802.11a and 802.11b standard in the flat fading and frequency selective fading scenario.

To accurately portray the multipath fading, a time domain linear filter is employed. Complex white Gaussian noise is passed through a linear filter to produce a Rayleigh fading process with a prescribed power spectral density. It should be noted that the fading process has to be run in continuous time. The packets may arrive at various time periods and the associated fading process has to take account of the

time gap between the transmission of each packet. There are a few other options to generate the Rayleigh fading process in addition to the linear time filter such as the famous Jakes model [37] or frequency domain method [38]. The time domain linear filter approach is chosen to generate the random fading process for the following reasons. First very minimal memory is required, which speeds up the simulation process. Second, it is convenient to generate a random fading process for an unknown period of time. In the simulation, the size of random fading parameters is dependent on the time period of the transmitted packet. The time domain linear filter approach produces random data for each realization while the Jakes model produces the same data for the same time instant. This property is a huge benefit when there are multi-links in the wireless network so each link can be guaranteed to have their own random fading process.

A third order filter is used to generate the random fading process with the transfer function [39]

$$H(s) = \frac{\omega_o^3}{(s^2 + 2\xi\omega_o s + \omega_o^2)(s + \omega_o)}, \tag{3.1}$$

where $\omega_o = 2\pi f_d/1.2$ and $\xi = 0.175$. The transfer function (3.1) is mapped into a discrete time filter using a bilinear transformation. Let f_s be the desired sample rate of the discrete time signal, the discrete time filter is described by

$$H(z) = H(s)\Big|_{s=2f_s\left(\frac{1-z^{-1}}{1+z^{-1}}\right)}. \tag{3.2}$$

The discrete time transfer function can be written as a ratio of two polynomials

$$H(z) = \frac{b_0 + b_1 z^{-1} + b_2 z^{-2} + b_3 z^{-3}}{a_0 + a_1 z^{-1} + a_2 z^{-2} + a_3 z^{-3}} \tag{3.3}$$
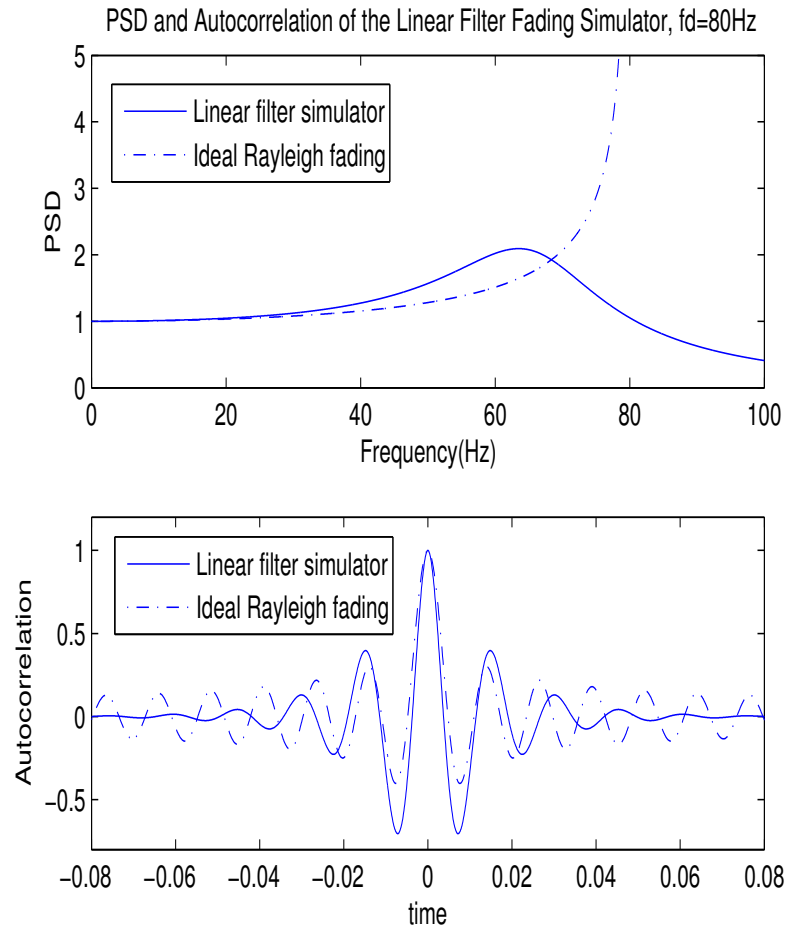
Fig. 15. Third order time domain linear filter fading simulator

which defines a difference equation

$$X[n] = -a_1 X[n-1] - a_2 X[n-2] - a_3 X[n-3] + b_0 N[n] + b_1 N[n-1] + b_2 N[n-2] + b_3 N[n-3].$$

(3.4)

The power spectral density and autocorrelation of a random fading process with the third order time domain linear filter are shown in Fig 15.

B.   Current Physical Layer Models

To approximate some key statistics of physical layer performance in a Rayleigh fading channel, a variety of channel models have been proposed and employed. Especially for research related to upper layer protocols and algorithms, block statistics of the physical layer are of primary concern and hence block-based channel models are commonly used to simplify and expedite simulations. Of all the current channel models, the two-state Markov model (2SMM) which is well known as the Gilbert-Elliott channel is most popular and has been widely used to characterize wireless fading channels due to the simplicity of its implementation. The Finite-state Markov model (FSMC) has been proposed by [17] to model a Rayleigh fading channel.

1.   Two-State Markov Model

The memoryless two-state Markov model shown in Fig. 16 enjoys prevalent popularity by researchers in network protocol design and evaluation, e.g. [40] [6] [41] [42] [41] [43] [44]. It is also well known at the Gilbert-Elliott channel [45]. The model is particularly popular in wireless applications where the physical channel is of the flat Rayleigh fading type. With its wide popularity, the validity of this model for wireless networks has been questioned in recent years [46] [47] [48]. But due to the simplicity of the two-state Markov model, it is still the most popular channel model in wireless networks.

The 2SMM provides the ability to emulate the burstiness caused by the underlying fading process. In the good state, all frames are transmitted successfully while in the bad state all frames will be in error. The transition probabilities [13] [49] and
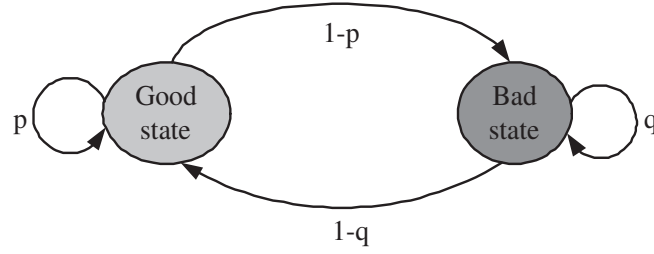
Fig. 16. Two-state Markov model

the steady state error rate are described as following:

$$\Pi_j = \begin{pmatrix} p & 1-p \\ 1-q & q \end{pmatrix}, \tag{3.5}$$

$$\varepsilon = \frac{1-p}{2-p-q}, \tag{3.6}$$

where p is the probability of successfully transmitting a frame given the previous frame was successfully transmitted and $1-q$ is the probability of successfully transmitting a frame given the previous frame was in error. The frame error rate is defined as ε and the average frame error length is equal to $1/(1-q)$. Values of both the frame error rate and average frame error length can be observed from simulations with the specific physical channel, coding, and modulation. With knowledge of ε and q, we can easily derive the remaining parameter p

$$p = 1 - \frac{(1-q)\varepsilon}{1-\varepsilon}. \tag{3.7}$$

Thus the 2SMM physical layer approximation is fully defined. The parameters of the 2SMM are dependent upon the frame size. Each state of the Markov Model indicates the channel state for the period of a frame duration.

As we can see, the two-state Markov Model is designed to match the statistics of frame error rate (FER) and average burst error length (ABEL) of the physical

layer. With regard to the accurateness of the Markov Models, Wang [13] argued from a mutual information perspective that with full knowledge of the current state, the knowledge of the previous state is insignificant to form the future realization. This argument became the foundation of using Markov models to approximate flat Rayleigh fading channels. In [50], it is suggested that a first order Markov model is adequate for representing the block error process for a slow fading channel.

The previous arguments of the adequateness of the two-state Markov model are mostly from the view of mutual information. Tan pointed out in [51] that a first order Markov model is typically unsuitable for applications requiring a large number of consecutive samples based on comparing the autocorrelation functions (ACF) and argued that comparing ACFs of consecutive samples is a more effective approach than the information theoretic metric [52]. To investigate the appropriateness of using the two state Markov model for wireless network simulation, wireless LAN 802.11a and 802.11b environments are simulated and the network throughput of the 2SMM and the representative 802.11a and 802.11b physical layer are compared. The network throughput of a two-node network with the TCP and UDP protocols are shown in Fig. 17 and Fig. 18. Note that we use the definition of SNR= E_b/N_o throughout all the physical layer simulations and ns2 simulations in this thesis.

As shown, the two-state Markov model substantially underestimated the network throughput especially for low to medium signal noise ratios. It does not picture the network performance accurately in terms of throughput. This result indicates that the commonly used two-state Markov model is not appropriate under some circumstances and may lead to improper conclusions of upper layer protocols. For researchers to validate or evaluate the upper layer protocols, an accurate physical layer model is imperative.
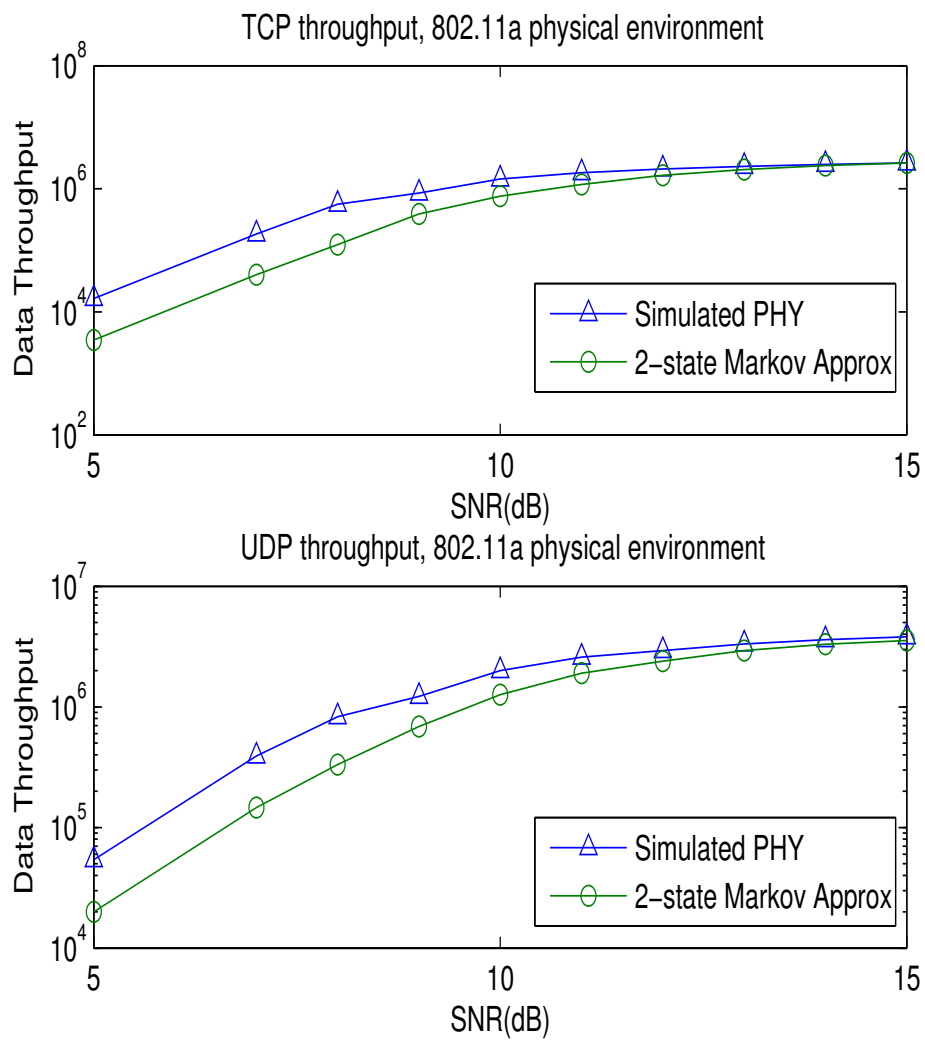
Fig. 17. TCP and UDP throughput with 2SMM, 802.11a environment
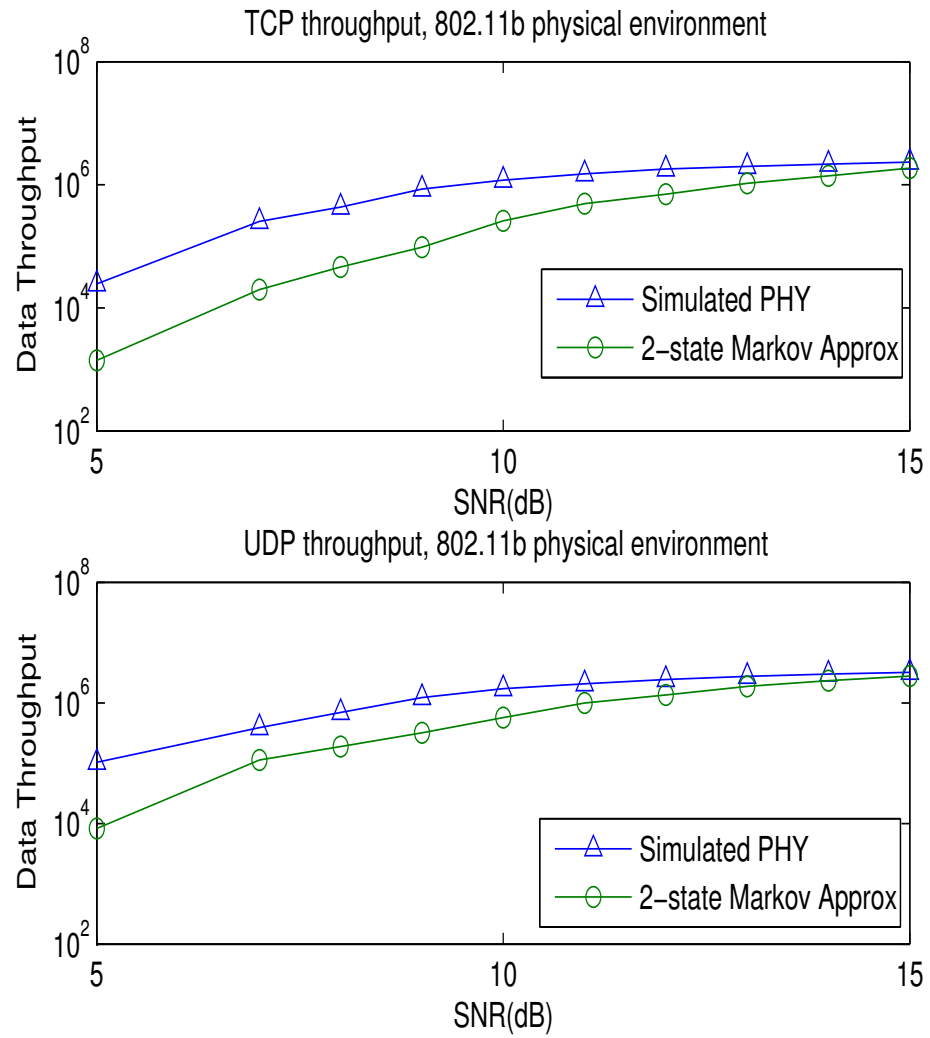
Fig. 18. TCP and UDP throughput with 2SMM, 802.11b environment
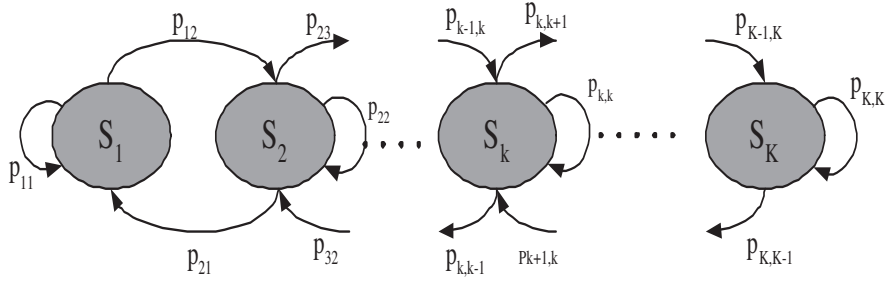
Fig. 19. Finite-state Markov model

2.   Finite-State Markov Model

Wang proposed a finite-state Markov model (FSMC) to a represent a Rayleigh fading channel by partitioning the received instantaneous signal-noise ratio into a finite number of intervals [17]. In [18], a methodology to partition the received signal-to-noise ratio into a finite number of states according to the time duration of each state is described.

The structure of the finite-state Markov model is shown in Fig. 19. P_{ij} is the transition probability from state s_i to state s_j [53]. A given state can only transfer to its two adjacent states. The states are divided by the received instantaneous signal to noise ratio. Each state is associated with a specific bit error rate which indicates the quality of the fading channel. The number of states is determined by the fading speed of the channel, which is implied by the normalized Doppler frequency shift.

The criterion of setting the SNR range for each state is to keep the average time duration of each state equal. The transition probabilities can be approximated based on the state thresholds and the level crossing rate at the state thresholds. Denote γ_0 as the average SNR, f_m as the Doppler frequency, $\vec{\Gamma} = [\Gamma_1, \Gamma_2, \cdots, \Gamma_{K+1}]^t$ as the state SNR threshold, where $\Gamma_1 = 0$ and $\Gamma_{K+1} = +\infty$. A received packet is in state s_k if the received instantaneous SNR is in the range $[\Gamma_k, \Gamma_{k+1})$. The average duration $\bar{\tau}_k$

of the received SNR interval $[\Gamma_k, \Gamma_{k+1})$ is given by [18]

$$\bar{\tau}_k = c_k T_p, \tag{3.8}$$

$$c_k = \frac{\exp(-\frac{\Gamma_k}{\gamma_0}) - \exp(-\frac{\Gamma_{k+1}}{\gamma_0})}{\sqrt{\frac{2\pi\Gamma_k}{\gamma_0}}\exp(-\frac{\Gamma_k}{\gamma_0}) + \sqrt{\frac{2\pi\Gamma_{k+1}}{\gamma_0}}\exp(-\frac{\Gamma_{k+1}}{\gamma_0})} \cdot \frac{1}{f_m T_p}, \quad k = 1, \cdots, K. \tag{3.9}$$

By constraining all the c_k to be equal to a constant c, there are K equations with K variables $\Gamma_2, \Gamma_3, \cdots, \Gamma_K$ and c. The value of state threshold Γ_k can then be solved. After setting the state threshold, the transition probability can be approximated by [17]

$$P_{k,k+1} \approx \frac{N(\Gamma_{k+1})T_p}{\pi_k}, k = 1, 2, \cdots, K-1. \tag{3.10}$$

$$P_{k,k-1} \approx \frac{N(\Gamma_k)T_p}{\pi_k}, k = 2, 3, \cdots, K. \tag{3.11}$$

Thus the finite-state Markov model has been set up. The number of states K needs chosen before finding the state threshold and transition probabilities. The value of c can be obtained by solving the K equations described in (3.9). It is important to have a suitable value of c set for the model. It is suggested that a choice of c between 3 and 8 should be reasonable [18]. The associated average probability of symbol error rate for state s_k is given by

$$P_{ek} = \frac{\int_{\Gamma_k}^{\Gamma_{k+1}} P_e(\gamma)p(\gamma)d\gamma}{\pi_k}, \tag{3.12}$$

$$p(\gamma) = \frac{1}{\gamma_0}\exp(-\frac{\gamma}{\gamma_0}), \ \gamma \geq 0 \tag{3.13}$$

$$\pi_k = \int_{\Gamma_k}^{\Gamma_{k+1}} p(\gamma)d\gamma = \exp(-\frac{\Gamma_k}{\gamma_0}) - \exp(-\frac{\Gamma_{k+1}}{\gamma_0}), \tag{3.14}$$

where P_{ek} is the average probability of symbol error for state s_k, $P_e(\gamma)$ is the probability of symbol error as a function of SNR γ, $p(\gamma)$ is the exponential distribution of the received instantaneous SNR γ with additive Gaussain noise, γ_0 is the average

SNR, π_k is the steady-state probability.

With an increasing of the number of states in the Markov model compared to the two-state Markov model, the accuracy of the finite-state Markov model is improved. However, a large amount complexity is added to the model set-up process as a tradeoff for better performance. For low Doppler frequencies or small packet lengths, the channel changes slowly and a larger number of states is required to keep the value of c within a reasonable range which results in a larger number of nonlinear equations to be solved. Moreover, it is uncertain how many states are needed until the array of equations are solved. One has to try it several times empirically before deciding the proper number of states. Also there is no analytical results indicating the appropriate value of the constant c. Furthermore, the error function $P_e(\gamma)$ versus SNR γ has to be acquired in order to resolve the average probability of symbol error P_{ek} for each state.

To validate the performance of the FSMC, TCP and UDP network simulations have been set up with $f_m T_p = 0.038$ and $\pi/4$-DQPSK modulation with coherent detection. The FSMC parameters are listed in [18], where $K = 11$ and $c = 3.0446$. The network throughput of a two-node network operating over a wireless channel is shown in Fig. 20.

In contrast to the two-state Markov model, the FSMC tends to overestimate network throughput for low to medium signal-to-noise ratios. The FSMC offers a relatively more accurate approximation for network throughput. However, the tradeoff is the substantially increased complexity of the model set-up process. The required number of states becomes large for lower Doppler frequencies or packet durations. For a different Doppler rate, the entire process of setting the parameters has to be redone. And there is no clear criterion about choosing the number of states and the appropriate value of the average time duration c. Due to this complexity, the FSMC
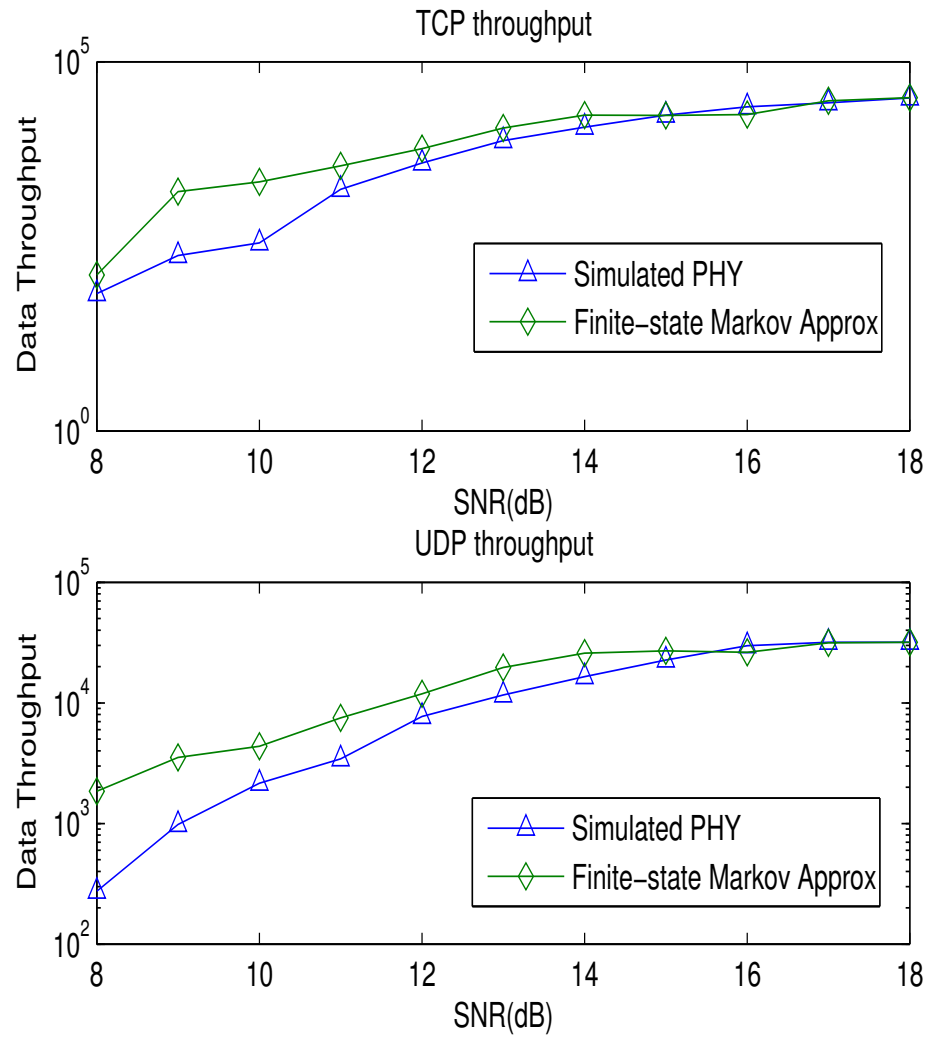
Fig. 20. TCP and UDP throughput with FSMC

has enjoyed very limited applications in practical experiments and simulations.

There are other partition approaches proposed for the FSMC model set-up available such as the equal probability method and the MMSE quantization method. For example, in [17], the equal probability method is used to partition the states by setting the SNR thresholds so that the steady probabilities of each state are equal to $1/K$. The MMSE quantization approach uses the quantization thresholds of the optimum Minimum Mean-Square Error (MMSE) Lloyd-Max quantizer for exponentially distributed SNR random variables. Compared to the equal average time duration method described above, the other two methods do not reflect the dynamics of the fading process since only the univariate fading signal random variable is considered. Zhang claimed that the other approaches cause deviations in the state transition probabilities [18] and the equal average time duration method described above gives the best representation of the fading channel. Although the finite-State Markov model has been used in the analysis of channel capacity and wireless network performance, e.g. in [54], [55], [56], [57], generally it is not chosen for the analysis of specific upper layer protocol stacks such as TCP and UDP because of the complexity issue.

C.   The Frame Error Process

To give an accurate representation of the underlying fading process of the physical layer, matching the first-order statistics is not sufficient anymore. It is demonstrated that the channel approximation provided by the 2SMM underestimates the network performance badly, especially when the SNR value is low to moderate. Apparently, the higher order characteristics of the frame error process are important to produce accurate network simulation results.

For the 2SMM, the probability density functions (PDF) of good and bad run

lengths are exponentially distributed and related to the value of p and q. However, as shown in Fig. 21 and Fig. 22, the distributions of good and bad frame run lengths for the wireless physical layer are more like a mixture of two exponential curves with a small slope matching the tail of the curve and a larger slope matching the initial part of the curve. In order to obtain frame error statistics of the physical channel, the 802.11a and 802.11b modulation scheme were simulated to send frames across a flat Rayleigh fading channel with a Doppler frequency of 100Hz. Greater than 430,000 good and bad frame run lengths were obtained through simulation, accounting for over 2 billion simulated bits for SNR values in the range 5-15dB. Parameters of the 2SMM were set by matching the FER and AFEL with the 802.11a and 802.11b wireless physical channel.

Good and bad run length distributions for FSMC with DPSK modulation across a flat Rayleigh fading channel are also simulated and compared in Fig. 23 and Fig. 24 at signal-to-noise ratios 8dB and 10dB. As we can see from the picture, the FSMC provides a good approximation of the physical layer bad run length distribution but it does not give an accurate approximation for the good run length distribution.

The higher order statistics of the physical layer frame error process have a great influence on the upper layer network performance. Fail to match the good and bad run length distributions can cause a deviation of the estimation of upper layer activities, which explains why the 2SMM is not providing accurate network results.

D.   Run Length Model

To further the understanding of how important it is to match the frame error process, we use a two-state run length model (2SRLM) to duplicate the good and bad frame run length distributions of the physical channel. The 2SRLM is illustrated in Fig. 25.
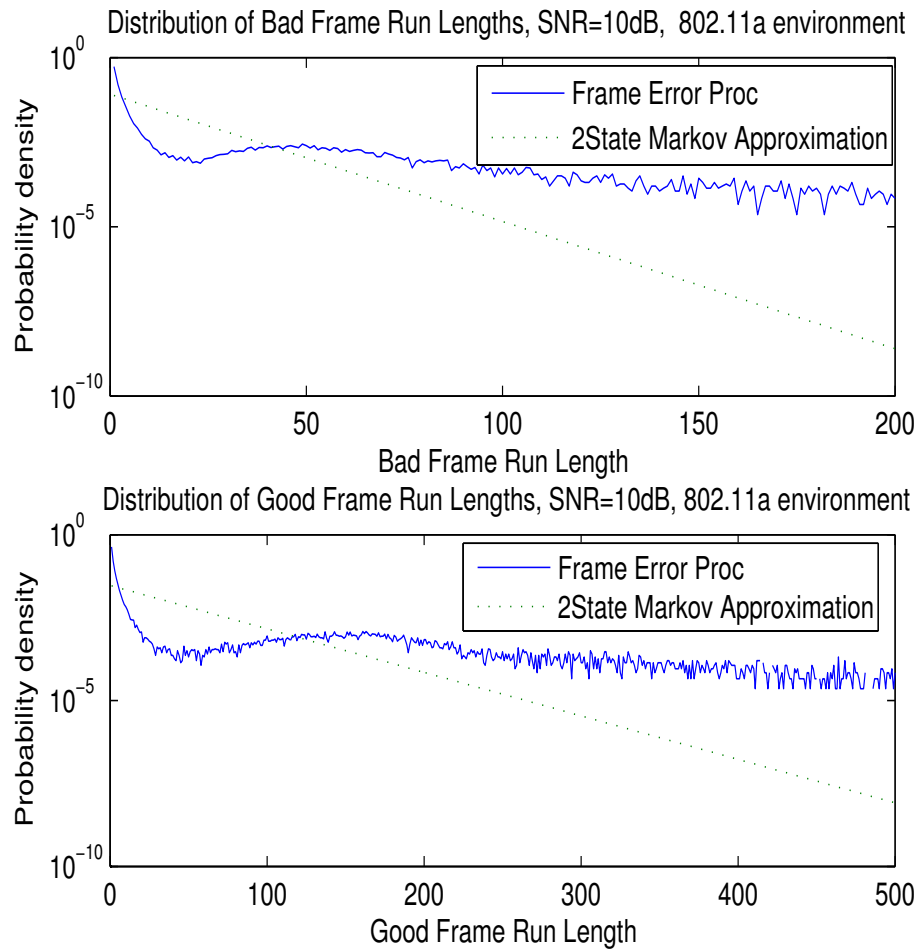
Fig. 21. Probability density function of the frame error process, 802.11a environment
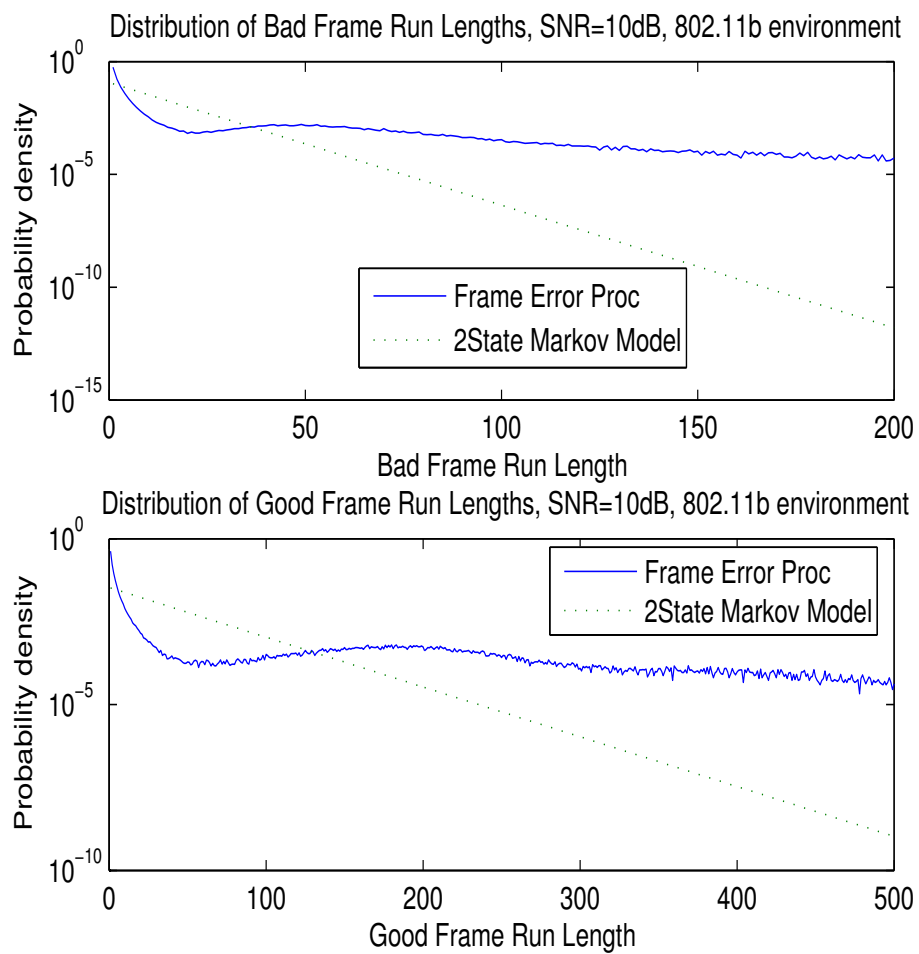
Fig. 22. Probability density function of the frame error process, 802.11b environment
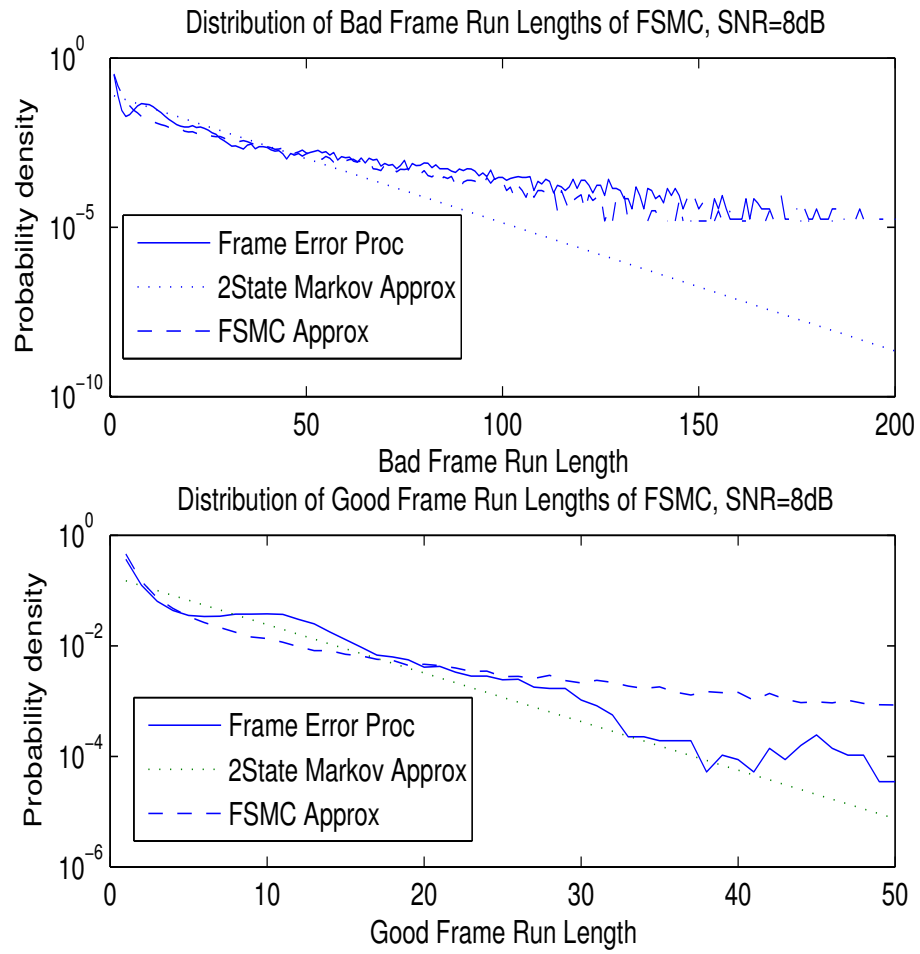
Fig. 23. Probability density function of the frame error process, FSMC, SNR=8dB
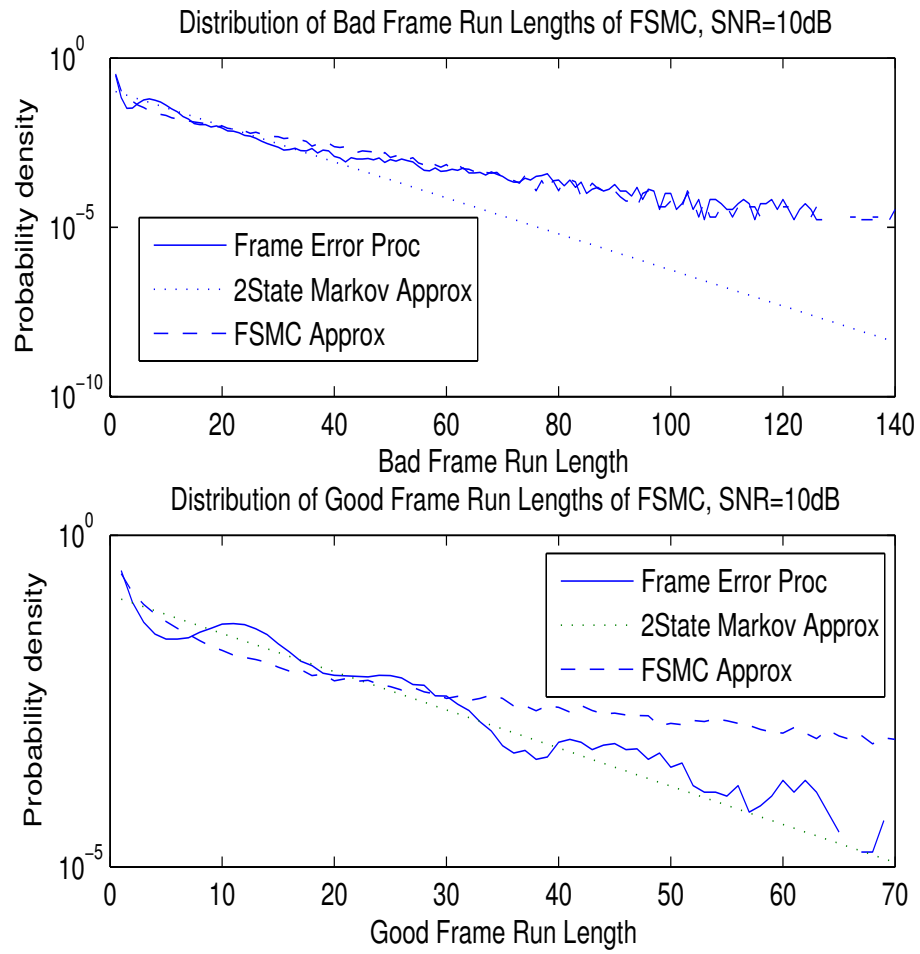
Fig. 24. Probability density function of the frame error process, FSMC, SNR=10dB
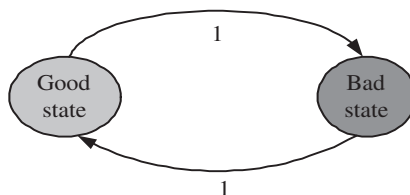
Fig. 25. Two-state run length model

In this model, the time duration staying in the good state, τ_g, and the time duration staying in the bad state, τ_b, are random variables whose distributions are set to exactly match the specific physical channel environment. From the good (bad) state, it transfers to the bad (good) state after a time duration of τ_g (τ_b). Unlike the 2SMM which is defined by the frame error rate and average frame error length, this two state run length model is described by the distributions of τ_g and τ_b. We made a PDF table from physical layer simulations to get the distributions of τ_g and τ_b. This table is lengthy and requires extensive simulation to obtain, but it's worthwhile to gain insight into how the network layer reacts if we use a model with accurate distributions of the good and bad frame run lengths.

With the two-state run length model, the network simulation performance is extremely close to what is obtained when the flat Rayleigh fading physical channel is employed in the ns2 simulation. The network results is shown in Fig. 26 and Fig. 27. This reveals the fact that using a physical layer model which generates accurate distributions of good and bad frame run lengths is sufficient to generate accurate network simulation results.

However, the two-state run length model is impractical in a network simulation because of the complexity of constructing the distribution table (and the difficulty in obtaining these tables). This complexity increases with the maximum good and bad frame run lengths. Also, because the distributions of τ_g and τ_b do not scale with
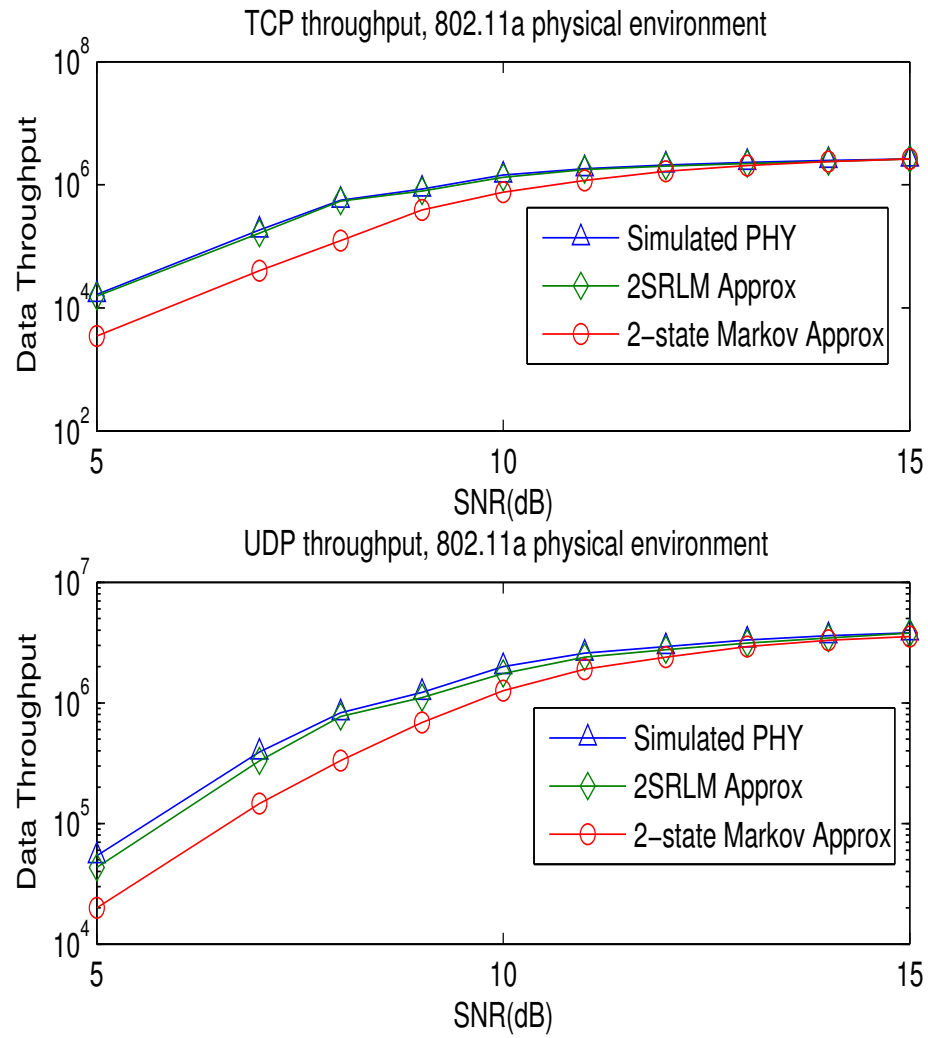
Fig. 26. TCP and UDP throughput with 2SRLM
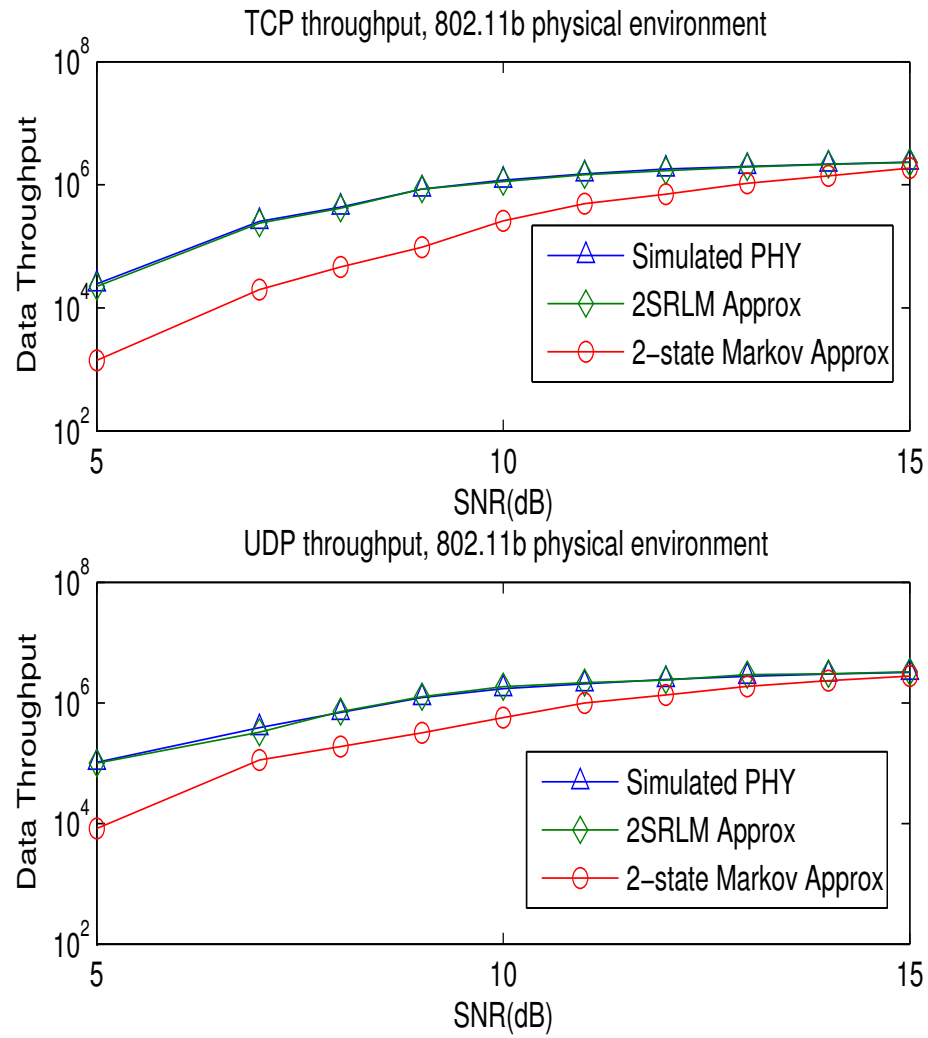
Fig. 27. TCP and UDP throughput with 2SRLM

different signal to noise ratios (SNR), one has to rerun the physical layer simulation for each different SNR value. The purpose in our using this model is that it helps to clarify the most important factors in the physical channel which affect network performance. The result is encouraging in that if we can build a model which reasonably matches the statistics of the good frame run lengths and bad frame run lengths, then the task of physical layer channel modeling is solved.

E.   Structure of the Four-State Markov Model

As shown in Fig. 21 and Fig. 22, from graphs of good and bad frame run length distributions, we notice that both ends of the frame run length distributions seem to follow an exponential behavior. Hence it is possible to approximate the run length distributions with a mixture of geometric distributions.

$$f(k) = p(1 - \alpha)\alpha^k + (1 - p)(1 - \beta)\beta^k, \tag{3.15}$$

where α is chosen to fit the slope of the initial part of the probability mass function (PMF), β is chosen to fit the slope of the tail part of the PMF, and p is the mixture parameter. One set of parameters $\{\alpha_g, \beta_g, p_g\}$ is used for the good frame run length distribution and another set $\{\alpha_b, \beta_b, p_b\}$ is used for the bad frame run length distribution. The resulting two-state RLM is illustrated in Fig. 28a.

Since the run length distributions are approximated using a mixture of geometric distributions, the resulting two-state RLM is equivalent to a four-state Markov Model
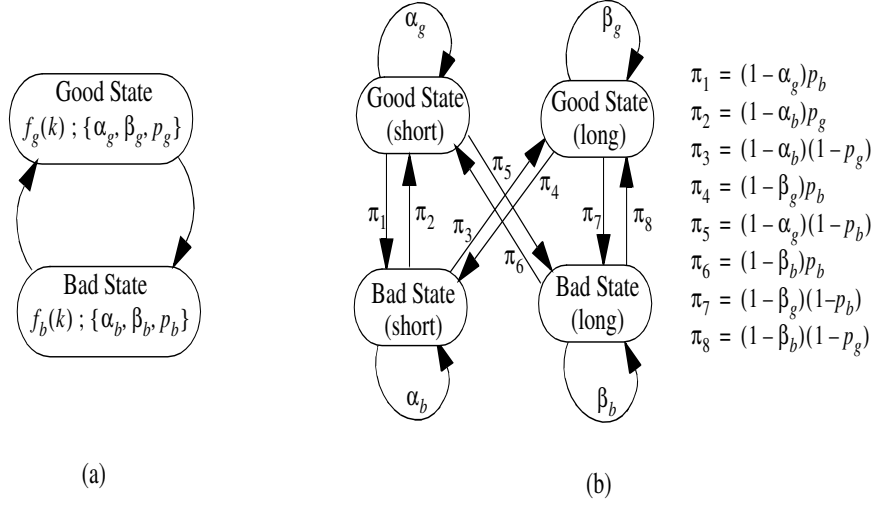
Fig. 28. Simplified models for the flat Rayleigh fading physical layer; (a) Two-state RLM (b) Equivalent four-state Markov model.

illustrated in Fig. 28b whose transition probability matrix is given by

$$
\Pi = \begin{array}{c}
 \\
GS \\
GL \\
BS \\
BL
\end{array}
\begin{array}{cccc}
GS & GL & BS & BL \\
\left(\begin{array}{cccc}
\alpha_g & 0 & (1-\alpha_g)p_b & (1-\alpha_g)(1-p_b) \\
0 & \beta_g & (1-\beta_g)p_b & (1-\beta_g)(1-p_b) \\
(1-\alpha_b)p_g & (1-\alpha_b)(1-p_g) & \alpha_b & 0 \\
(1-\beta_b)p_g & (1-\beta_b)(1-p_g) & 0 & \beta_b
\end{array}\right)
\end{array}, \quad (3.16)
$$

where GS = good state short, GL = good state long, etc.

Both the good state and the bad state have been split into two sub-states, one which tends to produce short runs and one which tends to produce long runs. In this model, any transition ending in one of the good states produces a correct frame while any transition ending in one of the bad states leads to a frame in error. The resulting physical layer model is very simple to implement.

In order to implement the 4SMM shown in Fig. 28b, we must have knowledge

of several model parameters, namely $\{\alpha, \beta, p\}$ for both the good and bad frame run length distributions. To obtain these via simulation would require substantial effort. Fortunately, these parameters can be linked to various physical channel characteristics. This set-up process will be described in the next chapter.

F. Summary

This chapter described the basic structure of the ns2 network simulator and the modifications we made to adapt ns2 to various physical layer modules. Current physical layer models, the two-state Markov model and the finite-state Markov model were investigated in detail. The two-state Markov model was shown not to be able to accurately approximate physical layer activities in terms of network performance. The limitation of using the Finite-state Markov model was discussed, which is mainly due to the complexity and uncertainty of setting up the model parameters. The network throughput of using both 2SMM and FSMC in 802.11a and 802.11b environment were both presented. Physical layer frame error statistics were studied and compared for the MM and FSMC. A run length model was set up to accurately present good and bad frame run length distributions of the physical layer. It was shown that by matching physical layer good and bad frame run length distributions, accurate network results can be gained. However, immense complexity for initial simulations to set up model parameters and requirement to re-run the simulations when one of the physcial layer conditions change make it impractical to use the run length model in practice. Inspired by the run length model, a new four-state Markov model was proposed by approximating the frame run length distributions with a mixture of geometric distributions. The diagram of the 4SMM was presented. The process of setting up the parameters of 4SMM for a flat Rayleigh fading channels will be

explored in the next chapter.

CHAPTER IV

FOUR-STATE MARKOV MODEL FOR RAYLEIGH FADING CHANNELS

In the previous chapter, the commonly used two-state Markov model has been demonstrated to badly underestimate network throughput especially when the signal-to-noise ratio is low to medium. There are other models proposed which provide better approximations but the complexity and inflexibility to establish the model parameters make them have limited application. The inaccuracy of the 2SMM can be explained by the deviance of the good and bad frame run length distributions. The 2SMM has exponential run length distributions while the real physical layer distributions are more like a mixture of two exponential slopes. The good and bad run length distributions are identified to be key factors in order to accurately present physical layer activities in a network environment. A four-state Markov model was proposed in the previous chapter. It is inspired by the two-state run length model and approximates the good and bad run length distributions with a mixture of exponential distributions. Two good and bad sub-states are introduced in the 4SMM with each one representing short and long runs respectively. The diagram was shown in the previous chapter. In this chapter, we will study the structure and property of the 4SMM. First frame error statistics of the 4SMM will be analyzed. The process of setting up model parameters for flat Rayleigh fading channels will be investigated thoroughly. An analytical approach is presented to estimate the model parameters with no initial simulations required. Moreover, the 4SMM parameter estimation with regard to varied Doppler frequency shift and frame size will be discussed. Network throughput in 802.11a and 802.11b flat Rayleigh fading environments will be presented and compared in this chapter.

A.   Frame Error Statistics

Run length distributions have been identified to be the key to accurately approximate physical layer activities. As shown in Fig. 29, both good and bad frame run length distributions can be approximated with a mixture of two exponential distributions. Compared with the 2SMM, the mixture of two exponential distributions exhibits considerable improvement in the run length distribution approximation. The run length distribution of the 4SMM can then be described as

$$f(k) = p(1 - \alpha)\alpha^{k-1} + (1 - p)(1 - \beta)\beta^{k-1} \ , \tag{4.1}$$

where α represents the exponential slope of the short run length distribution, β represents the exponential slope of the long run length distribution, p represents the weight factor of the two exponential distributions. $\{\alpha_g, \beta_g, p_g\}$ is denoted as the parameters of the good frame run length distribution, $\{\alpha_b, \beta_b, p_b\}$ is denoted as the parameters of the frame error run length distribution. The state diagram and transition probabilities for the 4SMM have been described in the previous chapter. Based on knowledge of two sets of parameters $\{\alpha_g, \beta_g, p_g\}$ and $\{\alpha_b, \beta_b, p_b\}$, the 4SMM can be easily set up and implemented in applications. Unlike the FSMC, for different physical layer conditions, the 4SMM only needs to adjust the value of $\{\alpha_g, \beta_g, p_g\}$ and $\{\alpha_b, \beta_b, p_b\}$. There is no additional efforts needed to alter the number of states and the value of state thresholds which is a necessary process for the FSMC. With only four states, by choosing the value of $\{\alpha_g, \beta_g, p_g\}$ and $\{\alpha_b, \beta_b, p_b\}$ appropriately, the four-state Markov model is quite simple to implement and is more easily adjusted with different physical layer conditions compared to the finite-state Markov model.
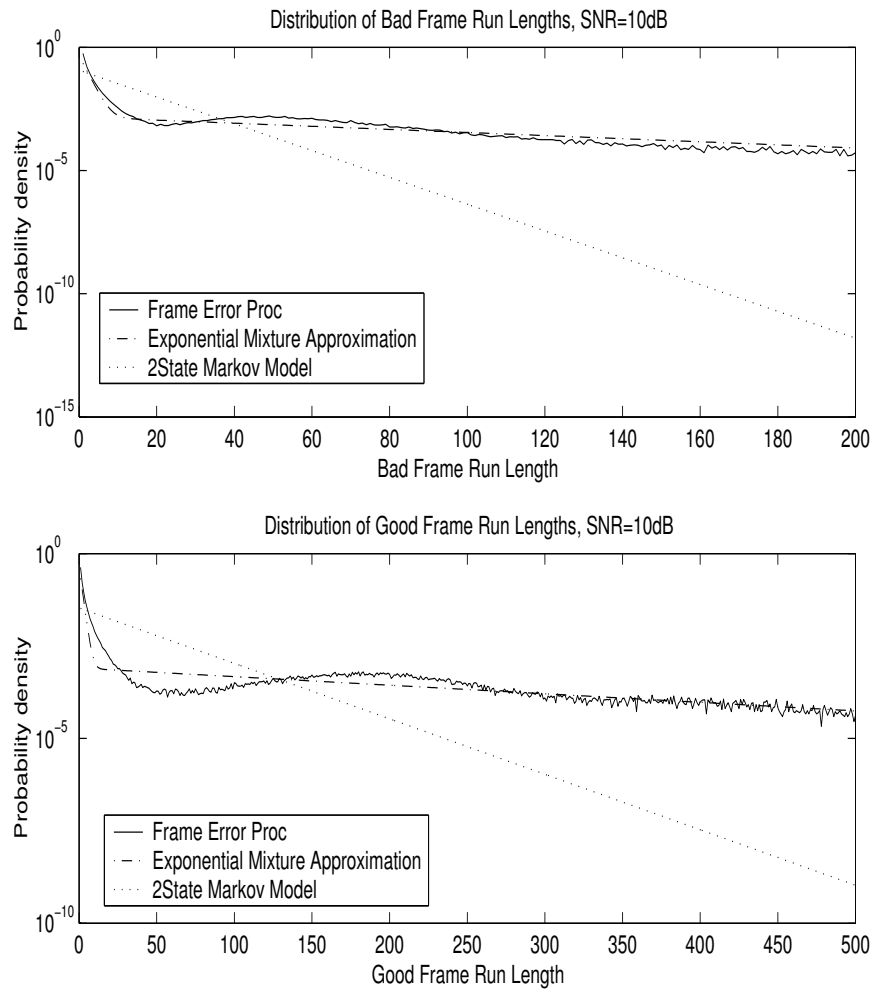
Fig. 29. Probability density function of the frame run lengths

B.   Parameter Setting

As stressed in the previous section, choosing the model parameters properly is critical for the 4SMM to have good approximations to the actual run length distributions. To obtain these via simulation would require substantial effort. Fortunately, these parameters can be linked to underlying physical channel characteristics.

1.   Tail Exponential Slope

The tail of the run length distributions indicates the probability of a long burst of frame errors or a long run of good frames and is seen to behave in an exponential manner. Long runs of frame errors are caused by long deep fades of the underlying Rayleigh fading process. Similarly, long continuous good frame runs occur when the fading process remains at a relatively high level. Suppose that any time the fading magnitude falls under a certain threshold r_1, the fading process will cause frame errors. Then the task of deriving the tail exponential slope of the bad run length distribution is converted into the problem of finding the tail exponential slope of the distribution of the time duration in which the Rayleigh fading process remains below r_1. Vice versa, assume that any time the fading remains above another threshold r_2, a run of good frames results. The task of deriving the tail exponential slope of the good run length distribution is converted into the problem of finding the tail exponential slope of the distribution of the duration in which the Rayleigh fading process stays above r_2. Considering the signal power at the transmitter end as well as the modulation/coding scheme employed, r_1 and r_2 are set based on two instantaneous SNR thresholds which decide if the frame is good or bad. The instantaneous SNR thresholds are chosen according to the frame error rate performance of the modulation/coding scheme in a Gaussian noise channel. For example, as shown in Fig. 30, for the 802.11a physical
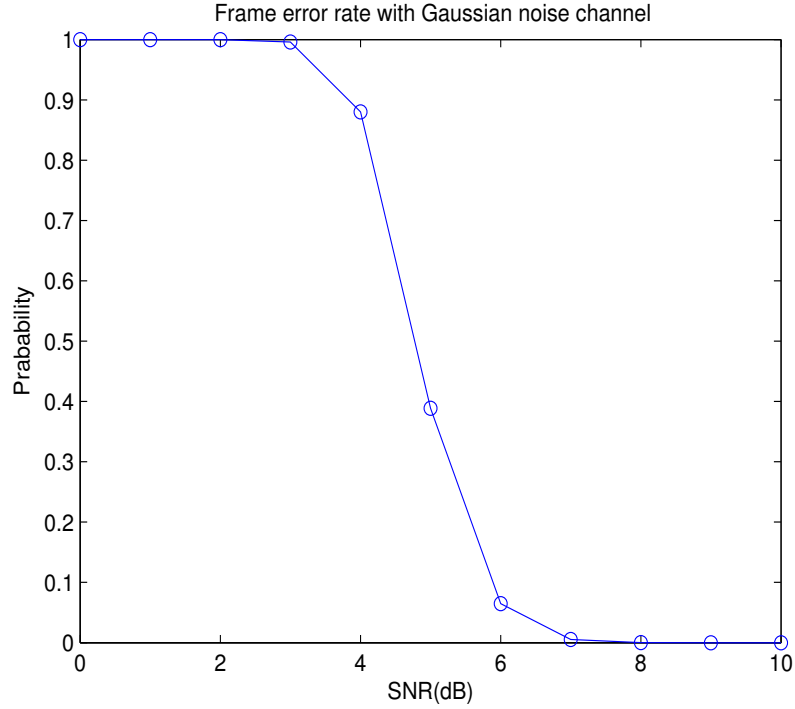
Fig. 30. Frame error rate with Gaussian noise channel

layer in a Gaussian noise channel, the frame error rate (FER) is near 1 when the SNR is lower than 3dB and the FER is near 0 when the SNR is higher than 8dB. Hence the two instantaneous SNR thresholds are set to be 3dB and 8dB. For example, if the long term average received SNR is 10dB, the two fading envelope thresholds r_1 and r_2 are set to be -7dB and -2dB respectively.

The distribution of time duration τ when the flat Rayleigh fading process falls below a certain threshold has been studied before, but to date no accurate mathematical description has been given. Although the average fading time below a certain threshold and the level crossing rate are well known [37], we require a more complete description here. Rice developed a method for approximating the distribution of fading time intervals for a Rayleigh process [58]. Unfortunately it is only asymptotically

applicable for the case when τ is small (i.e., short frame run lengths). We require the slope of the tail, that is, the long frame run lengths. The following describes an analytical procedure to estimate the tail distribution of τ.

Define a flat Rayleigh fading process as $x(t)$, the duration for which $x(t)$ falls below the lower threshold r_1 as τ, and periodic samples of the fading process $x_0, x_1, x_2, \ldots, x_N$, taken at a sampling interval of Δt. Then

$$\left\{\tau \geq t \big| |x_0| = r_1\right\} \Rightarrow \left\{|x_1| < r_1, |x_2| < r_1, \ldots, |x_N| < r_1 \big| |x_0| = r_1\right\}, \qquad (4.2)$$

where $N = \lfloor \frac{t}{\Delta t} \rfloor$. Note that the left event implies the right, but the right event does not necessarily imply the left.

However, if Δt is set to be small relative to the correlation time of the fading process, then the right event in (5.1) will almost always imply the left event. Hence when Δt is sufficiently small, the probability of $\left\{\tau \geq t \big| |x_0| = r_1\right\}$ can be well approximated by the joint probability of $\left\{|x_1| < r_1, |x_2| < r_1, \ldots, |x_N| < r_1 \big| |x_0| = r_1\right\}$.

On the other hand, if we choose the sample distance Δt sufficiently large we can claim the events $\{|x_i| < r_1\}, i = 0, 1, 2, \ldots, N$ are approximately independent of each other, thus

$$P_r(\tau \geq t) \approx P_r\left(|x_1| < r_1, |x_2| < r_1, \ldots, |x_N| < r_1 \big| |x_0| = r_1\right) \approx P_r(|x_n| < r_1)^N.$$
$$(4.3)$$

Utilizing the property that the magnitude squared of a Rayleigh process is exponentially distributed,

$$1 - F_r(t) \approx (1 - e^{-r_1^2})^{t/\Delta t}, \qquad (4.4)$$

where Δt is the time difference between each sample of the fading process. Notice that the analysis is in the continuous time domain here for the convenience of derivation.

Taking derivatives of each side, we get

$$f_r(t) \approx \frac{1}{\Delta t} \ln\left(\frac{1}{1 - e^{-r_1^2}}\right)(1 - e^{-r_1^2})^{t/\Delta t}. \tag{4.5}$$

From equation (4.11), we can easily get the exponential slope as $\frac{1}{\Delta t} ln\left(1 - e^{-r_1^2}\right)$. It is equivalent to a geometric distribution with $\beta_b = (1 - e^{-r_1^2})^{T_f/\Delta t}$ in discrete time, where T_f is the frame duration.

For the selection of Δt, we take advantage of the autocorrelation function of a flat Rayleigh fading process,

$$\phi(\tau) = \frac{\Omega}{2} J_0(2\pi f_m \tau), \tag{4.6}$$

where Ω is the envelope power and $J_0(x)$ is the zero-order Bessel function of the first kind. Δt is chosen as the smallest value so that the normalized correlation value $\phi(\Delta t)/(\frac{\Omega}{2})$ is about 0, which leads to

$$\Delta t = 1.2/(\pi f_m). \tag{4.7}$$

Thus we can reasonably approximate the samples of the fading process as independent while Δt is small enough to keep the left hand approximation in (4.10) reasonably accurate.

Similarly, for the distribution of the time duration above a certain threshold r_2,

$$P_r(\tau \geq t) \leq P_r\left(|x_1| > r_2, |x_2| > r_2, \ldots, |x_N| > r_2 \ \middle| \ |x_0| = r_2\right) \approx P_r(|x_n| > r_2)^N, \tag{4.8}$$

$$f_r(t) \approx \frac{-r_2^2}{\Delta t} e^{-r_2^2 t/\Delta t}. \tag{4.9}$$

Then the tail exponential slope for the good run length distribution is equal to $\frac{-r_2^2}{\Delta t}$. It is equivalent to a geometric distribution with $\beta_g = e^{\frac{-r_2^2 T_f}{\Delta t}}$ in discrete time.

By taking advantage of the bivariate Rayleigh distribution and using a smaller

Δt, the accuracy of the tail exponential slope estimation can be improved. In this case, the neighboring samples do not have to be independent to each other. Δt can be smaller so that only the neighboring samples are correlated, thus

$$
\begin{aligned}
P_r(\tau \geq t) \ &\approx\ P_r\Big(|x_1| < r_1, |x_2| < r_1, \ldots, |x_N| < r_1 \ \Big|\ |x_0| = r_1\Big) \\
&\approx\ \left(\frac{P_r(|x_{n-1}| < r_1, |x_n| < r_1)}{P_r(|x_{n-1}| < r_1)}\right)^{N-1} \cdot P_r\Big(|x_1| < |r_1| \big| |x_0| = r_1\Big) \\
&\approx\ \left(\frac{P_r(|x_{n-1}| < r_1, |x_n| < r_1)}{P_r(|x_{n-1}| < r_1)}\right)^{\frac{t}{\Delta t}-1} \cdot P_r\Big(|x_1| < |r_1| \big| |x_0| = r_1\Big).
\end{aligned}
$$
$$(4.10)$$

Taking derivatives of each side, we get

$$
f_r(t) \approx \frac{-1}{\Delta t} \ln\left(\frac{P_r(|x_{n-1}| < r_1, |x_n| < r_1)}{P_r(|x_{n-1}| < r_1)}\right)\left(\frac{P_r(|x_{n-1}| < r_1, |x_n| < r_1)}{P_r(|x_{n-1}| < r_1)}\right)^{\frac{t}{\Delta t}-1}. \quad (4.11)
$$

Then the tail exponential slope λ can be described as $\frac{1}{\Delta t}\ln\left(\frac{P_r(|x_{n-1}|<r_1,|x_n|<r_1)}{P_r(|x_{n-1}|<r_1)}\right)$, which is equivalent to geometric distribution with $\beta_b = \left(\frac{P_r(|x_{n-1}|<r_1,|x_n|<r_1)}{P_r(|x_{n-1}|<r_1)}\right)^{\frac{T_f}{\Delta t}}$ in discrete time.

The bivariate Rayleigh cumulative distribution function (cdf) was derived in [59] and [60]. Using an infinite series representation,

$$
P_r(|x_{n-1}| < r_1, |x_n| < r_1) = (1-\rho)\sum_{k=0}^{\infty} \rho^K \cdot P\Big(k+1, \frac{r_1^2}{(1-\rho)}\Big) \times P\Big(k+1, \frac{r_1^2}{(1-\rho)}\Big),
$$
$$(4.12)$$

where $\rho = cov(|x_{n-1}|^2, |x_n|^2)/\sqrt{var(|x_{n-1}|^2)var(|x_n|^2)} = J_0^2(2\pi f_m \tau)$, $P(\alpha, x) = (1/\Gamma(\alpha))\int_0^x e^{-t}t^{\alpha-1}dt$ is a common form of the incomplete gamma function.

Since the power of a Rayleigh process is exponentially distributed, it is easy to

get that $P_r(|x_{n-1}| < r_1) = 1 - \exp(-r_1^2)$. Then

$$\beta_b = \left(\frac{(1-\rho) \sum_{k=0}^{\infty} \rho^K \cdot P\left(k+1, \frac{r_1^2}{(1-\rho)}\right) \times P\left(k+1, \frac{r_1^2}{(1-\rho)}\right)}{1 - \exp(-r_1^2)} \right)^{\frac{T_f}{\Delta t}}. \qquad (4.13)$$

Similarly, the tail slope for the good run length distribution can be refined with the smaller Δt following the same procedure. The tail exponential slope λ for the good run length distribution can be described as $\frac{1}{\Delta t} \ln\left(\frac{P_r(|x_{n-1}|>r_2,|x_n|>r_2)}{P_r(|x_{n-1}|>r_2)} \right)$, which is equivalent to geometric distribution with $\beta_g = \left(\frac{P_\tau(|x_{n-1}|>r_2,|x_n|>r_2)}{P_r(|x_{n-1}|>r_2)} \right)^{\frac{T_f}{\Delta t}}$ in discrete time.

Using an infinite series representation for the bivariate Rayleigh cdf,

$$P_r(|x_{n-1}| > r_2, |x_n| > r_2) = (1-\rho) \sum_{k=0}^{\infty} \rho^K \cdot \left(1 - P\left(k+1, \frac{r_2^2}{(1-\rho)}\right) \right) \times \left(1 - P\left(k+1, \frac{r_2^2}{(1-\rho)}\right) \right). \qquad (4.14)$$

It is known that $P_r(|x_{n-1}| > r_2) = \exp(-r_2^2)$, so

$$\beta_g = \left(\frac{(1-\rho) \sum_{k=0}^{\infty} \rho^K \cdot \left(1 - P\left(k+1, \frac{r_2^2}{(1-\rho)}\right) \right) \times \left(1 - P\left(k+1, \frac{r_2^2}{(1-\rho)}\right) \right)}{\exp(-r_2^2)} \right)^{\frac{T_f}{\Delta t}}. \qquad (4.15)$$

2. Initial Exponential Slope

Now that the slopes of the tails of the run length distributions have been determined, we focus our attention on the other end of these distributions. Short bursts of bad (or good) frames occur when the fading process is in that region between the two thresholds r_1 and r_2. In that region, we model the frame error process as having each frame in error with some probability q_o independent of other frames. Note that since the fading process is in this in-between region, the frame error probability q_o is neither very small, nor very close to one. Hence, both frame errors and good frames are frequent, leading to many short bursts of both good and bad frames. Furthermore, under this model, the bad (good) frame run length distribution will be geometric with

parameter $\alpha_b = q_o$ $(\alpha_g = 1 - q_o)$.

Note that with this model, the initial slopes of the run length distributions do not depend on many of the physical channel parameters. For example, as long as the fading process is sufficiently slow so that the process tends to stay in the in-between region for much longer than the run lengths typically last, then the run length distribution will be largely unaffected by changes in the Doppler rate. Also, the long term SNR is irrelevant. The short runs occur when the instantaneous SNR falls in the in-between region. The long term average SNR will determine how often the process enters this region but it will not affect the behavior of the run lengths once the process is known to be in that region.

Simulations using the 802.11a and 802.11b physical layer operating over a flat Rayleigh fading channel have confirmed this hypothesis. Good and bad run length distributions under different SNR and Dopper rate in a flat Rayleigh fading channel are shown in Fig. 31 and Fig. 32. An 802.11a physical layer environment was simulated. We can see that the initial exponential slope almost stays constant for various SNR and Doppler rate. Namely, the initial slope of both the good and bad run length distributions seems to be independent of SNR, Doppler rate, frame size, and the choice of modulation/coding. Furthermore, we have found that using a value of $q_o = 1/2$ so that $\alpha_g = \alpha_b = 1/2$ seems to be adequate.

3. Combination Factor

The last parameter we need to set is the combination factor p, which combines the two different exponential distributions. Analytically, p means the percentage of short runs in the total number of good or bad runs. Short runs represent good or bad frame runs when the instantaneous SNR r belongs to the middle region, whereas long runs represent the frame errors occurring when the underlying Rayleigh fading process falls
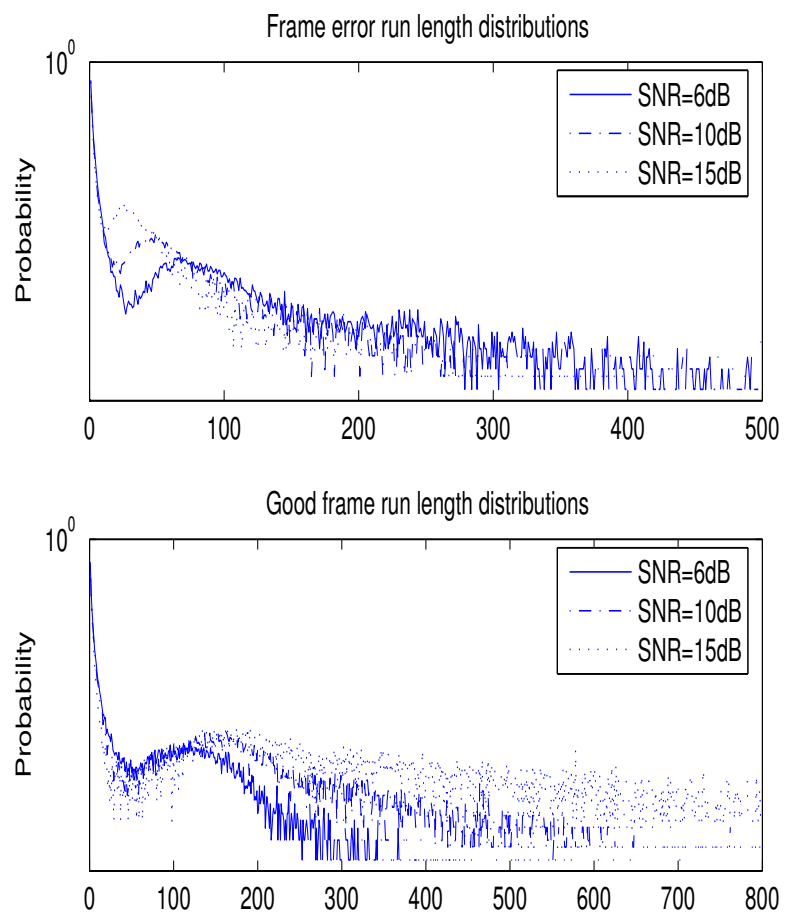
Fig. 31. Probability density function of the frame error process versus SNR
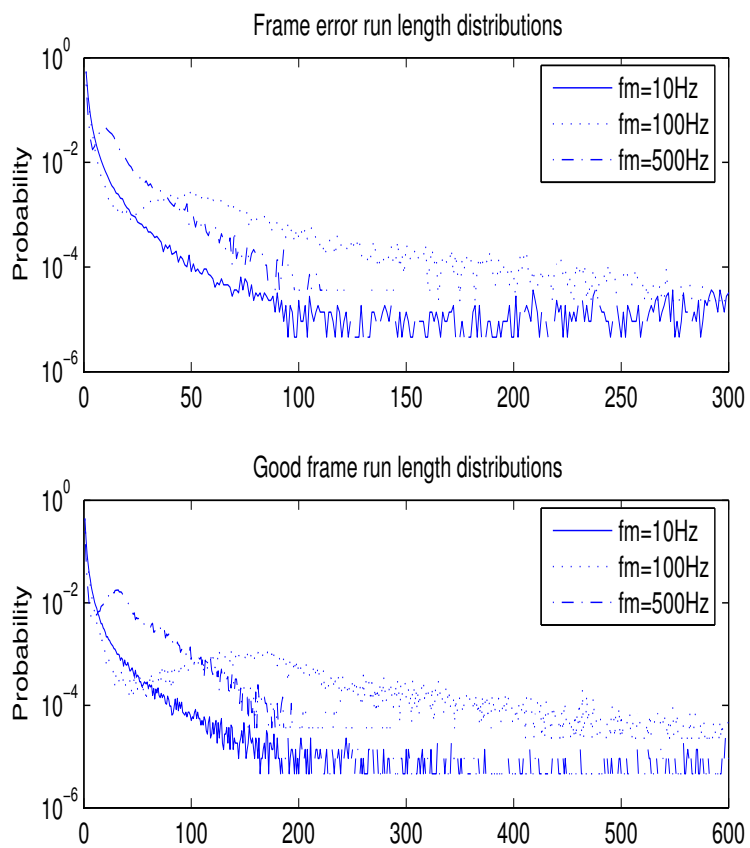
Fig. 32. Probability density function of the frame error process versus Doppler rate

below the threshold r_1 or the good frame runs occurring when the magnitude of the fading process is higher than threshold r_2. The value of p can be derived by utilizing the mathematical expression of level crossing rate.

The number of long runs N_l per second can be described as the level crossing rate at level γ [61] in the positive direction only (or in the negative direction only).

$$N_l = R\sqrt{\frac{2\pi\gamma}{\gamma_0}} f_m \exp(-\frac{\gamma}{\gamma_0}), \tag{4.16}$$

where γ_0 is the average SNR.

Each time the random process passes level r_1, one long error frame run will be generated. Each time the random process passes level r_2, one long good frame run will be generated.

The total number of runs is the sum of the number of long runs and short runs. Unlike those long runs, short runs occur when the magnitude of fading process r belongs to the middle region from r_1 to r_2. Assume the frame error rate as $r \in [r_1, r_2]$ is P_f, the average length of error runs in this region can be estimated as follows.

$$\bar{L} = \sum_{n=1}^{\infty} nP_f^{n-1}(1 - P_f) \tag{4.17}$$

$$= \frac{1}{1 - P_f}. \tag{4.18}$$

The total number of error frames per second is $\frac{P_f \int_{r_1^2}^{r_2^2} p(\gamma)d\gamma}{T_f}$, where $p(\gamma) = \frac{1}{\gamma_0}\exp(-\gamma)$ is the probability density function of the instantaneous power of the fading process, T_f is the frame duration. Since P_f is different for every instantaneous SNR, averaging P_f over $[r_1^2, r_2^2]$, the average number of short error runs per second N_s can be approximated by

$$N_s = \int_{r_1^2}^{r_2^2} p(r)\frac{1}{T_f}p_e(r)/\bar{L}dr$$

$$= \int_{r_1^2}^{r_2^2} \exp(-r) \frac{1}{T_f} p_e(r)(1 - p_e(r)) dr, \qquad (4.19)$$

where $p_e(r)$ is the frame error rate of instantaneous SNR $(\gamma_0 + r)(\text{dB})$ with no random fading process added.

Therefore, assume the average power of the fading process is 1, the percentage of short runs p can be approximated by

$$p = \frac{N_s}{N_s + N_l} \qquad (4.20)$$

$$= \frac{\int_{r_1^2}^{r_2^2} \exp(-r) p_e(r)(1 - p_e(r)) dr}{\int_{r_1^2}^{r_2^2} \exp(-r) p_e(r)(1 - p_e(r)) dr + \sqrt{2\pi\gamma^2} f_m T_f \exp(-\gamma^2)}, \qquad (4.21)$$

where γ is chosen to be r_1 if p is for the frame error run length distribution or r_2 for the good frame run length distribution.

Hence, all the parameters in the four-state Markov Model can be set analytically with no additional physical layer simulation.

An alternative approach to set up p is available by taking advantage of the average good frame run length $\bar{\tau}_g$ and average bad frame run length $\bar{\tau}_b$. With these additional measurements, p can be set up to model the physical layer more accurately. The average run length for the short bursts is $1/(1-\alpha)$ and the average run length for the long run lengths is $1/(1 - \beta)$. To make the model average run length consistent with the observed run length, we must set p to satisfy

$$p \cdot \frac{1}{1 - \alpha} + (1 - p) \cdot \frac{1}{1 - \beta} = \bar{\tau}, \qquad (4.22)$$

$$\Rightarrow p = \frac{\bar{\tau} - \frac{1}{1-\alpha}}{\frac{1}{1-\beta} - \frac{1}{1-\alpha}}. \qquad (4.23)$$

The results of using these two approaches to set up the combination factor p will be compared in the next section.

C. Statistical Approximation Results

In summary, the parameters of the 4SMM are set as follows:

1)α_g, $\alpha_b = 0.5$;

2)Set r_1 and r_2 according to the plot of the FER of the underlying modulation/coding scheme in a Gaussian noise channel.

3)$\beta_b = (1 - e^{-r_1^2})^{\frac{\pi f_m T_f}{1.2}}$, $\beta_g = e^{-\frac{r_2^2 \pi f_m T_f}{1.2}}$, where T_f is the frame duration and f_m is the Doppler rate.

Or improve the accuracy by choosing a smaller delta and use the β_b and β_g in (4.13) and (4.15)

4)

$$p_b = \frac{\int_{r_1^2}^{r_2^2} \exp(-r)p_e(r)(1 - p_e(r))dr}{\int_{r_1^2}^{r_2^2} \exp(-r)p_e(r)(1 - p_e(r))dr + \sqrt{2\pi r_1^2} f_m T_f \exp(-r_1^2)},$$

$$p_g = \frac{\int_{r_1^2}^{r_2^2} \exp(-r)p_e(r)(1 - p_e(r))dr}{\int_{r_1^2}^{r_2^2} \exp(-r)p_e(r)(1 - p_e(r))dr + \sqrt{2\pi r_2^2} f_m T_f \exp(-r_2^2)},$$

where $p_e(r)$ is the function of frame error rate when the instantaneous SNR is $(\gamma_0 + r)$(dB).

Or using the alternative approach when the average good and bad run length are available, then $p_b = (\frac{1}{(1-\beta_b)} - \bar{\tau}_b)/(\frac{1}{(1-\beta_b)} - \frac{1}{(1-\alpha_b)})$, $p_g = (\frac{1}{(1-\beta_g)} - \bar{\tau}_g)/(\frac{1}{(1-\beta_g)} - \frac{1}{(1-\alpha_g)})$.

Using the analytical approach(without taking advantage of the information of $\bar{\tau}_b$ and $\bar{\tau}_b$), the run length distributions in the 802.11a and 802.11b physical layer environment are shown in Fig. 33, Fig. 34 and Fig. 35. It can be seen that the 4SMM gives good approximations of the run length distributions, especially in that 4SMM matches the initial slope and the tail slope of the run length distributions very well. Thus the 4SMM estimates run length distributions properly by setting up model parameters analytically. By constraining the average run length to the

observed value(the alternative approach to set up p), the four-state Markov model is expected to perform better because now we have more information available to set up the model. As we can see in Fig. 34, Fig. 33 and Fig. 35, the alternative approach is slightly better for the good run length distributions when the SNR is lower but no apparent difference for medium to high SNRs. The performance of the four-state Markov model using these two approaches in a wireless network will be evaluated and compared in the next section.

We also increase the frame size to 1200 bytes to see if the frame size will affect the approximation accuracy of the 4SMM. The Doppler rate is chosen to be 8Hz, as a lower Doppler rate is more usual in an indoor environment. The 802.11a physical layer is simulated. As shown in Fig. 36 and Fig. 37, the 4SMM has a good run length distribution estimation with the increased frame size. This is expected because in the procedure of choosing the 4SMM parameters, the frame size and Doppler rate have been accounted for.

Another issue when setting up the 4SMM is that choosing the thresholds r_1 and r_2 can be empirical to a certain extent because these thresholds are chosen to make the instantaneous FER close to 1 or 0 and there is no precise definition of how close to 1 or 0 the FER should be. We found that generally choosing the thresholds so that the instantaneous FER is 1%/99% seems to be a reasonable choice. We move the thresholds so that the instantaneous FER is as high as 0.01%/99.99% at one extreme and as low as 5%/95% at the other extreme. As we can see in Fig.38 and Fig.39, changing the thresholds in this range does not affect the run length distributions much. Overall, the 4SMM is robust to a slight shift of the thresholds. We will also look at the network simulation results with varying thresholds in the next section.
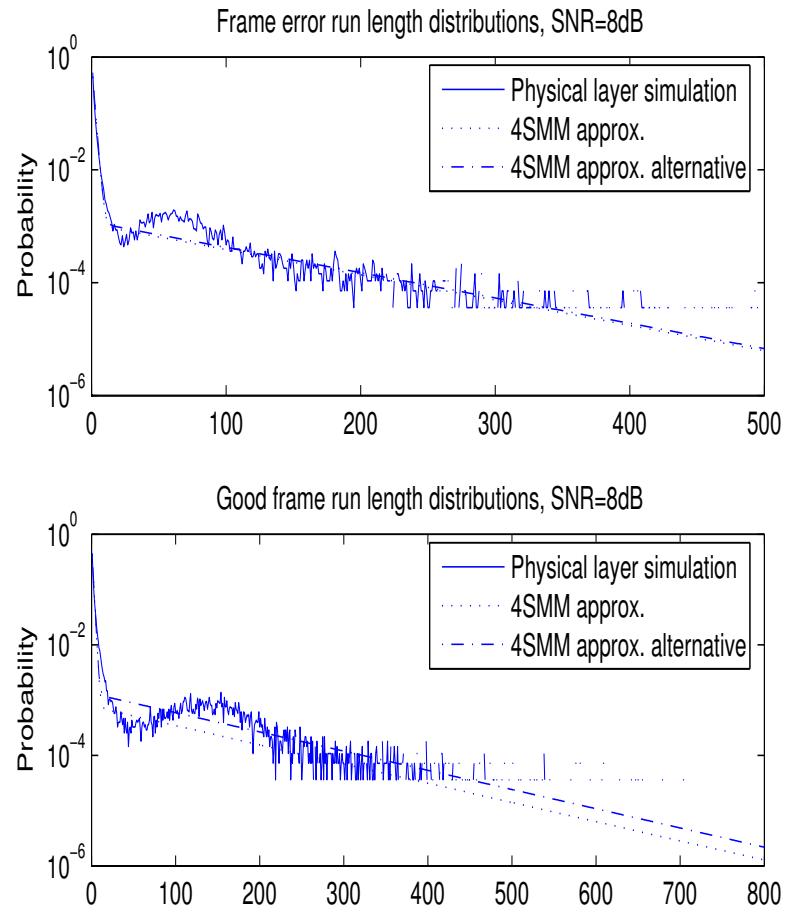
Fig. 33. 4SMM run length distribution approximations with lower SNR, 802.11a environment
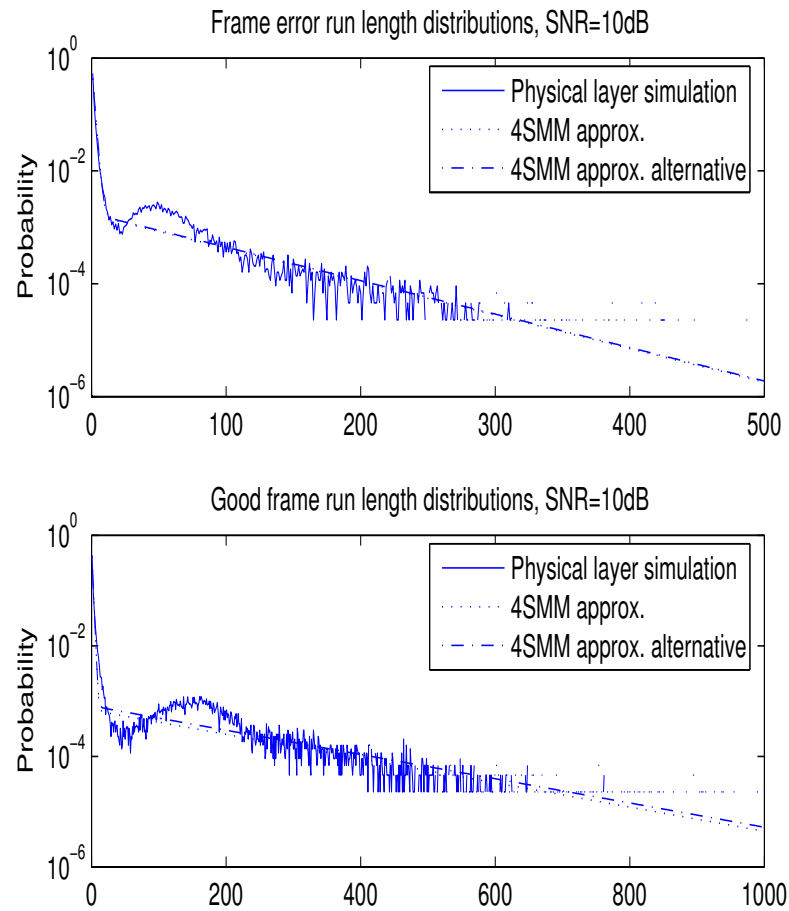
Fig. 34. 4SMM run length distribution approximations, 802.11a environment

Fig. 35. 4SMM run length distribution approximations, 802.11b environment
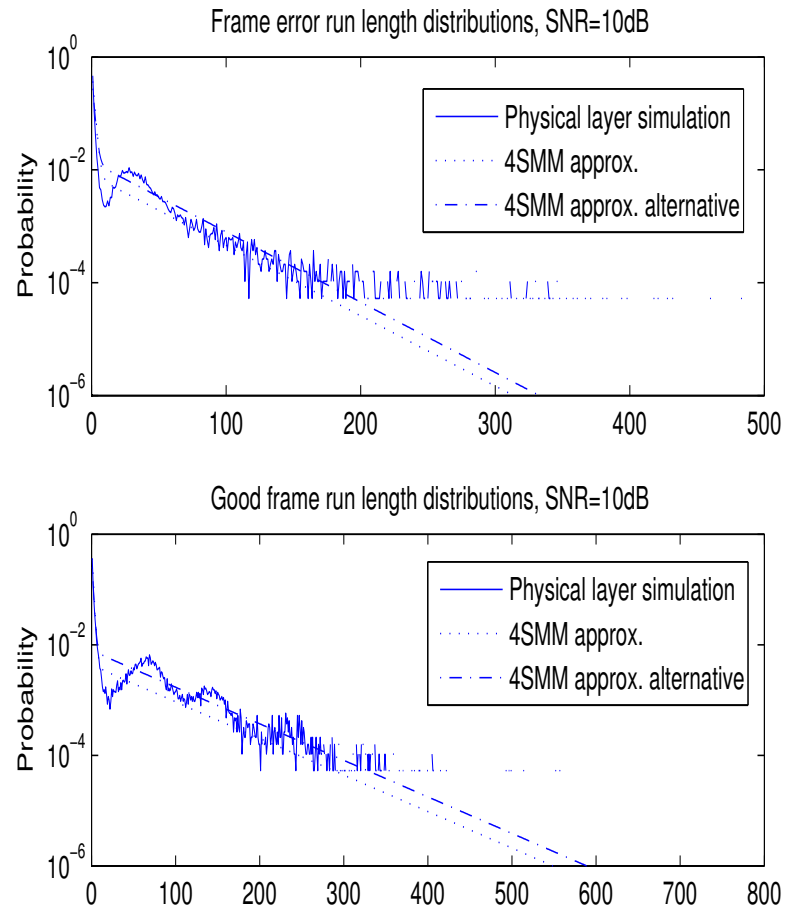
Fig. 36. 4SMM run length distribution approximations, frame size 1200 bytes, SNR=10dB
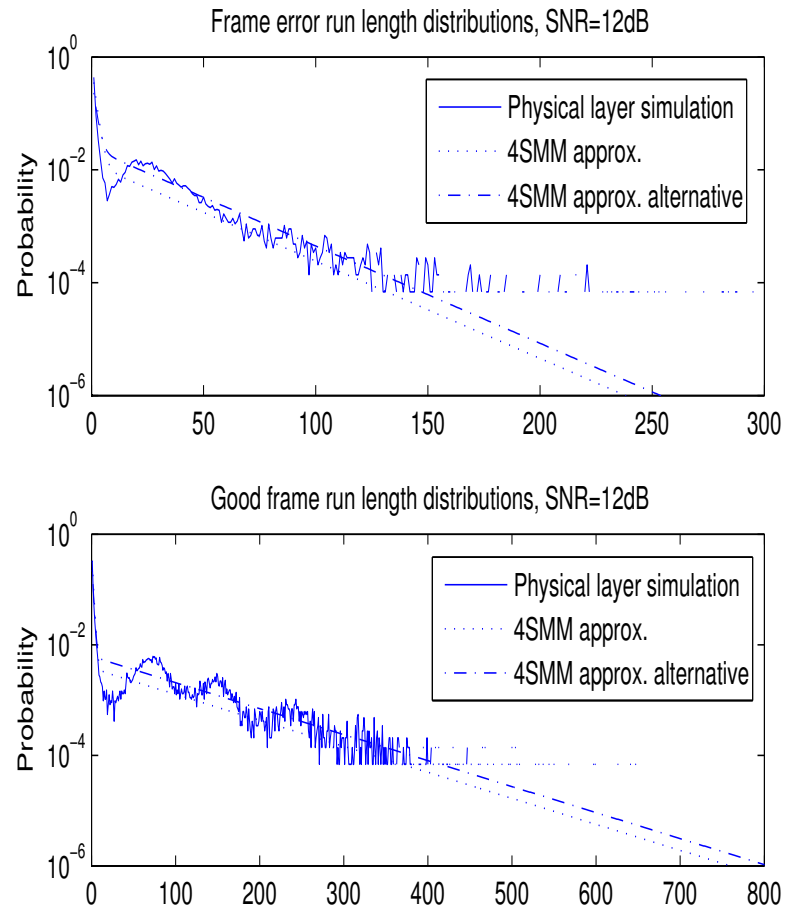
Fig. 37. 4SMM run length distribution approximations, frame size 1200 bytes, SNR=12dB
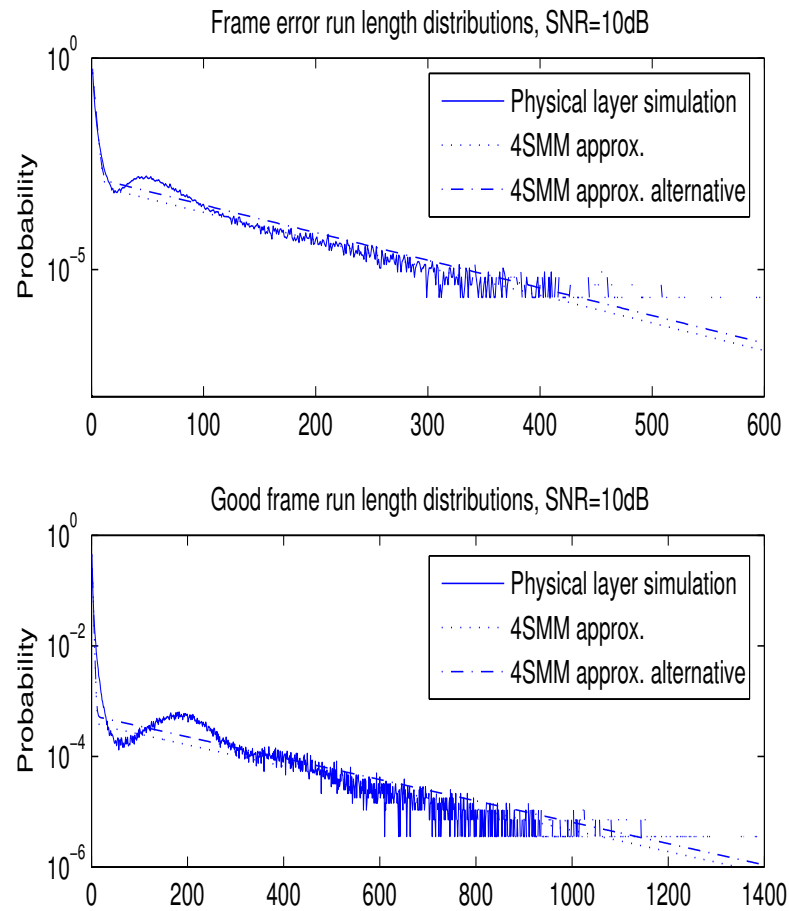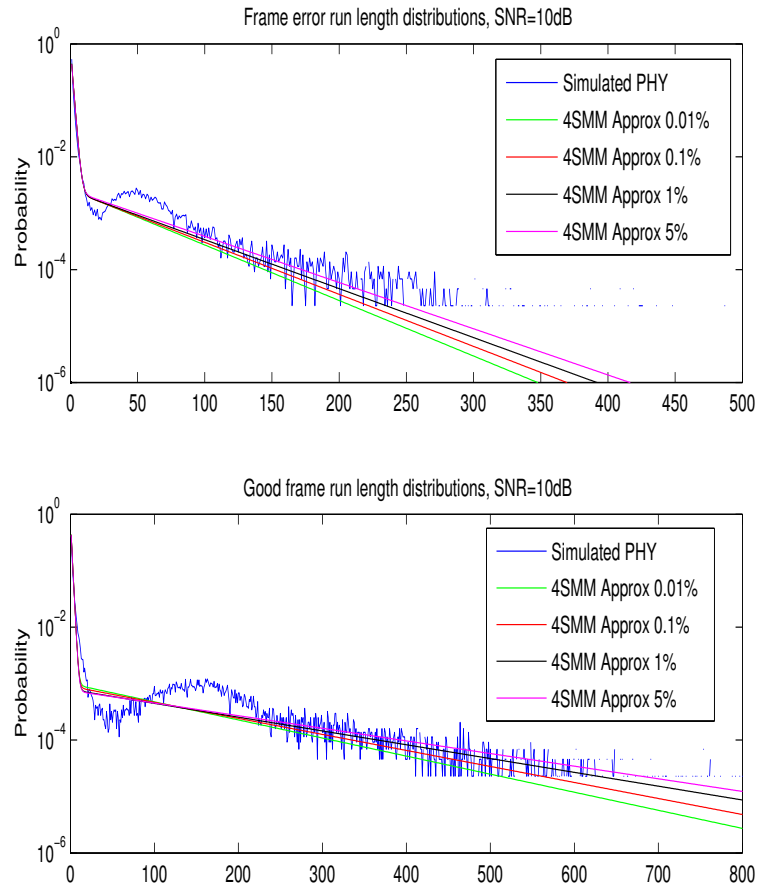
Fig. 38. 4SMM run length distribution approximations with varying thresholds, SNR=10dB
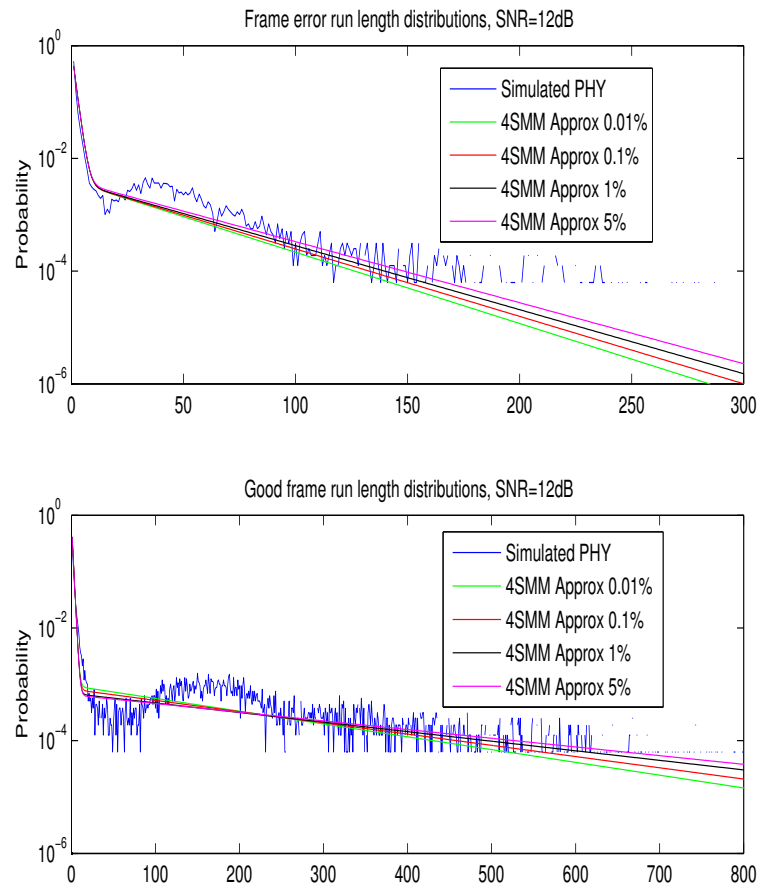
Fig. 39. 4SMM run length distribution approximations with varying thresholds, SNR=12dB

D. Network Performance

We apply the four-state Markov model in a wireless LAN 802.11a and 802.11b environment with the ns2 network simulation tool. To make a fair comparison, we also embed a simulated 802.11a and 802.11b physical channel with channel coding, modulation and flat Rayleigh fading into ns2 to get the simulated physical layer results. The Doppler frequency is selected to be 100Hz. The frame size and transmission rate chose for 802.11a and 802.11b are 384bits, 12Mb/s and 296bits, 11Mb/s respectively. The normalized Doppler, $f_m T_f$ is 0.0032 and 0.0027 for the 802.11a and 802.11b physical layers respectively.

Two finer points of model implementation need to be addressed here. When choosing the simulated frame, a frame size of 384 and 296 bits is chosen for 802.11a and 802.11b simulations respectively. The purpose of using a small frame size is to adapt to the different frame size definitions in the physical layer. In this way, longer frames can be split into several frames while for the shorter frames the accuracy can still be maintained. Another issue is about ensuring the accuracy of the temporal process. When the channel is not in use, the time between frame transmissions should be accounted for in the simulated frame error process. That is, the simulated error process must be advanced even when the channel is idle.

A simple two-node wireless network was set up by the ns2 simulation tool. Simulations were conducted for 30% channel loadings, with the following network setup: a constant SNR of 5-15dB, the 802.11a and 802.11b MAC protocols with the distributed coordination function and a queue length of 50 packets, TCP Reno with an initial window length of 100, and also the user datagram protocol (UDP). Each simulation was conducted for 10 minutes of simulation time. Note that this is the network simulation duration set before the ns2 simulation, while the ns2 simulator

can run for days to finish. A trace file was generated for each simulation and analyzed later for network characteristics. Parameters for the 4SMM were set as described in the previous section. Considering that the 2SMM is the most commonly used model, the network throughput of the 2SMM will be used for comparison. The parameters of the 2SMM and 4SMM are listed in tables I, II, III and IV. Note that we use the smaller Δt approach in (4.13) and (4.15) to get the β_b and β_g in the following tables.

The network simulation results are presented in Fig. 40 and Fig. 41. As shown, The four-state Markov Model makes a much more accurate estimation of the network performance compared to the 2SMM for both 802.11a and 802.11b environment. Using the alternative approach to estimate the combination factor p improves the network throughput for the lower SNR. For the medium SNR which is of the most interest for research purpose, the 4SMM with analytical approach provides very accurate network results. For the high SNR, the frame error rate becomes very low and network throughput comes close to the offered data load and becomes predictable. From a practical engineering point of view, when the SNR is too low(frame error rate close to 0.5) the system is not able to operate and when the SNR is very high(frame error rate close to 0) the physical layer errors can be easily recovered by MAC layer retransmission scheme and the upper layer sees almost an error-free physical layer. It is the medium SNR range that we are not clear about the behavior and the interaction of physical layer and upper layer and so the medium SNR range is worth the most attention for physical layer modeling. Overall, the four-state Markov model is substantially better than the traditional two-state Markov model. The physical layer interactions are simulated with a baseband equivalent simulation. We also compared the network results with different approach to select Δt described in the previous section. As shown in Fig.42 and Fig.43, using a smaller Δt to estimate the tail slope improves the model accuracy. The effect of choosing different thresholds are shown

Table I. Two-state Markov Model Parameters, 802.11a

SNR(dB)	ε	AFEL	p	q
8	0.37327	12.885	0.95378	0.92239
9	0.30252	12.77	0.96603	0.92169
10	0.25149	11.094	0.96971	0.90986
11	0.2024	11.934	0.97874	0.91621
12	0.18901	11.725	0.98012	0.91471
13	0.12654	10.871	0.98667	0.90801
14	0.11841	10.903	0.98768	0.90828
15	0.08024	10.068	0.99133	0.90067

Table II. Two-state Markov Model Parameters, 802.11b

SNR(dB)	ε	AFEL	p	q
8	0.3256	9.527	0.9493	0.8950
9	0.2797	8.9337	0.9565	0.8881
10	0.224	8.4995	0.9660	0.8823
11	0.1809	8.1269	0.9728	0.8770
12	0.1515	7.8329	0.9772	0.8723
13	0.1232	8.3289	0.9831	0.8799
14	0.0978	7.7794	0.9861	0.8715
15	0.076	8.0765	0.9898	0.8762

Table III. Four-state Markov Model Parameters, 802.11a

SNR(dB)	α_g	β_g	p_g	α_b	β_b	p_b
8	0.5	0.9904	0.90469	0.5	0.9857	0.89551
9	0.5	0.9918	0.88505	0.5	0.9830	0.88756
10	0.5	0.9931	0.86429	0.5	0.9802	0.8784
11	0.5	0.9942	0.84252	0.5	0.9773	0.86799
12	0.5	0.9951	0.81981	0.5	0.9742	0.85631
13	0.5	0.9959	0.79621	0.5	0.9710	0.84334
14	0.5	0.9966	0.77173	0.5	0.9677	0.82904
15	0.5	0.9972	0.74641	0.5	0.9643	0.81339

Table IV. Four-state Markov Model Parameters, 802.11b

SNR(dB)	α_g	β_g	p_g	α_b	β_b	p_b
8	0.5	0.9917	0.94037	0.5	0.9825	0.94067
9	0.5	0.9929	0.92575	0.5	0.9799	0.93662
10	0.5	0.9940	0.90995	0.5	0.9773	0.93175
11	0.5	0.9949	0.89309	0.5	0.9745	0.92604
12	0.5	0.9957	0.87523	0.5	0.9717	0.91947
13	0.5	0.9964	0.85638	0.5	0.9689	0.912
14	0.5	0.9971	0.83657	0.5	0.9659	0.90359
15	0.5	0.9976	0.81578	0.5	0.9630	0.89418

in Fig. 44. We can see that when choosing the thresholds so that the instantaneous FER is 5%/95% the estimated network throughput has a little deviation compared to the results of choosing the thresholds so that the instantaneous FER is within 1%/99%. When the thresholds are chosen so that the instantaneous FER is 1%/99%, the network throughputs are well approximated. This confirms our argument in the previous section that although choosing the thresholds is somewhat empirical, the 4SMM is robust to varying thresholds as long as they are chosen within a reasonable range. We recommend choosing the thresholds so that the FER is 1%/99%. Overall, the four-state Markov Model is shown to be efficient, accurate, easy to set up and suitable for different physical environments. Since most of the network simulations are conducted with a 30% offered load, we varied the load from 10% to 90% of the channel bandwidth for the SNR= 12dB in the 802.11b system. As seen in Fig.45, changing the offered load does not affect our previous observation of the model performance. The four-state Markov model is able to estimate the network throughput accurately with varying offered load.

E.   Summary

A novel four-state Markov model was presented to approximate physical layer frame error statistics in this chapter. The procedure to establish the transition probabilities for the four-state Markov model was described in detail. By approximating the good and bad run lengthes distributions with a mixture of geometric distribution, the four-state Markov model captures the essential physical layer characteristics so that it can be used for upper layer wireless network simulations and analysis in a flat Rayleigh fading channel. By choosing the tail slope and initial slope based on the underlying fading process statistics, the parameters in the four-state Markov model can be set
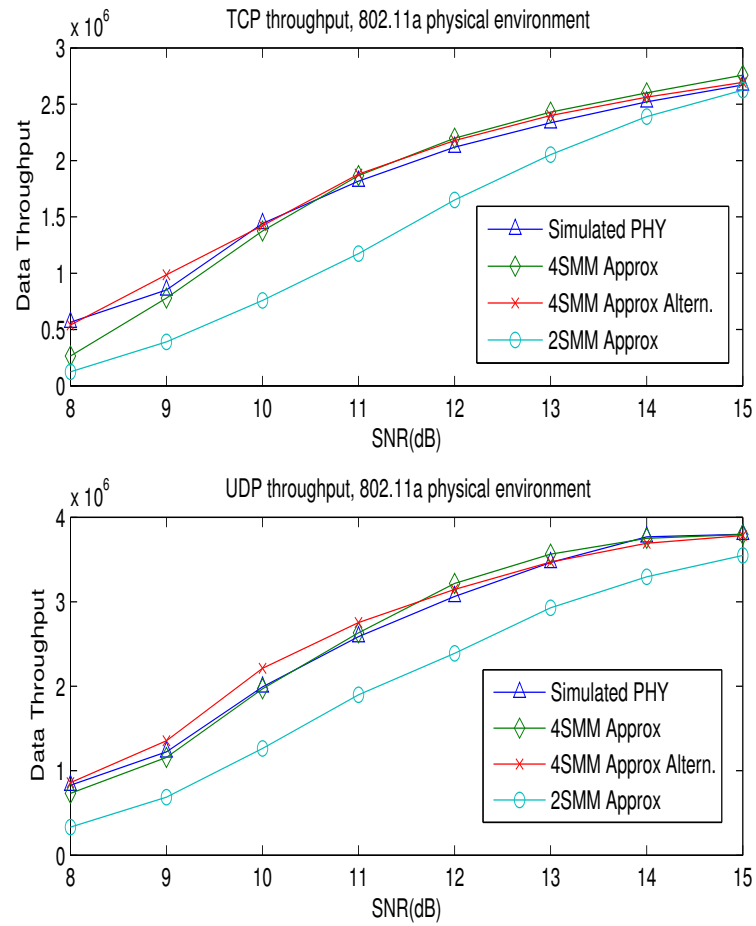
Fig. 40. Network performance of channel approximations, 802.11a environment
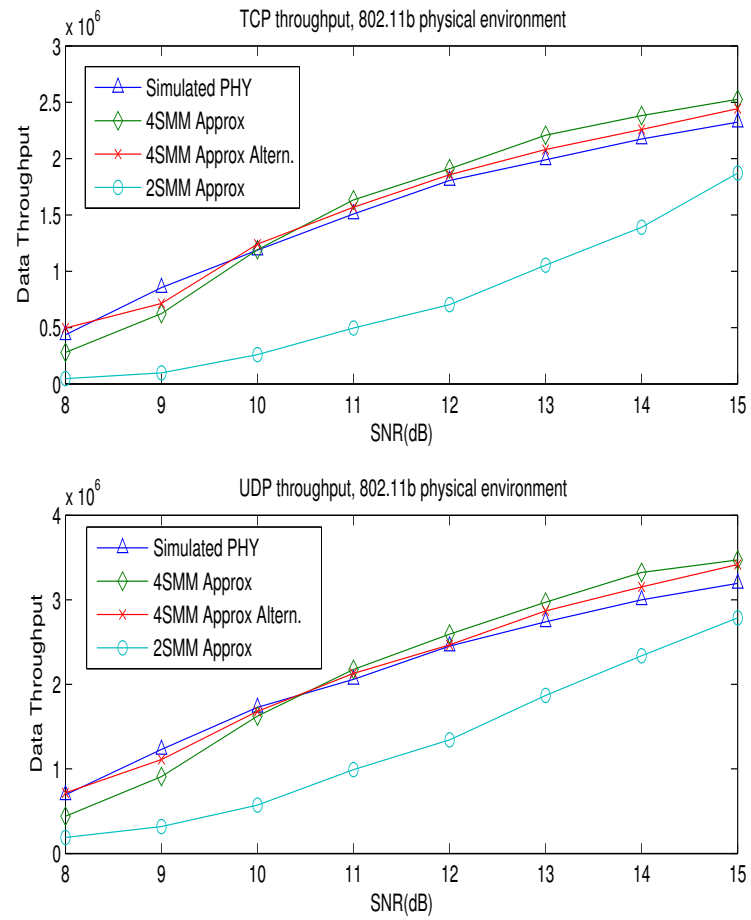
Fig. 41. Network performance of channel approximations, 802.11b environment
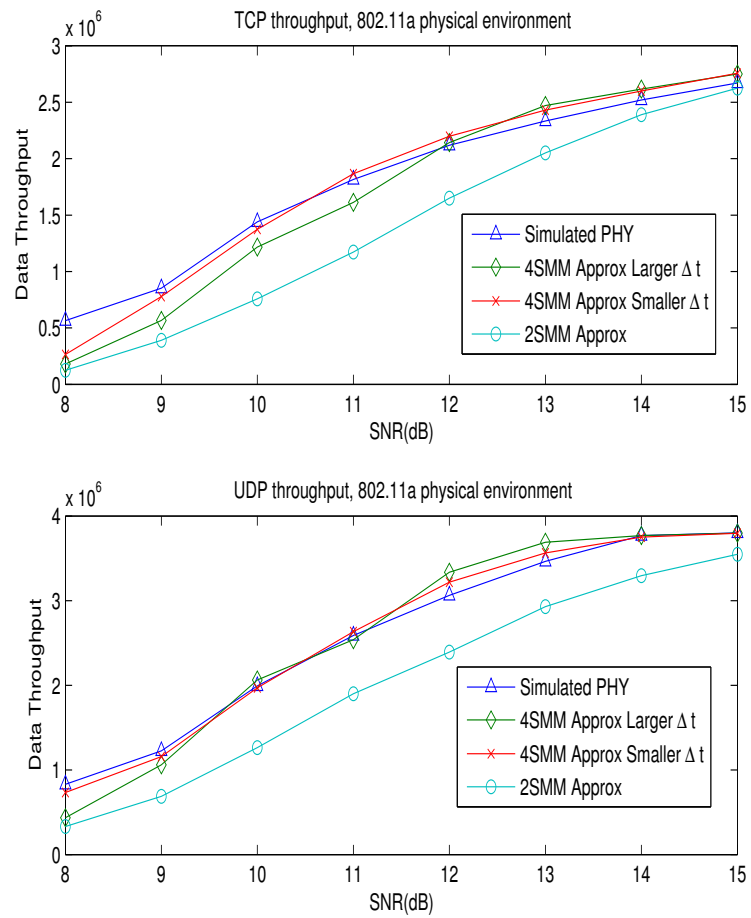
Fig. 42. Network performance comparison with different Δt , 802.11a environment
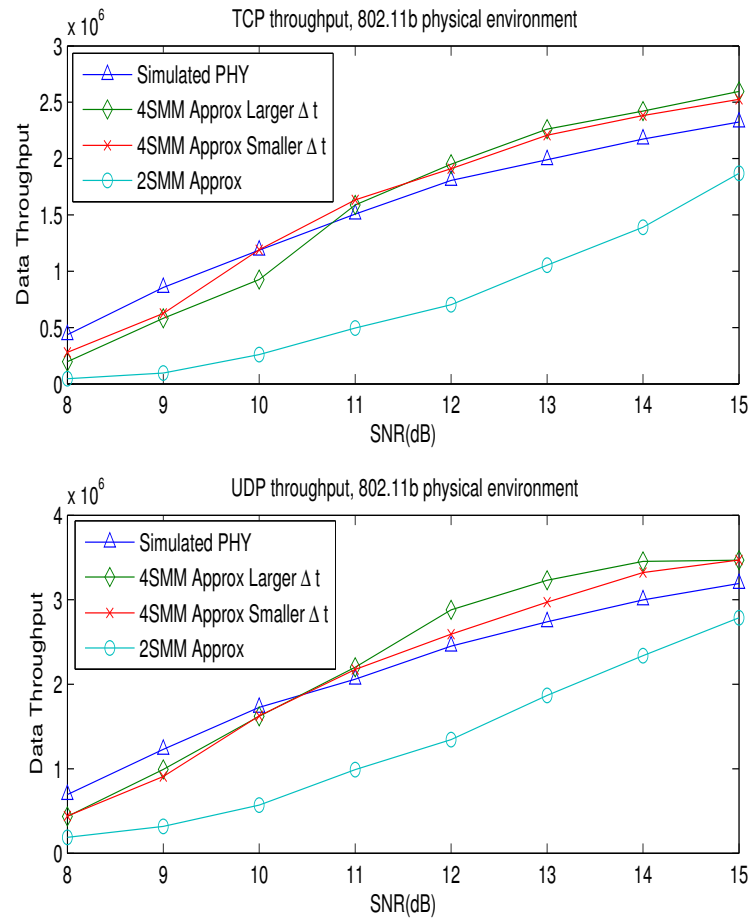
Fig. 43. Network performance comparison with different Δt, 802.11b environment
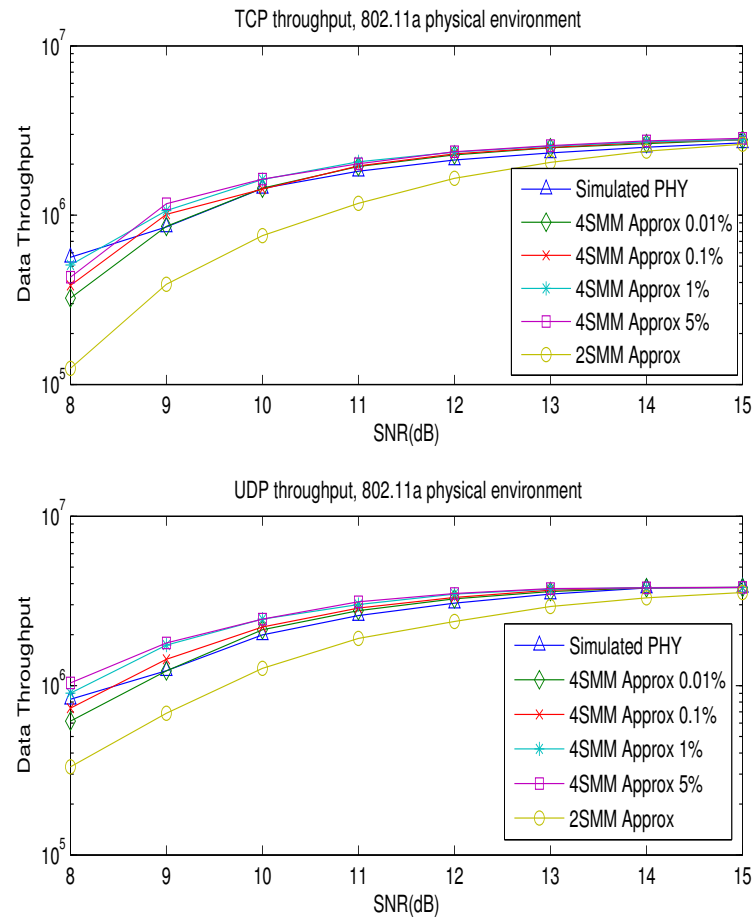
Fig. 44. Network performance comparison with varying thresholds, 802.11a environment
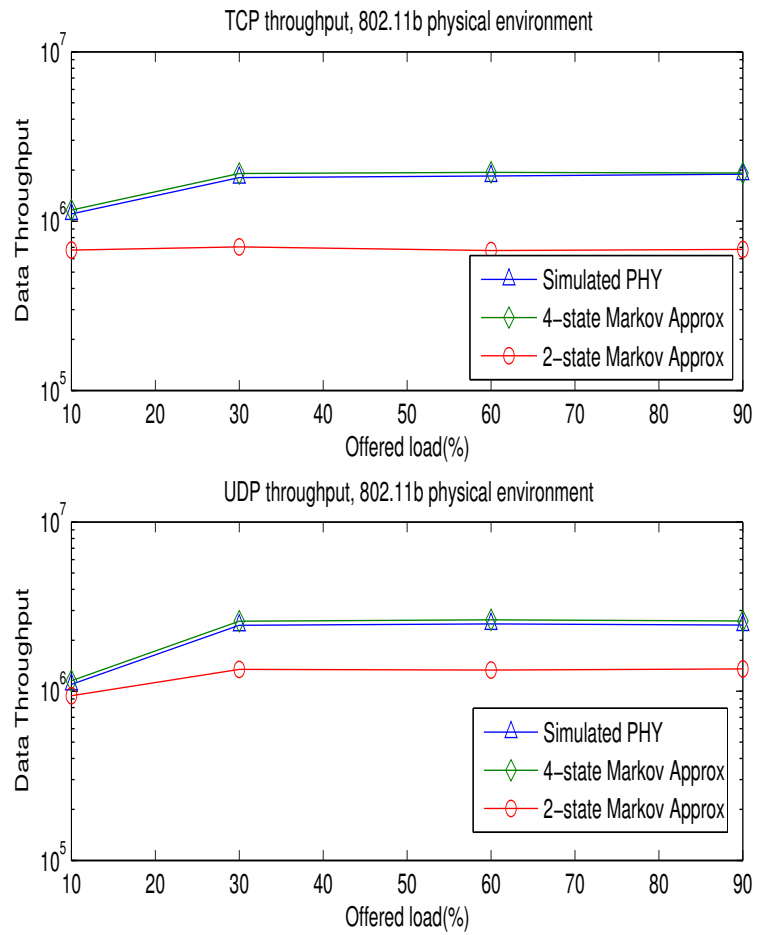
Fig. 45. Network performance comparison with different traffic load, 802.11b environment, snr=10dB

up without having to run initial simulations while most of the current models require simulations to obtain certain physical layer statistics such as the frame error rate and average frame error run length before setting up the model parameters. Besides accurate network simulation results, this advantage sets the four-state Markov model apart from most of the other physical layer models. The ns2 simulation for 802.11a and 802.11b environments showed that the four-state Markov model is superior than the most popular two-state Markov model. Especially for the medium SNR range, which is of the most interest for upper layer designers, the four-state Markov model produces close network results with the actual simulated physical layer. An alternative approach to derive the combination factor p was also presented in this chapter. This approach requires the information of the average good frame run length and the average bad frame run length of the physical layer. With this additional information, the performance of the four-state Markov model can be further improved. The approach is suitable when the physical layer statistics are available. The simple structure of the four-state Markov model provides a valuable tool for wireless network analysis and simulations based on the frame level error statistics in a flat fading channel.

CHAPTER V

FOUR-STATE MARKOV MODEL FOR DIVERSITY CHANNELS

In the previous chapter, we established an accurate and efficient physical layer model for wireless flat Rayleigh fading channels. It will be helpful if the model can be adapted for multi-path frequency selective channels. Instead of generating different paths separately and combining them, a more efficient way is to directly generate the error process at the output of a diversity receiver. Iskander and Mathiopoulos extended the FSMC model for diversity channels with different combining schemes [62] [63]. However, as pointed out in [18], an inappropriate method to partition the states can cause substantial deviation in the transition probabilities and hence inaccurate modeling of the fading process. Again, to partition the state using the equal duration method proposed by Zhang involves large complexity to solve the equations and the number of states and equations will become too many to deal with if the Doppler frequency shift is low, which makes the FSMC model less attractive in practice. In this chapter, the four-state Markov model is used to emulate the frame error process with frequency selective channels and diversity gain out of the frequency selective channel. The process of establishing parameters for the 4SMM will be investigated for diversity channels. The physical layer frame error statistics are analyzed in order to set up the model parameters. An 802.11a coded OFDM system and an Alamouti scheme STBC will be studied and simulated for the physical layer to provide real data to compare with. In the end, network throughput for the 4SMM, 2SMM and simulated physical layer environment will be compared and discussed.

A.   Frame Error Statistics

In chapter IV, we established the procedure to set up the transition probabilities for the four-state Markov model by examining the physical layer frame error process and matching the run length distributions. For a wideband communication system, the channel becomes frequency selective and diversity gain may be obtained at the receiver with appropriate signal processing techniques.

To build up an adequate model for a physical layer with a frequency selective channel and diversity gain, the physical layer run length distributions are simulated. In an 802.11a OFDM physical layer environment, assume there are 4 independent paths available in the channel and each of them experiences independent fading. By using a convolutional code with a large enough free distance, a diversity order of approximately 4 can be achieved. The parameters for the simulation are as follows: data rate 12Mbps, frame size 384 bits, maximum Doppler frequency shift 100Hz, $f_m T_f = 0.0032$, SNR 8dB, the good and bad run length distributions are shown in Fig. 46.

It can be seen that the good and bad run length distributions follow a mixture of two exponential slopes as well as in the flat fading case. Therefore, the run length distributions for the frequency selective channel and diversity gain can still be approximated by the mixture of two exponential slopes. The structure of the four-state Markov model described in the previous chapter can be applied to a physical layer with a frequency selective channel. However, the transition probabilities of the 4SMM need to be adapted appropriately. With L uncorrelated fading paths, the probability of the instantaneous SNR dropping below a certain threshold is much lower. The procedure to set up a 4SMM for a physical layer with a frequency selective channel and diversity gain will be investigated in the next section.
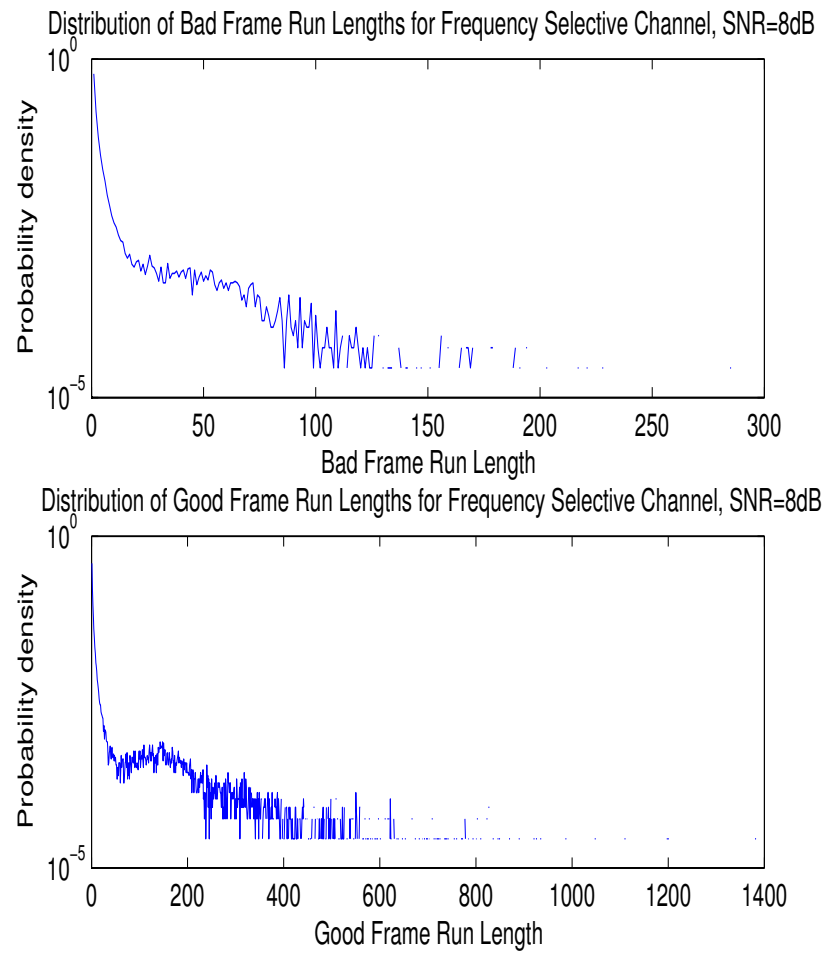
Fig. 46. Probability density function of the frame error process, frequency selective channel

B.   Parameter Setting

As shown in chapter IV, the 4SMM transition probabilities depend on the two exponential slopes and the combining factor of the run length distributions, which need to be reevaluated when the fading channel becomes frequency selective with diversity. The goal is to identify these quantities by analysis so that the model can be set up without having to run the pre-simulations to acquire the slopes and the combining factor.

1.   Tail Exponential Slope

As discussed in the flat fading scenario, the tail slope can be related to the distribution of the time duration in which the instantaneous fading magnitude falls below a threshold r_1 or above a threshold r_2. The process of finding the threshold for the frequency selective channel is the same as for the flat fading channel. Running the physical layer with the same modulation and coding scheme through an AWGN channel, look at the plot of FER versus SNR and find the low SNR S_1 when the FER is close to 1 and the high SNR S_2 when FER is close to 0. Then r_1 is the average SNR minus S_1 and r_2 is the average SNR minus S_2 (in dB scale).

For a frequency selective channel with diversity order L, define the equivalent diversity combined fading process as $x(t)$, the duration for which $x(t)$ falls below the lower threshold r_1 as τ, and periodic samples of the diversity combined fading process $x_0, x_1, x_2, \ldots, x_N$, taken at a sampling interval of Δt. Let $|x_i|, i = 0, 1, 2, \ldots, N$ be the diversity combined envelope at the sample time. Then

$$\left\{ \tau \geq t \big| |x_0| = r_1 \right\} \Rightarrow \left\{ |x_1| < r_1, |x_2| < r_1, \ldots, |x_N| < r_1 \, \big| |x_0| = r_1 \right\}, \qquad (5.1)$$

where $N = \lfloor \frac{t}{\Delta t} \rfloor$.

By choosing Δt so that the correlation value $R(x_i, x_j)$ of $x_i, x_j, i \neq j$ is approximately 0, the distribution of τ can be written as

$$P_r(\tau \geq t) \approx P_r\Big(|x_1| < r_1, |x_2| < r_1, \ldots, |x_N| < r_1 \,\Big|\, |x_0| = r_1\Big) \approx P_r(|x_n| < r_1)^N. \tag{5.2}$$

Assume the branches are equal strength, the sum of the branch powers are 1 and they are independent Rayleigh fading processes. The distribution of the diversity combined envelope square γ is a chi-square distribution with $2L$ degrees of freedom [64],

$$p_\gamma(x) = \frac{1}{(L-1)!x}(Lx)^L e^{-Lx}. \tag{5.3}$$

The cdf of γ is

$$F_\gamma(x) = 1 - e^{-Lx}\sum_{k=0}^{L-1}\frac{1}{k!}(Lx)^k. \tag{5.4}$$

Hence we have

$$1 - F_r(t) \approx (1 - e^{-Lr_1^2}\sum_{k=0}^{L-1}\frac{1}{k!}(Lr_1^2)^k)^{t/\Delta t}, \tag{5.5}$$

where Δt is the time difference between each sample of the diversity combined fading process. Notice that the analysis is in the continuous time domain here for the convenience of derivation. Taking derivatives of each side, we get

$$f_r(t) \approx \frac{1}{\Delta t}ln\Big(\frac{1}{1 - e^{-Lr_1^2}\sum_{k=0}^{L-1}\frac{1}{k!}(Lr_1^2)^k}\Big)(1 - e^{-Lr_1^2}\sum_{k=0}^{L-1}\frac{1}{k!}(Lr_1^2)^k)^{t/\Delta t}. \tag{5.6}$$

From equation (5.6), we can get the exponential slope λ_b as

$$\lambda_b = \frac{1}{\Delta t}ln\Big(1 - e^{-Lr_1^2}\sum_{k=0}^{L-1}\frac{1}{k!}(Lr_1^2)^k\Big). \tag{5.7}$$

It is equivalent to a geometric distribution in discrete time with

$$\beta_b = (1 - e^{-Lr_1^2}\sum_{k=0}^{L-1}\frac{1}{k!}(Lr_1^2)^k)^{T_f/\Delta t}, \tag{5.8}$$

where T_f is the frame duration.

For the selection of Δt, a similar procedure can be followed as with the flat fading case. The difference is now the autocorrelation we need to characterize is $\alpha_M = \sum_{k=1}^{L} \alpha_k^2$. Since α_i, α_j are independent for $i \neq j$, the autocorrelation of the process $\alpha_M(t)$ is the sum of correlation value for each branch. Hence,

$$
\begin{aligned}
\phi_{\alpha_M}(\tau) &= \sum_{k=1}^{L} \phi_{\alpha_M}(\tau) \\
&= \frac{\pi}{16} J_0^2(2\pi f_m \tau).
\end{aligned}
\tag{5.9}
$$

Δt is chosen as the smallest value so that the correlation value ϕ_{α_M} is about 0, which leads to $J_0^2(2\pi f_m \tau) = 0$. Note that this is the same result as in the flat fading scenario. The relationship of autocorrelation of the diversity combined fading process does not change since each of the branches is independently Rayleigh distributed. Therefore, the value of Δt is

$$
\Delta t = 1.2/(\pi f_m).
\tag{5.10}
$$

Thus we can reasonably approximate the samples of the fading process as independent while Δt is small enough to keep the left hand approximation in (5.2) reasonably accurate.

For the distribution of the time duration above a certain threshold r_2, a similar procedure can be followed.

$$
P_r(\tau \geq t) \leq P_r\Big(|x_1| > r_2, |x_2| > r_2, \ldots, |x_N| > r_2 \ \big| \ |x_0| = r_2\Big) \approx P_r(|x_n| > r_2)^N,
\tag{5.11}
$$

$$
f_r(t) \approx \frac{-Lr_2^2 + \ln(\sum_{k=0}^{L-1} \frac{1}{k!}(Lr_2^2)^k)}{\Delta t} (e^{-Lr_2^2} \sum_{k=0}^{L-1} \frac{1}{k!}(Lr_2^2)^k)^{t/\Delta t}.
\tag{5.12}
$$

Then the tail exponential slope for the good run length distribution λ_g is equal to

$$
\lambda_g = \frac{-Lr_2^2 + \ln(\sum_{k=0}^{L-1} \frac{1}{k!}(Lr_2^2)^k)}{\Delta t}.
\tag{5.13}
$$

It is equivalent to a geometric distribution in discrete time with

$$\beta_g = \left(e^{-Lr_2^2} \sum_{k=0}^{L-1} \frac{1}{k!} (Lr_2^2)^k \right)^{T_f/\Delta t}. \tag{5.14}$$

Similar to the flat fading scenario, the accuracy of the tail slope can be improved by taking advantage of the bivariate Rayleigh distribution and using a smaller Δt. The tail exponential slope λ can be described as $\frac{1}{\Delta t} \ln \left(\frac{P_r(|x_{n-1}|<r_1, |x_n|<r_1)}{P_r(|x_{n-1}|<r_1)} \right)$, which is equivalent to geometric distribution with $\beta_b = \left(\frac{P_\tau(|x_{n-1}|<r_1, |x_n|<r_1)}{P_r(|x_{n-1}|<r_1)} \right)^{\frac{T_f}{\Delta t}}$ in discrete time.

Then the tail exponential slope λ can be described as

$$\lambda = \frac{1}{\Delta t} \ln \left(\frac{P_r(|x_{n-1}| < r_1, |x_n| < r_1)}{P_r(|x_{n-1}| < r_1)} \right), \tag{5.15}$$

which is equivalent to a geometric distribution in discrete time with

$$\beta_b = \left(\frac{P_r(|x_{n-1}| < r_1, |x_n| < r_1)}{P_r(|x_{n-1}| < r_1)} \right)^{\frac{T_f}{\Delta t}}. \tag{5.16}$$

The bivariate Rayleigh cumulative distribution function (cdf) was derived in [59] and [60]. Using an infinite series representation,

$$P_r(|x_{n-1}| < r_1, |x_n| < r_1) = \frac{(1-\rho)^L}{\Gamma(L)} \sum_{k=0}^{\infty} \rho^K \cdot P\left(k+L, \frac{r_1^2 L}{(1-\rho)}\right) \times P\left(k+L, \frac{r_1^2 L}{(1-\rho)}\right), \tag{5.17}$$

where $\rho = cov(|x_{n-1}|^2, |x_n|^2)/\sqrt{var(|x_{n-1}|^2)var(|x_n|^2)} = J_0^2(2\pi f_m \tau)$,

$P(\alpha, x) = (1/\Gamma(\alpha)) \int_0^x e^{-t} t^{\alpha-1} dt$ is a common form of the incomplete gamma function.

Since $P_r(|x_{n-1}| < r_1) = 1 - e^{-Lr_1^2} \sum_{k=0}^{L-1} \frac{1}{k!}(Lr_1^2)^k$, then

$$\beta_b = \left(\frac{(1-\rho)^L/\Gamma(L) \sum_{k=0}^{\infty} \rho^K \cdot P\left(k+L, \frac{r_1^2}{(1-\rho)}\right) \times P\left(k+L, \frac{r_1^2}{(1-\rho)}\right)}{1 - e^{-Lr_1^2} \sum_{k=0}^{L-1} \frac{1}{k!}(Lr_1^2)^k} \right)^{\frac{T_f}{\Delta t}}. \tag{5.18}$$

The tail slope for the good run length distribution can be refined with the smaller

Δt following the same procedure. The tail exponential slope λ_g for the good run length distribution can be described as

$$\lambda_g = \frac{1}{\Delta t} \ln \left(\frac{P_r(|x_{n-1}| > r_2, |x_n| > r_2)}{P_\tau(|x_{n-1}| > r_2)} \right), \tag{5.19}$$

which is equivalent to a geometric distribution in discrete time with

$$\beta_b = \left(\frac{P_r(|x_{n-1}| > r_2, |x_n| > r_2)}{P_r(|x_{n-1}| > r_2)} \right)^{\frac{T_f}{\Delta t}}. \tag{5.20}$$

Using an infinite series representation for the bivariate Rayleigh cdf,

$$P_r(|x_{n-1}| > r_2, |x_n| > r_2) = (1-\rho)^L/\Gamma(L) \sum_{k=0}^{\infty} \rho^K \cdot \left(1 - P\left(k+L, \frac{r_2^2}{(1-\rho)} \right) \right)^2. \tag{5.21}$$

It is known that $P_r(|x_{n-1}| > r_2) = e^{-Lr_2^2} \sum_{k=0}^{L-1} \frac{1}{k!}(Lr_2^2)^k$, so

$$\beta_g = \left(\frac{(1-\rho)^L/\Gamma(L) \sum_{k=0}^{\infty} \rho^K \cdot \left(1 - P\left(k+L, \frac{r_2^2}{(1-\rho)} \right) \right)^2}{e^{-Lr_2^2} \sum_{k=0}^{L-1} \frac{1}{k!}(Lr_2^2)^k} \right)^{\frac{T_f}{\Delta t}}. \tag{5.22}$$

Therefore, the tail slopes for good and bad run length distributions are determined. The procedure to set up the tail slope for a frequency selective channel with diversity is no different than with the flat fading case except that the probability of the envelope of the combined diversity fading process falling above or below certain threshold needs to be adjusted accordingly.

2.   Initial Exponential Slope

As in the flat fading channel, the initial slope of the run length distributions represents the short bursts occurring when the instantaneous fading envelope falls between the middle region from r_1 to r_2. Although the channel is frequency selective with diversity gain now, it does not change the fact that the appearances of short runs are associated with the instantaneous fading envelope falling between the middle region. Once the

instantaneous fading envelope falls into that region, we model the frame error process independent with each frame with an average frame error rate of $1/2$.

Therefore, we have the same results as we have in the flat fading channel. Under this model, the bad (good) frame run length distribution will be geometric with parameter $\alpha_b = \alpha_g = 1/2$. And the argument that the initial slopes of the run length distributions do not depend on many of the physical channel parameters such as Doppler rate and long term SNR still holds here for the frequency selective channel with diversity gain. The frequency selective channel with diversity only changes how often or how long the fading process stays in this region. While once the fading process enters this region, the behavior of run lengths will be the same and will not be affected by those physical layer parameters.

Fig. 47 illustrates the initial slope of good and bad run length distributions. An 802.11a OFDM system with 4 independent fading channels are simulated. It is seen that the invariance of the initial slope still exists as in the flat fading channel. The initial slope does not depend on Doppler rate, average SNR or diversity order, which is a nice result considering it remains constant and does not have to be recalculated when the physical layer condition differs.

3. Combination Factor

The combination factor p represents the percentage of short runs in the total number of good or bad runs. Long runs are supposed to occur when the underlying Rayleigh fading process falls below the threshold r_1 or the good frame runs occurr when the magnitude of the fading process is higher than the threshold r_2. Short runs occur when the instantaneous SNR r belongs to the middle region.

The number of long runs N_l per second can be described as the level crossing rate of the composite fading process at level γ in the positive direction only (or in
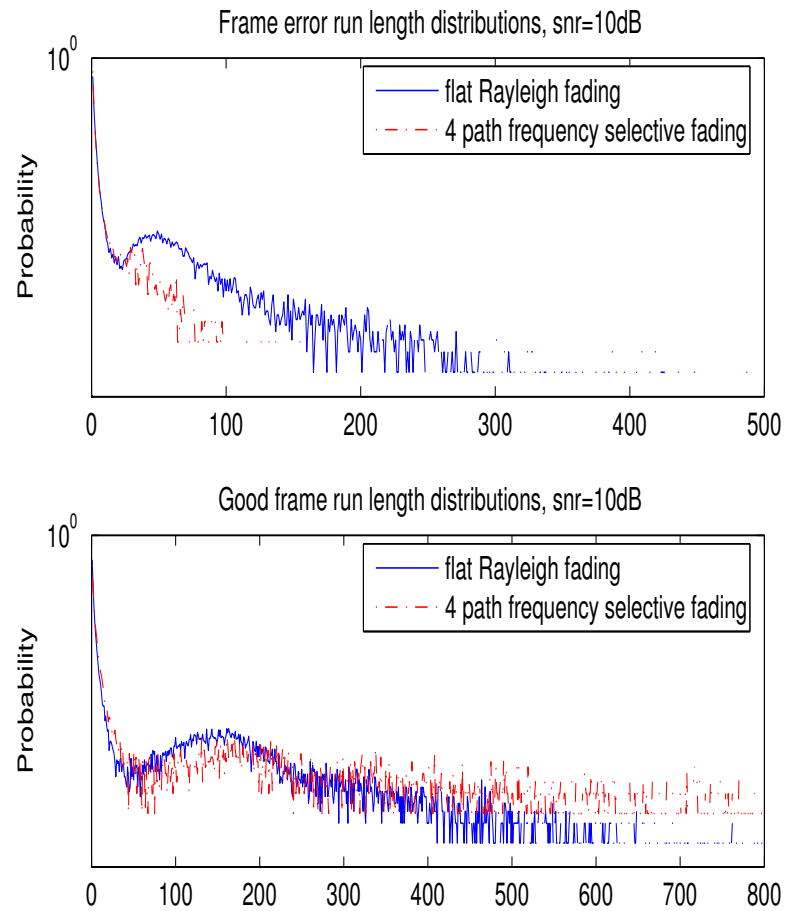
Fig. 47. Initial slope of the run length distribution, frequency selective channel with diversity gain

the negative direction only), which is given by Iskander and Mathiopoulos [65].

$$N_l = R\frac{\sqrt{2\pi}f_m}{\Gamma(L)}(\frac{\gamma^2}{\gamma_0})^{L-\frac{1}{2}}e^{(-\frac{\gamma^2}{\gamma_0})}, \tag{5.23}$$

where γ_0 is the average SNR, L is the diversity order.

Assume the frame error rate as $r \in [r_1, r_2]$ is P_f, the average length of error runs in this region can be estimated as follows

$$\bar{L} = \sum_{n=1}^{\infty} nP_f^{n-1}(1 - P_f) \tag{5.24}$$

$$= \frac{1}{1 - P_f}. \tag{5.25}$$

Let the average SNR be γ_0, the average number of short error runs per second N_s can be approximated by

$$N_s = \int_{r_1^2}^{r_2^2} p(r)\frac{1}{T_f}p_e(r)/\bar{L}dr$$

$$= \int_{r_1^2}^{r_2^2} \frac{1}{(L-1)!r}(Lr)^L e^{-Lr}\frac{1}{T_f}p_e(r)(1 - p_e(r))dr, \tag{5.26}$$

where $p_e(r)$ is the frame error rate of instantaneous SNR (γ_0+r)(dB) with no random fading process added.

Therefore, assume the average power of the fading process is 1, the percentage of short runs p can be approximated by

$$p = \frac{N_s}{N_s + N_l} \tag{5.27}$$

$$= \frac{\int_{r_1^2}^{r_2^2} \frac{1}{(L-1)!r}(Lr)^L e^{-Lr}p_e(r)(1 - p_e(r))dr}{\int_{r_1^2}^{r_2^2} \frac{1}{(L-1)!r}(Lr)^L e^{-Lr}p_e(r)(1 - p_e(r))dr + \frac{\sqrt{2\pi}f_m}{\Gamma(L)}(\gamma^2)^{L-\frac{1}{2}}e^{-\gamma^2}}, \tag{5.28}$$

where γ is chosen to be r_1 if p is for the frame error run length distribution or r_2 for the good frame run length distribution.

Thus all the parameters in the four-state Markov Model can be set analytically

for a frequency selective channel with diversity combining with minimum physical layer simulation.

4. Statistical Approximation Results

In summary, the parameters of the 4SMM are set as follows:

1)α_g, $\alpha_b = 0.5$;

2)Set r_1 and r_2 according to the plot of the FER of the underlying modulation/coding scheme in a Gaussian noise channel.

3)$\beta_b = (1 - e^{-Lr_1^2} \sum_{k=0}^{L-1} \frac{1}{k!} (Lr_1^2)^k)^{\frac{\pi f_m T_f}{1.2}}$, $\beta_g = \left(e^{-Lr_2^2} \sum_{k=0}^{L-1} \frac{1}{k!} (Lr_2^2)^k\right)^{\frac{\pi f_m T_f}{1.2}}$, where T_f is the frame duration, f_m is the Doppler rate and L is the diversity order.

Or improve the accuracy by choosing a smaller delta and use the β_b and β_g in (5.18) and (5.22)

4)

$$p_b = \frac{\int_{r_1^2}^{r_2^2} \frac{1}{(L-1)!r} (Lr)^L e^{-Lr} p_e(r)(1 - p_e(r))dr}{\int_{r_1^2}^{r_2^2} \frac{1}{(L-1)!r} (Lr)^L e^{-Lr} p_e(r)(1 - p_e(r))dr + \frac{\sqrt{2\pi} f_m}{\Gamma(L)} (r_1^2)^{L-\frac{1}{2}} e^{-r_1^2}},$$

$$p_g = \frac{\int_{r_1^2}^{r_2^2} \frac{1}{(L-1)!r} (Lr)^L e^{-Lr} p_e(r)(1 - p_e(r))dr}{\int_{r_1^2}^{r_2^2} \frac{1}{(L-1)!r} (Lr)^L e^{-Lr} p_e(r)(1 - p_e(r))dr + \frac{\sqrt{2\pi} f_m}{\Gamma(L)} (r_2^2)^{L-\frac{1}{2}} e^{-r_2^2}},$$

where $p_e(r)$ is the function of frame error rate when the instantaneous SNR is $(\gamma_0 + r)$(dB).

Using this approach, the run length distributions of 802.11a environment in a 4 path frequency selective fading channel are shown in Fig. 48. Note that for the coded OFDM system, the actual achieved diversity order may not be the diversity available in the channel depending on the adopted coding, modulation scheme and average SNR. One needs to verify the real diversity order achieved before conducting the physical layer modeling to ensure the accurateness when setting up the 4SMM.

Run length distributions of an Alamouti scheme [30] with 2 transmit antennas and 2 receive antennas in a flat Rayleigh fading channel are shown in Fig. 49. The diversity order is 4 for an Alamouti system with 2 transmit antennas and 2 receive antennas. One reason we choose an Alamouti scheme to justify the models is because the diversity order is only dependent on the number of transmit and receive antenna if we assume all the fading branches are independent. There will be no confusion about the diversity order in the physical layer system. No channel coding is included in the Alamouti system. Channel coding only changes the value of two thresholds r_1 and r_2 but will not change the diversity of the system. We can see that the 4SMM gives good approximations to the run length distributions for both cases, especially the 4SMM matches the initial slope and the tail slope of the run length distributions very well. Thus the 4SMM estimates run length distributions for frequency selective channel with diversity and Alamouti MIMO scheme properly by setting up model parameters analytically. It is encouraging that the 4SMM can be easily adapted for a diversity channel with a similar procedure to establish the state transition probabilities. This result for diversity channel confirms the idea of approximating the run length distribution with two exponential distributions and choosing the parameters by utilizing the inherent behavior of the underlying fading process. The performance of the four-state Markov model in a wireless network will be evaluated in the next section.

C.   Network Performance

We apply the four-state Markov model in a wireless LAN 802.11a frequency selective channel and Alamouti MIMO environment with the ns2 network simulation tool. To make a fair comparison, we also embed a simulated 802.11a physical channel
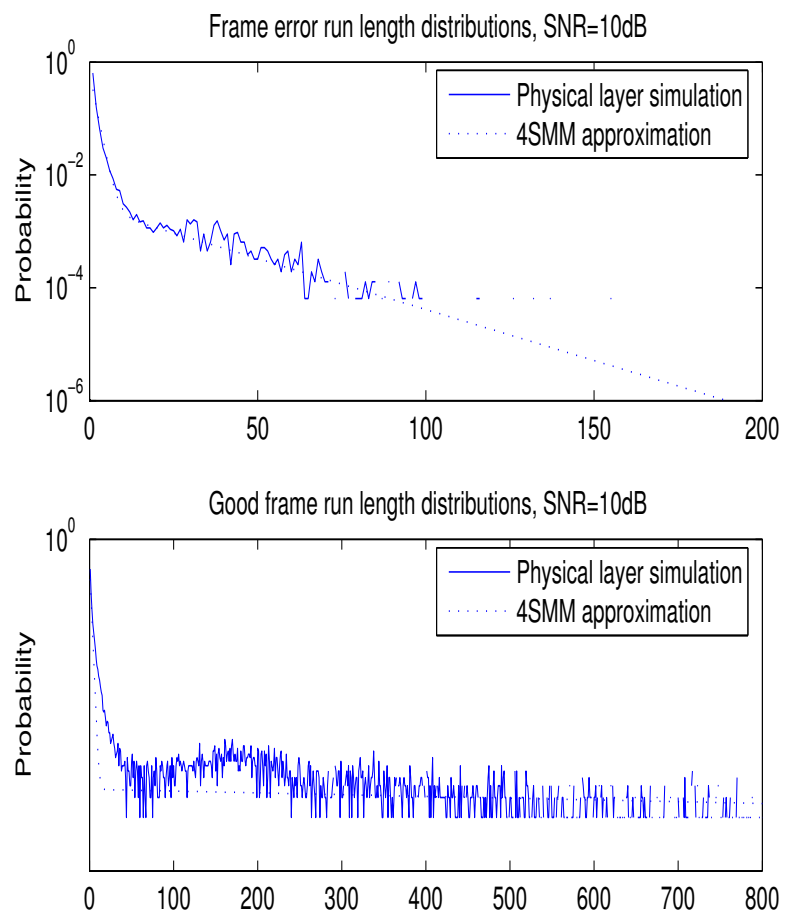
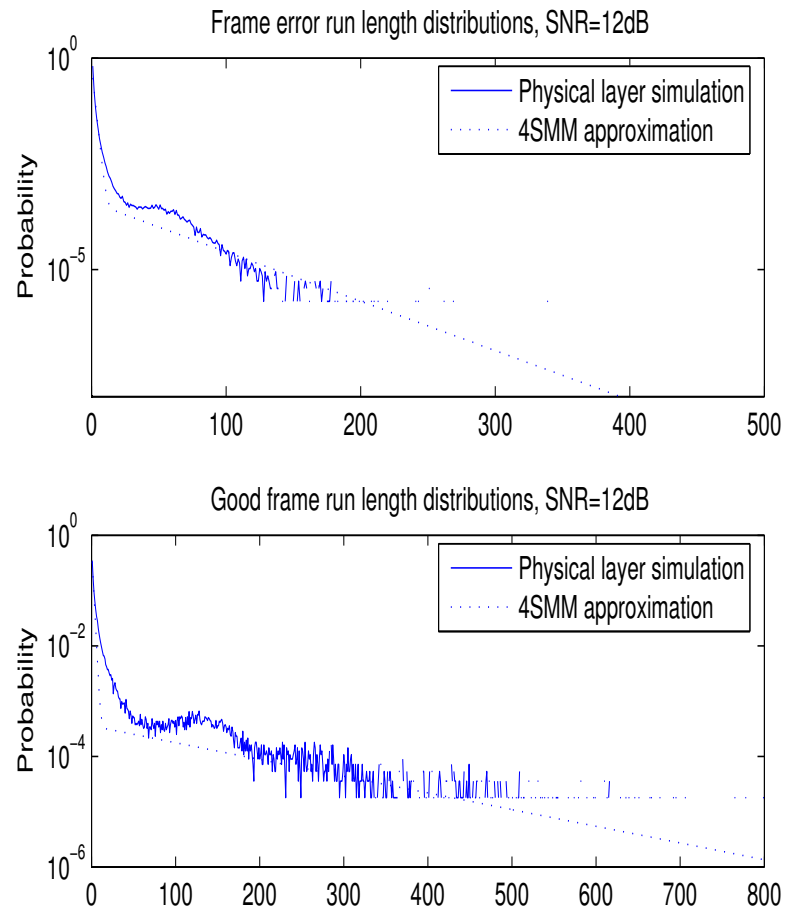Fig. 48. 4SMM run length distribution approximations in a frequency selective channel, 802.11a environment

Fig. 49. 4SMM run length distribution approximations for Alamouti scheme

with channel coding, modulation in a 4 path frequency selective channel into ns2 to get the simulated physical layer results. A similar simulation is performed for the Alamouti scheme. The Doppler frequency is selected to be 100Hz. The frame size and transmission rate chosen are 384bits, 12Mb/s. The normalized Doppler $f_m T_f$ is 0.0032.

A simple two-node wireless network was set up by the ns2 simulation tool. Simulations were conducted for 30% channel loadings, with the following network setup: a constant SNR of 5-15dB, the wireless LAN MAC protocols with the distributed coordination function and a queue length of 50 packets, TCP Reno with an initial window length of 100, and also the user datagram protocol (UDP). Each simulation was conducted for 10 minutes of simulation time. A trace file was generated for each simulation and analyzed later for network characteristics. Note that this is the network simulation duration set before the ns2 simulation, while the ns2 simulator can run for days. For a physical layer with a number of independent fading paths, it takes substantial time to simulate the physical layer with diversity. Moreover, the simulation time increases with the average SNR because the better the frame error rate the more data packets will be transmitted through the network and more simulation time will be consumed. For example, it could take five to seven days on a dual 1800MP+ processor computer with 2GB of DDR RAM to execute a 600 second simulation for a 4 path 802.11a environment with 10dB SNR. In comparison, the 4SMM only takes 3 minutes to complete the ns2 simulation.

Another issue one should be careful about is the selection of the diversity order. In a coded OFDM system which is employed in the 802.11a physical layer, the maximum diversity order is the number of independent fading paths L available in the channel. But that is the asymptotic result and for a specific SNR, the achieved diversity order may be less than L. For instance, with a constraint length 7, mini-

Table V. Two-state Markov Model Parameters, 802.11a coded OFDM system

SNR(dB)	ε	AFEL	p	q
9	0.09167	3.6979	0.9727	0.7296
10	0.04811	3.2376	0.9844	0.6911
11	0.03097	2.9300	0.9891	0.6587
12	0.0145	2.7938	0.9947	0.6421
15	0.00262	2.4486	0.9989	0.5916

Table VI. Two-state Markov Model Parameters, Alamouti MIMO scheme

SNR(dB)	ε	AFEL	p	q
12	0.1693	2.8923	0.9295	0.6543
13	0.0957	2.5746	0.9589	0.6116
14	0.0498	2.3599	0.9778	0.5763
15	0.0240	2.1926	0.9888	0.5439
16	0.0114	2.0999	0.9945	0.5238
20	0.0004	1.8151	0.9998	0.4491

mum free distance 10, 1/2 convolutional code [66], the diversity order for a 4 path frequency selective channel at 10dB is about only 2. When setting the 4SMM parameters according to the described procedures, it is necessary to use the actual achieved diversity order at the specific SNR not the asymptotic results.

The parameters of the 2SMM and 4SMM are listed in tables V, VI, VII and VIII. As shown in Fig.50 and Fig.51, the four-state Markov model approximates the TCP throughput more accurately compared to the two-state Markov model.

Table VII. Four-state Markov Model Parameters, 802.11a coded OFDM system

SNR(dB)	α_g	β_g	p_g	α_b	β_b	p_b
9	0.5	0.9953	0.7727	0.5	0.9710	0.8551
10	0.5	0.9969	0.7274	0.5	0.9622	0.8660
11	0.5	0.9979	0.6837	0.5	0.9550	0.8622
12	0.5	0.9986	0.6382	0.5	0.9472	0.8579
15	0.5	0.9998	0.4793	0.5	0.9138	0.8565

Table VIII. Four-state Markov Model Parameters, Alamouti MIMO scheme

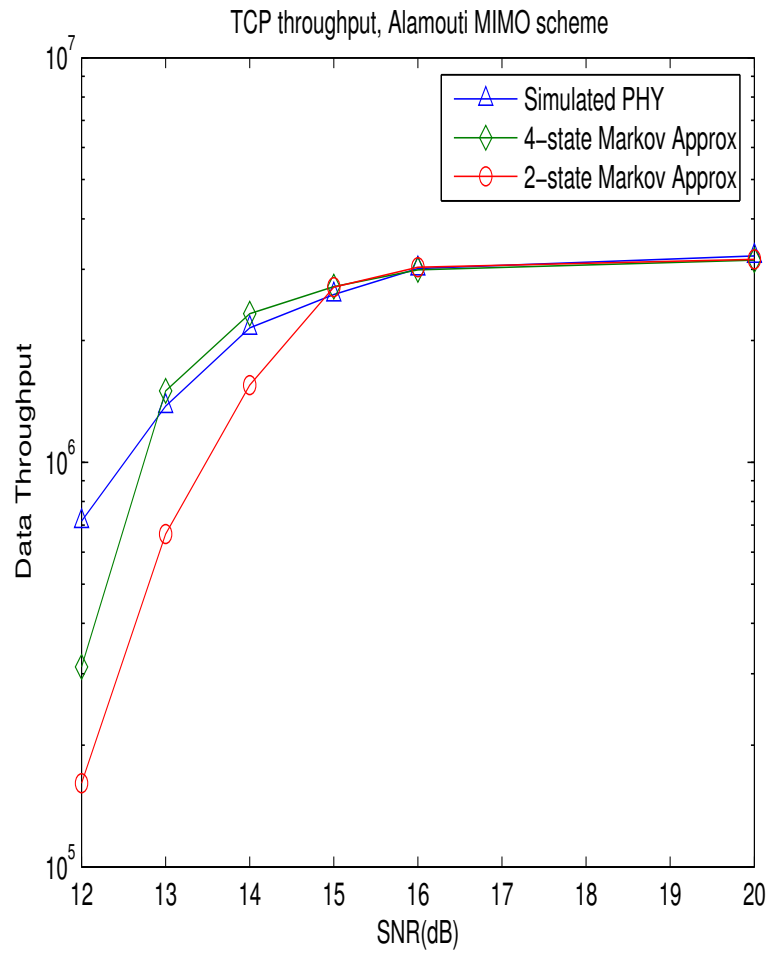| SNR(dB)	α_g	β_g	p_g	α_b	β_b	p_b
12	0.5	0.9828	0.9761	0.5	0.9574	0.9920
13	0.5	0.9877	0.9429	0.5	0.9481	0.9934
14	0.5	0.9915	0.8882	0.5	0.9379	0.9943
15	0.5	0.9944	0.8139	0.5	0.9272	0.9948
16	0.5	0.9965	0.7277	0.5	0.9159	0.9951
20	0.5	0.9997	0.4173	0.5	0.8681	0.9949

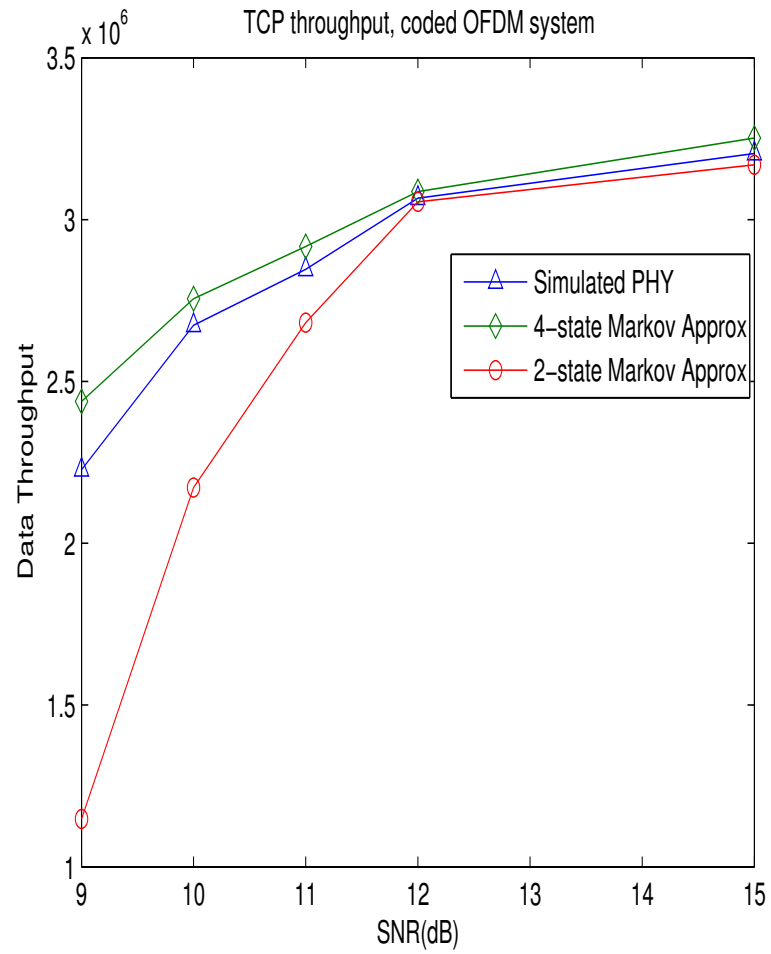Fig. 50. Network performance of channel approximations, Alamouti MIMO scheme

Fig. 51. Network performance of channel approximations, coded OFDM system

D.   Summary

The four-state Markov model was applied to model physical layer block level statistics in diversity channels in this chapter. By approximating the frame good and bad run length distributions with a mixture of geometric distributions, the four-state Markov model successfully captured the essential physical layer characteristics and provided good network simulation results. The procedure to set up the 4SMM parameters was described in detail. The transition probabilities of the 4SMM were obtained by matching the physical layer frame run length distributions. Without having to run initial simulations, the parameters of the 4SMM can be acquired analytically, which provides great convenience for upper layer analysis and simulations. Coded OFDM system and Alamouti MIMO scheme were studied as examples of the application of the 4SMM. By simulating physical layers of the coded OFDM system and Alamouti MIMO scheme in ns2, we compared the network performance of the 4SMM, which provides excellent network results. The four-state Markov model is shown to be a simple, accurate and easily set-up model for wireless physical layer with diversity channels.

CHAPTER VI

CONCLUSION

In this dissertation, current widely used physical layer models were examined and shown to be deficient. An inaccurate physical layer model can lead to incorrect upper layer protocol judgements and analysis when applied to simulations and analytical derivations. To address this problem, physical layer statistics were investigated. We identified the key properties of the physical layer to be the good and bad frame run length distributions for the purpose of approximating the physical layer activities accurately and thus providing a good physical layer model for upper layer simulations and analysis. A two-state run length model was presented in which the duration of each state was set to duplicate the exact physical layer frame run length distribution. In the two-state run length model, from the good (bad) state, it transfers to the bad (good) state after a certain time duration. To make a fair comparison of the performance of all the physical layer models, the actual physical layer with channel coding and fading were implemented and embedded into the ns2 simulator so that we can know what to expect and compare with the upper layer network simulation results. The ns2 network throughput with the two-state run length model is extremely close to the network throughput with simulated actual physical layer. However, the two-state run length model is impractical because the knowledge of the exact frame run length distribution is required in order to set up the model. If one of the physical layer parameters varies such as the signal-to-noise ratio and Doppler frequency shift, the frame run length distribution will be completely different and physical layer simulation has to be conducted to obtain the frame run length distributions. Although the two-state run length model is unrealistic for applications, it verifies the point that if we can approximate the physical layer frame run length distributions accurately in

the physical layer the model will generate accurate upper layer simulation results.

Encouraged by the results of the two-state run length model, we examined the physical layer frame run length distributions in the flat Rayleigh fading channel. Fortunately, we found that the frame run length distributions can be well approximated by a mixture of two exponential distributions. Approximating the run length distribution in such a manner will result in an innovative four-state Markov model. The transition probabilities of the four-state Markov model are linked with the slopes and the combination factors of the mixture exponential distributions. The four-state Markov model can be easily set up if the parameters of the mixture exponential distributions are known. The main idea when deriving the parameters of the approximated frame run length distributions is that we assume all the good or bad long runs occur when the instantaneous signal-to-noise ratio is above or below certain thresholds. And all the good or bad short runs occur when the instantaneous signal-to-noise ratio falls in the middle region. By carefully choosing the upper and lower thresholds for the fading process, a procedure to estimate the initial and tail slope has been developed. The combination factor of the mixture exponential slope can also be estimated by taking advantage of the level crossing rate of the flat fading process. Following the described procedure, the four-state Markov model can be easily established. Ns2 simulation showed that the proposed four-state Markov model performs superior to the popular two-state Markov model. The generated ns2 TCP and UDP throughput with the four-state Markov model were shown to be quite accurate. In addition to the accuracy of the four-state Markov model, the process of setting it up does not require previous physical layer simulations in a fading environment, whereas the traditional method to set up two-state Markov model needs to run previous physical simulations for each signal-to-noise ratio or Doppler frequency shift. The only condition one needs to know in order to set up the four-state Markov model is the physical layer frame

error rate versus signal-to-noise ratio in a Gaussian channel, which is very easy to obtain. The advantage of setting up the parameters analytically makes the model much favorable for upper layer analysis and simulations.

We also looked at the problem of physical layer modeling in a diversity channel. We start by investigating the frame run length distributions. The frame run length distributions for the diversity channel still presents a behavior of mixture exponential distributions. Thus it is possible to apply the four-state Markov model to the diversity channel if we can choose the slopes and combination factor appropriately. With a similar procedure to divide the instantaneous signal-to-noise ratio into three regions by choosing the upper and lower threshold, the procedure of setting up the model parameters has been adapted for the diversity channel. The procedures were similar with what we did in the flat fading scenario. A coded OFDM system with a frequency selective channel and an Alamouti MIMO system with 2×2 antennas were embedded and simulated in the ns2 simulator to provide benchmark results for the comparison of physical layer models. One should make sure that the actual achieved diversity order is in agreement with the diversity order used for model parameter derivation before trying to set up the model. The four-state Markov model was shown to approximate the frame run length distributions and network throughput nicely. Whereas the two-state Markov model presented a completely different behavior with respect to the frame run length distributions and underestimated the network throughput badly especially for low to medium signal-to-noise ratio. It took up to weeks to execute a 600 seconds network simulation for a 4 path 802.11a environment on a dual 1800MP+ processer computer while utilizing the four-state Markov model the simulation can be finished in minutes. Moreover, the simplicity of the four-state Markov model could make it a valuable tool for the analysis of the upper layer properties. This four-state Markov Model makes a practical and efficient model for the research of

wireless network which is generic and can be applied for many different kinds of physical environments. The four-state Markov Model is shown to be an excellent physical layer block level model for wireless network analysis and simulations and holds significant potential.

REFERENCES

[1] D.W. Davies, D.L.A.Barger, W.L.Price, and C.M. Solomonides, *Computer Networks and Their Protocols*, New York, NY: John Wiley and Sons, 1979.

[2] D.M. Piscitello and A.L.Chapin, *Open Systems Networking: TCP/IP and OSI*, Reading, MA: Addison-Wesley, 1993.

[3] Stevens and W.R., *TCP/IP Illustrated, Volume 1: The Protocols*, Reading, MA: Addison-Wesley, 1994.

[4] G.Kessler and S.Shepard, "Internet & TCP/IP tools and utilities," RFC 2151, Informational, June 1997.

[5] A.Kumar, "Comparative performance analysis of version of TCP in a local network with a lossy link," *IEEE Trans. on Networking*, vol. 6, pp. 485–498, Aug. 1998.

[6] N.M.Chaskar, T.V.Lakshman, and U.Madhow, "TCP over wireless with link level error control: analysis and design methodology," *IEEE Trans. Networking*, vol. 7, pp. 605–615, Oct. 1999.

[7] M.Zorzi, A.Chockalingam, and R.R.Rao, "Throughput analysis of TCP on channels with memory," *IEEE JSAC*, vol. 18, pp. 1298–1300, July 2000.

[8] A. Bakre and B. R. Badrinath, "Indirect TCP for mobile hosts," in *Proc.15th Int'l Conf. on Distributed Computing Systems (ICDCS)*, Vancouver, BC, Canada, May 1995.

[9] S. Kopparty, Krishnamurthy S.V., M. Faloutsos, and S.K. Tripathi, "Split TCP for mobile ad hoc networks," in *IEEE Globecom.*, Taipei, Taiwan, 2002.

[10] H.Balakrishnan, S.Seshan, E.Amir, and R.H.Katz, "Improving TCP/IP performance over wireless networks," in *ACM Conference on Mobile Computing and Networking*, Berkeley, CA, Nov. 1995.

[11] S.Floyd and T.Henderson, "The new Reno modification to TCP's fast recovery algorithm," RFC 2582, Informational, Apr. 1999.

[12] C.P.Fu and S.C.Liew, "TCP Veno: TCP enhancement for transmission over wireless access networks," *IEEE JSAC*, vol. 21, no. 2, pp. 216–228, Feb. 2004.

[13] H. S. Wang, "On verifying the first-order Markovian assumption for a Rayleigh fading channel model," in *Proc. ICUPC*, San Diego, CA, Sep. 1994, pp. 160–164.

[14] Xunqi Yu, James W. Modestino, and Xusheng Tian, "The accuracy of Gilbert models in predicting packet-loss statistics for a single-multiplexer network model," in *INFOCOM 2005. 24th Annual Joint Conference of the IEEE Computer and Communications Societies*, Miami, FL, Mar. 2005, vol. 4, pp. 2602–2612.

[15] J.McDougall and S.Miller, "Sensitivity of wireless network simulations to a two-state Markov model channel approximation," in *IEEE Globecom.*, San Francisco, CA, Dec. 2003, vol. 2, pp. 697–701.

[16] H.Sanneck, G.Carle, and R.Koodli, "A framework model for packet loss metrics based on loss run length," in *Proc. of SPIE/ACM SIGMM Multimedia Computing and Networking Conference*, San Jose, CA, Jan. 2000.

[17] H.S.Wang and N.Moayeri, "Finite-state Markov channel-a useful model for radio communication channels," *IEEE Trans. Veh. Technology*, vol. 44, pp. 163–171, Feb. 1995.

[18] Qinqing Zhang and S.A. Kassam, "Finite-state Markov model for Rayleigh fading channels," *IEEE Trans. Commun.*, vol. 47, pp. 1668–1692, Nov. 1999.

[19] Turin W and Van Nobelen R., "Hidden Markov modeling of flat-fading channels," *IEEE JSAC in Commun.*, vol. 16, no. 9, pp. 1234–1238, Dec. 1998.

[20] Turin W and Zorzi M., "Performance analysis of delay-constrained communications over slow Rayleigh fading channels," *IEEE Trans. Wireless Commun.*, vol. 1, no. 4, pp. 801–807, Oct. 2002.

[21] J.McDougall, Y.Yu, and S.Miller, "A statistical approach to developing channel models for network simulations," in *IEEE WCNC.*, Atlanta, GA, 2004.

[22] J. McDougall, "Low complexity channel models for approximating flat Rayleigh fading in network simulations," Ph.D. dissertation, Texas A&M University, College Station, TX, August 2003.

[23] Alberto Lopez Toledo, Xiaodong Wang, and Ben Lu, "A cross-layer TCP modelling framework for MIMO wireless systems," *IEEE Trans. Wireless Commun.*, vol. 5, no. 4, pp. 920–929, April 2006.

[24] T.S.Rappaport, *Wireless Communcations: Principles and Practice*, Upper Saddle River, NJ: Prentice Hall, 1996.

[25] W.C.Jakes, *Microwave Mobile Communications*, New York, NY: John Wiley & Sons, 1974.

[26] Jr. L.Cimini, "Analysis and simulation of a digital mobile channel using orthogonal frequency division multiplexing," *IEEE Trans. Commun.*, vol. 33, pp. 665–675, July 1985.

[27] R.Van Nee, G.Awater, M.Morikura, H.Takanashi, M.Webster, and K.W.Halford, "New high-rate wireless LAN standards," *IEEE Commun. Mag.*, pp. 82–88, Dec. 1999.

[28] David Gesbert, Mansoor Shafi, Da shan Shiu, Peter J.Smith, and Ayman Naguib, "From theory to practice: An overview of mimo space-time coded wireless systems," *IEEE JSAC in Commun.*, vol. 21, no. 3, pp. 281–302, April 2003.

[29] I.E.Telatar, "Capacity of multiantenna Gaussian channels," *Eur. Trans. Commun.*, vol. 10, no. 6, pp. 585–595, 1999.

[30] Siavash M. Alamouti, "A simple transmit diversity technique for wireless communcations," *IEEE JSAC in Commun.*, vol. 16, no. 8, pp. 1451–1458, Oct. 1998.

[31] V.Tarokh, H.Jafarhani, and A.R.Calderbank, "Space-time block codes from orthogonal designs," *IEEE Trans. Inform. Theory*, vol. 45, pp. 1456–1467, July 1999.

[32] S.Keshav, "REAL:A network simulator," Tech. report, Univ.California, Berkeley, 1988.

[33] K.Fall and K.Varadhan, *The ns Manual (formerly ns Notes and Documentation)*, http://www.isi.edu/nsnam/ns/doc, accessed August,2003.

[34] *Monarch Extensions to the ns-2 Network Simulator*, http://www.monarch.cs.cmu.edu/cmu-ns.html, 1999.

[35] *Additions to the NS network simulator to handle Ricean and Rayleigh fading*, http://www.ece.cmu.edu/wireless/, 2000.

[36] Ratish J. Punnoose, Pavel V. Nikitin, and Daniel D. Stancil, "Efficient simulation of ricean fading within a packet simulator," in *Vehicular Technology Conference*, Boston, MA, Sept. 2000.

[37] W.C.Jakes, *Microwave Mobile Communication*, New York, NY: IEEE Press, 1993.

[38] Gordon L.Stuber, *Principles of Mobile Communication*, Norwell, MA: Kluwer Academic Publishers, 2001.

[39] Scott L. Miller, "ELEN 489," Class notes, Department of Electrical Engineering, Texas A&M University, College Station, TX, Spring 2005.

[40] A.A Abouzeid, Roy.S, and Azizoglu.M, "Comprehensive performance analysis of a TCP session over a wireless fading link with queueing," *IEEE Trans. Wireless Communication*, vol. 2, pp. 344–356, March 2003.

[41] Chiani M., Milani E., and Verdone R., "A semi-analytical approach for performance evaluation of TCP-IP based mobile radio links," in *IEEE Global Telecommunications Conference*, San Francisco, CA, 2000, pp. 937–942.

[42] A.Chockalingam and B.Gang, "Performance of TCP/RLP protocol stack on correlated fading DS-CDMA wireless links," *IEEE Trans. on Vehicular Technology*, vol. 49, pp. 28–33, Jan. 2000.

[43] F. Vacirca, A. De Vendictis, A. Todini, and A. Baiocchi, "On the effects of ARQ mechanisms on TCP performance in wireless environments," in *Global Telecommunications Conference*, San Francisco, CA, Dec. 2003, vol. 2, pp. 671–675.

[44] Kim JG, Krunz M., and Verdone R., "Quality of service over wireless ATM links," in *IEEE Eighteenth Annual Joint Conference of the IEEE Computer and Communications Societies*, New York, NY, 1999, pp. 1003–1010.

[45] E.N.Gilbert, "Capacity of burst noise channels," *The Bell System Technical Journal*, vol. 39, pp. 1253–1256, 1960.

[46] J.Arauz and P.Krishnamurthy, "Markov modeling of 802.11 channels," in *IEEE Vehicular Technology Conference*, Orlando, FL, Fall 2003.

[47] A.Konrad et al., "A Markov-based channel model algorithm for wireless networks," *The Bell System Technical Journal*, , no. 9, pp. 189–199, Sept. 2003.

[48] J.A. Hartwell and A.O. Fapojuwo, "Modeling and characterization of frame loss process in ieee 802.11 wireless local area networks," in *IEEE Vehicular Technology Conference*, Los Angeles, CA, Sept. 2004, vol. 6, pp. 4481–4485.

[49] M.Zorzi, R.R.Rao, and L.B.Milstein, "On the accuracy of a first-order Markov model for data block transmission on fading channel," in *Proc.IEEE ICUPC95*, Tokyo, Japan, Nov. 1995, pp. 211–215.

[50] M.Zorzi, R.R.Rao, and L.B.Milstein, "Error statistics in data transmission over fading channels," *IEEE Trans. Commun.*, vol. 46, pp. 1468–1477, Nov. 1998.

[51] Christopher C.Tan and Norman C. Beaulieu, "On first-order Markov modeling for the Rayleigh fading channel," *IEEE Trans. Commun.*, vol. 48, no. 12, pp. 2032–2040, Dec. 2000.

[52] J.Arauz and P.Krishnamurthy, "Discrete Rayleigh fading channel modeling," *Wireless Communications and Mobile Computing*, vol. 4, pp. 413–425, July 2004.

[53] D.L.Isaacson and R.W. Madsen, *Markov Chains, Theory and Applications*, New York, NY: Wiley, 1976.

[54] Qingwen Liu, Shengli Zhou, and G.B. Giannakis, "Queuing with adaptive modulation and coding over wireless links: cross-layer analysis and design," *IEEE Trans. Wireless Communications*, vol. 4, pp. 1142–1153, May 2005.

[55] P. Sadeghi and P. Rapajic, "Capacity analysis for finite-state Markov mapping of flat-fading channels," *IEEE Trans. Commun.*, vol. 53, pp. 833–840, May 2005.

[56] Jungnam Yun and M. Kavehrad, "Markov error structure for throughput analysis of adaptive modulation systems combined with ARQ over correlated fading channels," *IEEE Trans. Vehicular Technology*, vol. 54, pp. 235–245, Jan. 2005.

[57] H. Rutagemwa and Xuemin Shen, "Modeling and analysis of wap performance over wireless links," *IEEE Trans. Mobile Computing*, vol. 2, pp. 221–232, July-Sept. 2003.

[58] S.O.Rice, "Distribution of the duration of fades in radio transmission: Gaussian noise model," *Bell System Tech. Journal*, vol. 38, pp. 581–635, May 1958.

[59] C.C.Tan and N.C.Beaulieu, "Infinite series representation of the bivariate Rayleigh and Nakagami–m distributions," *IEEE Trans. Commun.*, vol. 45, pp. 1159–1161, Oct. 1997.

[60] Marvin K. Simon and Mohamed-Slim Alouini, "A simple single integral representation of the bivariate Rayleigh distribution," *IEEE Communications Letters*, vol. 2, no. 5, pp. 128–130, May 1998.

[61] M.D.Yacoub, *Foundations of Mobile Radio Engineering*, Boca Raton, FL: CRC Press, 1993.

[62] Cyril-Daniel Iskander and P.Takis Mathiopoulos, "Fast simulation of diversity nakagami fading channels using finite-state Markov models," *IEEE Trans. Broadcasting*, vol. 49, pp. 269–277, Sept. 2003.

[63] C. D. Iskander and P. T. Mathiopoulos, "Finite-state Markov modeling of diversity Nakagami channels," in *Proc. Seventh Canadian Workshop on Info. Theory*, Vancouver,BC,Canada, June 2001.

[64] M.Nakagami, "The m-distribution—A general formula of intensity distribution of rapid fading," in *Statistical Methods in Radio Wave Propagation*, New York, NY: Pergamon, 1960, pp. 3–36.

[65] Cyril-Daniel Iskander and P.Takis Mathiopoulos, "Analytical level crossing rates and average fade durations for diversity tecniques in nakagami fading channels," *IEEE Trans. Commun.*, vol. 50, pp. 1301–1309, Aug. 2002.

[66] Stephen B Wicker, *Error control systems for digital communication and storage*, Englewood Cliffs, NJ: Prentice Hall, 1995.

VITA

Yi Yu, was born in 1979 in Jiangxi Province, P.R.China. She received her B.S. and M.S. degrees in electrical engineering from Southeast University in 1998 and 2001. Since 2001, she has been studying electrical engineering at Texas A&M University, College Station. She received her Ph.D degree in electrical engineering at Texas A&M University in August, 2006. Her permanent address is: Department of Electrical Engineering MS303, Texas A&M University, College Station, TX 77843.

The typist for this thesis was Yi Yu.